A STUDY OF THE REACTION $^{6}Li(^{12}C, d)^{16}O^{*}$ ABOVE THE COULOMB BARRIER

Thesis by

Clyde Stewart Zaidins

In Partial Fulfillment of the Requirements

For the Degree of

Doctor of Philosophy

California Institute of Technology

Pasadena, California

1967

(Submitted April 5, 1967)

ACKNOWLEDGMENTS

I hereby gratefully acknowledge and am deeply indebted to:

The entire staff of the Kellogg Radiation Laboratory for providing a friendly and productive place in which to work.

Dr. Hubert Winkler, Dr. Michael Loebenstein, and Dr. Donald Mingay for their essential collaboration in the completion of this experiment and all that they have taught me.

Dr. Gerard J. Stephenson, Jr., for valuable advice and assistance on the analysis of the data.

Professor Ward Whaling for helpful guidance of all types throughout my stay in the Kellogg Laboratory.

Professor W. A. Fowler and Dr. T. A. Tombrello for informative discussions during this undertaking.

The Office of Naval Research, the United States Steel Foundation, and the National Science Foundation for financial assistance at various stages of this project.

My wife, Florence, for her infinite patience, valuable help and continued moral support without which this work could never have been completed.

And all others not individually mentioned by name, who have made this project possible.

ABSTRACT

The angular distributions of deuterons from the reaction $^{6}Li(^{12}C, d)^{16}O^{*}$ leading to the ground state and first eight excited states of ^{16}O have been measured at a center of mass energy of 7 MeV. The angular distributions of deuterons leading to the third, fourth, and fifth excited states have been also measured at 8 MeV, and excitation functions for these levels at $\theta_{LAB} = 30^{o}$ and 50^{o} have been taken for these levels from 6 to 8 MeV. The results have been analyzed by calculating a theoretical contribution to the total cross sections due to the formation and decay of the compound nucleus ^{18}F in a statistical region of excitation by a Hauser-Feshbach calculation. This contribution is then subtracted from the total, neglecting any interference effect, and the difference is related to a reduced alpha width of the ^{16}O final states that might be measured in a purely direct alpha transfer reaction. The astrophysical significance of the reduced alpha width of the fourth excited state is discussed.

TABLE OF CONTENTS

I. INTRODUCTION

A. The Heavy Ion Reaction $^{6}Li(^{12}C, d)^{16}O^{*}$

The reaction $^{6}Li(^{12}C, d)^{16}O^{*}$ was investigated in the center-of-mass energy region around 7 MeV leading to the ground state and first eight excited states of ^{16}O. The pertinent energy level diagram for this reaction is shown in Figure 1. This reaction is interesting for several reasons. Although all the levels in ^{16}O that are investigated here have well known spins and parities tabulated by Ajzenberg-Selove and Lauritsen (1959), we may hope to gain additional information about certain intrinsic properties of these states that are of interest to nuclear structure theorists and nuclear astrophysicists. Furthermore, this is a heavy-ion-induced reaction and the experience gained in such an investigation, both in terms of experimental technique and interpretation of the results, may well be an aid in further reactions where both nuclei in the entrance channel are heavier than helium. Such reactions are of increasing importance because many of them afford a unique way to investigate certain nuclear properties and mass and excitation regions of the residual nuclei. The importance of heavy ion reactions in studying nuclear surfaces, highly excited nuclear matter, high angular momentum systems, and the transfer of various nuclear clusters have been extensively reviewed by Zucker (1960).

B. Reduced Alpha Widths

One parameter of great interest in describing an excited state of ^{16}O is the reduced alpha width, θ_{α}^{2}. A value of 0 for θ_{α}^{2}

corresponds to a state which in no way looks like a ^{12}C core plus an alpha particle, whereas a level having θ_α^2 of the order of unity can be well described by such a picture. The value of θ_α^2 for a level is also a parameter which influences cross-sections for $\alpha + {}^{12}C$ reactions in the region of that level. In particular, the reduced alpha width of the fourth excited state of $^{16}0$ is of importance to nuclear astrophysicists in the determination of the reaction rate of $^{12}C(\alpha, \gamma)^{16}0$ in the helium burning stage of red giant stars.

Originally, widths were extracted from cross-section measurements involving resonant reactions and the Breit-Wigner formula (1936) of the form

$$\sigma_{if} = \frac{(2\ell + 1)\pi}{k_i^2} \frac{\Gamma_{\lambda i}\Gamma_{\lambda f}}{(E_\lambda - E)^2 + \Gamma_\lambda^2/4} \qquad \text{(I. B. 1)}$$

where $\Gamma_{\lambda i}$ and $\Gamma_{\lambda f}$ refer to the width for decay of the compound state λ into the initial and final states respectively and E_λ and Γ_λ are the energy and total width of the compound state. Then the reduced width $\gamma^2_{\lambda\alpha}$ was defined in terms of the width for decay of a compound nucleus into, for example, an alpha particle and residual nucleus, $\Gamma_{\lambda\alpha}$, by

$$\gamma^2_{\lambda\alpha} = \frac{\Gamma_{\lambda\alpha}}{2k\, P_{\alpha\ell}} \qquad \text{(I. B. 2)}$$

where k is the wave number and $P_{\alpha\ell}$ is the Gamow penetration factor for the alpha particle at the nuclear surface. In this sense $\gamma^2_{\lambda\alpha}$ is a measure of the probability that the state λ has a configuration with an alpha particle at the nuclear surface of the residual nucleus, and the

product of this factor and the penetrability gives the rate of alpha decay of this level. The nature of γ^2 was discussed by Teichmann and Wigner (1952) and by means of the sum rule on γ^2, the dimensionless quantity

$$\theta^2 = \gamma^2 \Big/ \left(\frac{3\hbar^2}{2Ma}\right) \qquad \text{(I. B. 3)}$$

(where M is the reduced mas and a the nuclear radius) was introduced as a convenient measure of how well a compound state looks like a single particle state or, as in our case, an alpha particle state.

For states in which the particles are bound, such a straightforward procedure is impossible. However, single-particle reduced widths, θ_p^2 and θ_n^2, have been derived for (d, n) and (d, p) stripping reactions populating both bound and unbound levels in the residual nucleus, and have been discussed by Macfarlane and French (1960). Here they introduced the term, spectroscopic factor, $\mathcal{S}$, which is the ratio of the measured stripping width to the theoretical single particle width. This definition is equivalent to the dimensionless quantity θ^2 obtained from resonance reactions.

Butler (1957) showed that in general, a stripping cross-section was proportional to the probability density for finding the transferred particle at the surface of the final nucleus. In principle, one could then obtain the standard reduced widths of states in the final nucleus from stripping reactions. However, the uncertainties in the projectile wave function and the fact that the reduced width was evaluated at only a radius equal to r_0 in the Butler theory, allowed only the evaluation of relative reduced widths. The ratios of reduced widths

of two individual levels in a final state nucleus could then be used to determine the magnitude of a bound state reduced width in the following way. If a stripping reaction determined the ratio of relative reduced widths (or spectroscopic factors) to two final states m and n $R = \frac{\theta^2(m)}{\theta^2(n)}$ and the reduced width θ_n^2 for state n was determined independently, then to good approximation $\theta_m^2 = R \cdot \theta_n^2$. In addition, the value of R should be insensitive to the form of direct reaction theory analysis used to obtain it although $\theta^2(m)$ and $\theta^2(n)$ alone may be theory dependent. Therefore, a measurement comparing bound state reduced widths to that of an unbound level whose reduced width is known from a compound nuclear experiment should yield a value for the bound state reduced width. The procedure for such an extraction was reviewed by French (1960).

Since such a procedure for obtaining reduced widths seems relatively successful for single nucleon transfers, it was suggested that if an alpha transfer reaction could be found, it might yield the reduced alpha widths for states stable to alpha emission in nuclei such as ^{16}O. One prerequisite for such a reaction is that one nucleus in the incoming channel must have a relatively high amplitude for containing a loosely bound alpha particle, in the same way that a deuteron is a loosely bound (p + n).

The nucleus ^6Li suggests itself as a good candidate. It may be looked at as an (α + d) with a binding energy of only 1.471 MeV. A reasonable model might be an alpha plus deuteron bound in a state of zero relative orbital momentum with the ^6Li spin 1 due to the

deuteron spin. The validity of this model has been discussed by Tang et al. (1961). With this model, one could then possibly interpret the $^{12}C(^{6}Li, d)^{16}O^{*}$ reaction as an alpha transfer reaction which could measure the reduced alpha width of levels in ^{16}O in the same way that a $^{15}N(d, n)^{16}O^{*}$ reaction measures the reduced proton width of ^{16}O levels. The major uncertainty in such a procedure would be the strength of this reaction mode compared to competing mechanisms. This question is dealt with in Section III on data analysis.

C. Previous $^{6}Li + ^{12}C$ Experiments

The reaction $^{12}C(^{6}Li, d)^{16}O^{*}$ has been studied previously by various experimenters. The first investigations [Blair and Hobbie, (1962) and Bashkin et al. (1963)] observed only the ground state deuterons in the C. M. energy region between 2.0 and 2.7 MeV. The conclusion reached was that the reaction mechanism at this energy was predominantly compound nuclear. Norbeck et al. (1963) surveyed the gamma-rays from the bombardment of ^{12}C by ^{6}Li and concluded that the observed gamma-rays could all be explained by the reactions $^{12}C(^{6}Li, \alpha\gamma)^{14}N$ and $^{12}C(^{6}Li, p\gamma)^{17}O$. Their result implies that these competing exit channels will probably predominate in any $^{6}Li + ^{12}C$ reaction.

The most comprehensive study of the $^{6}Li + ^{12}C$ reaction has recently been carried out by Heikkinen (1966) at C. M. energies between 3.0 and 3.7 MeV, still below the Coulomb barrier (of about 4.5 MeV). At eleven equally spaced bombarding energies he obtained angular distributions for the $^{12}C(^{6}Li, d)^{16}O^{*}$ reaction for all the bound

alpha levels of ^{16}O: the ground state, 6.05 - 6.13 [unresolved], 6.92 and 7.12 MeV levels. The experiment employed a dE/dx - E counter telescope connected to a computer. His conclusion, based on the energy dependence and angular distributions of the excited state deuteron groups, is that the reaction mechanism has a strong direct reaction contribution, whereas the ground state deuterons show a compound nuclear behavior. He suggests that this is due to the favorable penetration factor for the ground state deuterons. The relation between his data and those of this experiment will be discussed in the interpretation of the results in Section III.

The $^{6}Li + ^{12}C$ reaction was studied in a very much higher C.M. energy region by Ollerhead et al. (1964). Their investigation at C.M. energies of 24 and 42 MeV showed that the ^{6}Li breaks up directly into α + d with a cross-section comparable to the geometric size of the nucleus. No deuterons corresponding to the formation of ^{16}O were found. These results, together with the fact that our experiment shows a marked decrease in $^{6}Li(^{12}C, d)^{16}O^{*}$ cross-section with increasing energy, imply that it is quite probable that information concerning states in ^{16}O will become more difficult to extract as the bombarding energy rises very much above the Coulomb barrier.

The inverse reaction $^{16}O(d, ^{6}Li)C^{12}$ was studied by Daehnick and Denes (1964) at a C.M. energy which corresponds to 7.3 MeV in the $^{6}Li(^{12}C, d)^{16}O$ system investigated here. Although the inverse reaction can be related only to the forward reaction leading to the ground state of ^{16}O, the principle of detailed balance has been applied

and we find agreement between the two cross-sections.

In order to investigate this reaction at energies between those of previous measurements, it was necessary to use a ^{12}C beam of energies around 21 MeV. Several attempts to accelerate ^{6}Li beams in the tandem accelerator were unsuccessful, so ^{12}C beams and ^{6}Li targets were used instead. The reaction $^{6}Li(^{12}C, d)^{16}O^{*}$ had several disadvantages compared to $^{12}C(^{6}Li, d)^{16}O^{*}$ for alpha-transfer studies, but remained the only alternative in the absence of a ^{6}Li beam.

The first advantage of a ^{6}Li beam is the ability to probe the very forward C. M. angles that might be favored in an alpha transfer reaction. Due to the geometry of the magnetic spectrometer, the incident carbon beam experiment was limited to C. M. angles which correspond to those greater than $\theta_{LAB} = 20^{o}$ for the corresponding lithium beams. For highly excited states in ^{16}O, this limiting angle was even greater due to the very low energy of the emitted deuteron. In some cases the deuteron energy distribution versus C. M. angle limited measurements to only the backward hemisphere in a C. M. system in which ^{6}Li would be the projectile.

In general, the kinematics would be more favorable if the lighter particle were the projectile. For example, to obtain a C. M. energy of 7 MeV, a 21 MeV ^{12}C beam is necessary while only 10.5 MeV is needed for the ^{6}Li beam. The extreme energies of the deuteron at very forward and very backward angles are shown in Table 1. One can see that the far smaller spread in energies from the $^{12}C(^{6}Li, d)^{16}O^{*}$ reaction, would make less severe demands on the detection system.

Another great difficulty is the fact that lithium foils are not self-supporting so that some other material must be used as a backing. In addition, the reactivity of lithium required preparation of the target in the target chamber, at considerable inconvenience in time. This same property led to time-dependent deterioration of the targets. These are discussed in Section II. C3. On the other hand, self-supporting foils of carbon of accurate thickness and great stability are quite easy to prepare, and may be manufactured prior to beam bombardment.

With these difficulties and the previous experiment in mind, this experiment was initiated in the region high enough above the Coulomb barrier in order to excite alpha unbound levels, but low enough that one might hope to see a major direct reaction contribution. This C. M. energy of about 7 MeV lay in a region between the previous measurements discussed above.

D. Astrophysical Significance of the Reaction $^{12}C(\alpha, \gamma)^{16}O$

Salpeter (1957) estimated the stellar reaction rate for the radiative capture of alpha particles by ^{12}C. The reaction cross section at energies corresponding to effective stellar temperatures is so low, about 10^{-20} barns at 200 keV, that it is not likely to be measured directly in the near future. Some of the difficulties of such an experiment are outlined by Larson (1965) who measured the cross section $^{12}C(\alpha, \gamma)^{16}O$ down to energies where the excitation in ^{16}O corresponds to the 9.58 MeV level. The threshold for $\alpha + {}^{12}C$ occurs at an excitation of 7.162 MeV in ^{16}O and the region of interest in stellar reactions

is only slightly above threshold. The energy level diagram is shown in Figure 1.

The absence of levels in this region excludes the possibility of resonant capture of the alphas. The level at 8.88 has been assigned a spin and parity of 2^-. (For information on all $^{16}0$ levels refer to the tabulation of Ajzenberg-Selove and Lauritsen [1959]). The unnatural parity of this state excludes any measurable resonant alpha capture as both reacting particles have spin and parity of 0^+.

The inability to measure the cross section necessitates the calculation of the non-resonant reaction rate. Such extrapolations below the lowest measured energy are routine. The stellar reaction rate is dependent upon such stellar conditions as density of the reacting nuclei and the temperature, and upon nuclear reaction properties. The standard procedure outlined by Burbidge, Burbidge, Fowler, and Hoyle (1957) is to gather the nuclear parameters and temperature dependent properties into a velocity averaged quantity, $\langle \sigma v \rangle$, which is calculated by integrating the product of the normalized Maxwell-Boltzmann velocity distribution, $\phi_T(v)dv$ at a given temperature T, with the velocity (energy) dependent cross-section times the velocity

$$\langle \sigma v \rangle = \int_0^\infty \phi_T(v)\, \sigma(v) v \, dv \text{ in cm}^3/\text{sec.} \qquad \text{(I. D. 1)}$$

Then, the mean reaction rate, P, is given by

$$P = n_c n_\alpha \langle \sigma v \rangle \text{ reaction/cm}^3\text{sec} \qquad \text{(I. D. 2)}$$

where n_c and n_α are the density of carbon and helium nuclei, respectively, in nuclei/cm^3. All the nuclear physics is contained in the quantity $\langle \sigma v \rangle$ and the rest of the problem is one of astrophysics. We shall concentrate here on the calculation of σ.

In this particular case the presence of a level just below threshold at 7.12 MeV excitation, with the same spin and parity (1^-) as the nearest level (9.58 MeV) above threshold, complicates the calculation of $\langle \sigma v \rangle$. In order to make an estimate of the energy dependence of the cross section, the alpha width for both levels is necessary. In addition, if the alpha width for the 7.12 MeV level is comparable to that for the 9.58 MeV level, then the interference term in the energy region between them may be important and will be either constructive or destructive. Such information is essential in estimating cross-sections.

The $^{12}C(\alpha,\gamma)^{16}O$ reaction must be considered in stellar reactions when the helium burning process, $3\alpha \rightarrow {}^{12}C$ has begun to build up a concentration of ^{12}C. This problem has been reviewed by Salpeter (1957). Due to the low $^{16}O(\alpha, \gamma)^{20}Ne$ non-resonant radiative capture cross section, the alpha burning stages should end with the core containing essentially only a mixture of carbon and oxygen, the relative amounts depending upon the rate of the reaction $^{12}C(\alpha, \gamma)^{16}O$ and the mass of the star. The ratio of carbon to the oxygen at the termination of helium burning in these stars has been calculated by Deinzer and Salpeter (1964) as a function of stellar mass and for reduced alphas widths of the 7.12 MeV level of 0.1, 0.4 and 1.

At the stage where the helium burning takes place, the temperature is slightly above 10^8 ^oK. The star had previously contracted and the release of gravitational energy increased the temperature until the $3\alpha \rightarrow {}^{12}C + Q$ reaction ignited. After the helium is totally consumed, the temperature equilibrium is destroyed and the gravitational collapse of the core resumes. This collapse will continue until the temperature rises to a value where the next nuclear reaction ignites. The temperature will have to rise at least a factor of six in order to begin consuming the carbon in a ${}^{12}C + {}^{12}C$ reaction. Because of the Coulomb barrier, even higher temperatures are necessary to ignite the oxygen. The future course of the star depends upon what temperature equilibrium is established and that in turn depends on its relative oxygen and carbon content when gravitational collapse commences. This problem has been studied by Reeves and Salpeter (1959) and by Reeves (1964), and a recent discussion of the consequences has been summarized by Larson (1965). The major uncertainty in the problem is the ${}^{12}C(\alpha, \gamma){}^{16}O$ reaction rate.

II. EXPERIMENTAL PROCEDURE

A. Experimental Configuration

In this experiment ^{6}Li targets evaporated on 1000 Å Ni foil backings were first bombarded by $^{12}C^{(4+)}$ ions with an energy of 21 MeV, corresponding to C.M. energy of 7 MeV. Angular distributions of the deuterons leading to the ground state and first eight excited states of ^{16}O were measured at this energy and at θ_{LAB} from 0^{o} to 155^{o} where energetically possible. In addition, excitation functions for the third, fourth, and fifth excited states deuterons were taken between 6 and 8 MeV at $\theta_{LAB} = 30^{o}$ and $\theta_{LAB} = 50^{o}$, and angular distributions for these levels were taken at a C.M. energy of 8 MeV. The deuterons were detected by a sixteen counter array in the focal plane of a 61 cm double-focusing magnetic spectrometer. The absolute cross section was obtained by measuring all cross sections relative to that for the third excited state at $\theta_{LAB} = 30^{o}$ and then normalizing this cross-section to the $^{6}Li(p, p)^{6}Li$ elastic scattering previously measured by Harrison and Whitehead (1962). The experimental procedure and data reduction are described in this chapter. The particle detection system and magnetic spectrometer chamber have been described previously (McNally 1966; Groce 1963).

A beam of $^{12}C^{(4+)}$ particles was focused on the target to an elliptical spot with a vertical axis of 1.5 mm and a horizontal axis of 1 mm on the average. The current was typically about 15 nA or $\approx 1 \times 10^{11}$ particles per second. The positive beam produced in the CIT-ONR Tandem Van de Graaff accelerator was derived from an

injected C^- beam out of the negative ion source. The negative beam was produced from methane (CH_4) in the duoplasmatron ion source; this operation is described in Appendix II. The gas pressure in the stripper canal where the negative beam becomes positively charged was about 20% higher than for a proton beam under optimum conditions. The subsequent acceleration and magnetic analysis were carried out in the standard way, but the low intensity of the beam required extra care in steering and focusing procedures. The terminal voltage, V, was determined from the equation $(Q + 1)V = E$, where Q is the charge of the positive beam and E is the desired energy of the beam on target.

A solid state detector mounted in the target chamber served as a monitor counter (see Fig. 2). It subtended a solid angle of 5×10^{-4} steradians and was normally kept at an angle of 135° with respect to the beam direction. By noting the position, width, and the number of counts under the elastic peak from the scattering reaction $^{58}Ni(^{12}C, ^{12}C)^{58}Ni$, it was possible to detect changes in the beam position, the foil position and condition, and the current integration accuracy for each run.

B. Lithium Targets

The targets were prepared in the following way: A 1000 Å thick nickel foil was mounted over a circular hole of 10 mm diameter on a stainless steel rectangular target holder 15 mm by 25 mm and thickness about 1 mm. This target was then mounted on the end of the target rod in the spectrometer chamber. After the beam was

optimized and focused with the aid of a quartz also mounted on the target rod, the height of the target was adjusted so that the beam struck the center of the nickel covered opening as closely as possible. This target position, with the foil perpendicular to the beam direction, could then be accurately reset after the target had been lowered for the ^{6}Li evaporation. First, however, an accurate determination of the energy of ^{12}C particles elastically scattered from the nickel was made in the spectrometer at $\theta_{LAB} = 30^{o}$, for use as a reference energy.

The target rod was then lowered until the nickel foil was centrally located in the 'accepting' area of the furnace (see Fig. 3). At this point the foil was about 15 cm from the tantalum boat which contained several slivers (each approximately 10 mg) of 97.6% pure ^{6}Li (obtained from the Isotope Branch of the Oak Ridge National Labs.). This 'donor' area of the furnace was not only far removed from the foil but about midway between them was a collimating aperture about 1.5 cm in diameter. With this geometry uniform deposition of Li on the target was possible. It was also possible to slide a shield up to prevent deposition on the back of the target.

After a visible amount of ^{6}Li was condensed on the nickel foil the target was returned to the original scattering position with the Li surface facing the beam and the energy of the carbon scattered from Ni was remeasured in the spectrometer.

We obtained an energy loss value for 21 MeV ^{12}C beams from the data of Demirlioglu and Whaling (1962) and the $\langle Z^2 \rangle$ from Appendix I, in order to determine the thickness of the ^{6}Li layer by

the change in energy of the scattered ^{12}C. This entire procedure was repeated, when necessary, several times until the thickness of the ^{6}Li layer corresponded to a total energy loss by the 21 MeV ^{12}C beam of between 100 and 140 keV. A typical example of the scattered particle spectrum is shown in Figure 4. However, because impurities with atomic number higher than three were present in varying and unknown concentrations, this approach is not a very precise method for measuring the amount of ^{6}Li present in the target.

The ^{6}Li thickness determination was made by comparison with a known cross section. For each target, all cross sections were measured relative to that for the 6.92 MeV level at $\theta_{LAB} = 30^{0}$. The absolute normalization of this cross section and the effects of target deterioration are discussed in later sections.

C. Cross-Section Measurement

C.1. Deuteron Detection

The deuterons were detected by an array of sixteen solid-state Au-Si surface barrier detectors located in the focal plane of the 61 cm double-focusing magnetic spectrometer. The operation of this spectrometer is described by D. E. Groce (1963). The general approach to the analysis of data obtained with the array is to present the data from each detector at the equivalent magnetic field as if all detectors were at the same radius of curvature, whereas the detectors really accept particles that traverse different orbits in the magnetic field of the spectrometer. This frequency for each detector was determined to be a factor times the frequency for detector eight located on the

central ray, the same position used for single detector operation. These frequency factors are listed in Table 2 and are described by J. H. McNally (1966) within a very good general discussion of the array design and operation.

The output of each detector was analyzed into sixty-four channels of energy in the Nuclear Data Pulse Height Analyzer. Measurements of deuteron energies could be taken from about 1.1 MeV to 13 MeV. The low energy limit was due to the pulse height threshold in routing the signal from each detector to its proper 64 channel address in the memory.

The spectrometer field for each deuteron energy was determined using the fluxmeter constant with its slight field dependence as determined by McNally (1966). In all cases the deuteron peak was found to be within 30 keV of the value predicted by kinematics, ^{16}O excitation, and energy loss.

In order to separate deuterons from any other particles of the same magnetic rigidity, the following procedure was followed. A complete set of energy versus pulse height calibrations of the array were taken by scattering deuterons from a thick target. These pulse height calibrations in each of the sixteen detectors for 1-10 MeV deuterons in steps of 0.5 MeV were measured as a function of the attenuator setting at the pulse input into the Nuclear Data Analyzer. At the same time the minimum detector bias necessary to stop deuterons in each counter was determined at each energy. These calibrations made it possible to separate and identify the deuteron

group in the energy spectrum of each counter.

Heavy ions were stopped in aluminum foils of 1.7 to 6.8 mg/cm^2, which could be placed just in front of the counter array. The energy loss of deuterons in this foil was computed and taken into account in the group identification. At angles $\theta_{LAB} > 90^{\circ}$ the flux of heavy ions was less intense and in the forward hemisphere was probably due to recoil impurities from the target which presented a broad spectrum of energies and magnetic rigidities.

Alpha particles at a given magnetic field setting have twice the energy of the deuterons, but approximately four times the value of dE/dx. They are easily separated by their energy from the deuterons.

The energy of protons at a given field setting was likewise twice that of deuterons. However, in the case of protons the dE/dx was sufficiently low that the protons were often not stopped in the detectors and therefore did not deposit their full energy. Since the maximum energy of a proton that could be stopped in all counters was 7 MeV at the maximum bias of 60 volts, deuterons of energy less than 3.5 MeV could be separated from protons by running the bias at the full 60 volts. For deuterons with energy above 3.5 MeV the bias was always set to the minimum value which just stopped the deuterons. This then permits so little loss of energy in the protons that their energy pulses always fell far below those of the deuterons.

The majority of the particles other than deuterons were the heavy ions, and alphas and protons from the highly exoergic reactions

$^{6}Li(^{12}C, \alpha)^{14}N$ and $^{6}Li(^{12}C, p)^{17}O$. The proper adjustment of input gain, bias, and degrading foil thickness allowed the unique determination of deuteron yields at most desired energies and angles. Examples of deuteron spectra are shown in Figures 7 and 8.

C.2. Measurements Using the 16-Detector Array

The total line intensity, I, that one measures with the 16-counter array must be extracted in a somewhat less direct manner than with the single counter in the focal plane of the spectrometer. This has been discussed previously by McNally (1966). Of course, if there were a single detector which had a large enough acceptance in the focal plane so that the entire line fell completely within the detector, the intensity would simply be the total number of counts. Similarly, if the array had no dead-space between the counters, the total line intensity would be equal to the sum of the counts in the appropriate detectors.

In the case of this 16-detector array, the dead space is of the order of one-half the area in the focal plane. Therefore one can approximate the intensity fairly well by taking a second measurement which shifts the frequency of each detector approximately half the frequency interval between the detectors, thereby counting in the area covered by "dead space" in the first measurement. Then the sum of the counts in the two runs multiplied by the ratio of this actual dead space fraction to one-half will give a good value or the total intensity.

In order to arrive at a more accurate value for the intensity, the non-uniformity of the detectors must be taken into consideration.

The approach we used is as follows, described by McNally (1966).

Suppose measurements are taken with a single detector located on the central ray in the focal plane and the frequency f_8 corresponding to the field is measured for this detector. Then a series of measurements over the breadth of the line will yield a number of counts N(f) as a function of frequency.

The acceptance in the frequency, Δf, is linearly related to the frequency f by the constant R

$$\Delta f = Rf \qquad \text{(II. C. 2. 1)}$$

and the differential number of counts n(f) per unit frequency is given

$$n(f) = \frac{N(f)}{\Delta f} = \frac{N(f)}{Rf} \qquad \text{(II. C. 2. 2)}$$

Thus the total yield is given by the expression

$$I = \int n(f)df = \frac{1}{R} \int \frac{N(f)}{f} df \qquad \text{(II. C. 2. 3)}$$

integrated over the region of interest. This is the standard method outlined by Snyder et al. (1950).

The normal method for using the sixteen detector array is to convert the counts in each detector to the number of counts that would have been observed if the measurement were taken at the corresponding frequency by detector 8. This conversion procedure, described by McNally (1966), is made with the use of a smooth spectrum of particles scattered from a thick target. Correction

factors are chosen so that each detector yield, when corrected, falls on the smooth spectrum measured by detector 8. In this way one arrives at a set of sixteen correction factors, k_i, which must multiply the number M_i of raw counts in each counter, to convert the array data to equivalent single-counter measurements for evaluating the intensity.

The yields for the various levels were then calculated using the yield correction factors listed in Table 2 for angles $\Delta\phi < 3^{\circ}$. These values were obtained by averaging results of the data kindly supplied to us by D. C. Hensley and Professor W. Whaling. The uncertainty associated with the use of these correction factors is less than 5%.

C. 3. General Data Reduction

The data had to be further analyzed in order to arrive at meaningful cross-sections. All yields were measured relative to the 6.92 MeV level deuteron yield at $\theta_{LAB} = 30^{\circ}$ and then later a normalization was performed to obtain absolute cross-sections.

Frequent measurements of the 6.92 MeV level yield were made as a basis for normalization of the data taken from the more than twenty targets necessary in completing the experiment. As a rule the targets were usable for about forty-eight hours of continuous beam bombardment. At intervals of about twelve to sixteen hours the 6.92 MeV level calibration runs were taken in order to monitor the change in thickness of the targets. It was possible to measure the 7.12 MeV level at the same time and in this way the "tail" effect was

monitored also.

The "tail" effect describes the development of a small satellite line or tail on the low energy side of the deuteron line which may be seen for example in Figure 7 near 47 MHz. This effect occurred simultaneously with the time- or bombardment-dependent depletion of the ^{6}Li content of the evaporated side of the target. In a single line, such as the ground state, this could be seen by a slow decrease in counts in the main peak and an increase in deuteron counts in the counters immediately below the main peak. With many foils the total number of counts in the peak plus tail was a constant, but this was not always true. This effect may have been caused by diffusion of lithium into the Ni-foil and the eventual formation of a very thin Li-layer on the back side of the foil. In the case of the 6.92 - 7.12 MeV lines at $\theta_{LAB} = 30^{o}$, the higher group tail fell under the main peak of the lower line. The frequent checks on the shape and intensity of these two lines permitted a correction for these effects described here.

Two factors, the target thickness factor, F_1, and the tail factor F_2 were plotted as a function of time as shown in a typical example, Figures 5 and 6. Their definition is as follows.

The target thickness factor, F_1, is the number by which one multiplies the yield for a given line in order to get the yield which would have been measured with a stable target. The time-dependent function, F_1, was determined by fitting the values of the yield leading to the 6.92 MeV level calibration points taken at various time intervals.

The form of this function was either linear with time or asymptotically approaching some constant factor (see Figs. 5 and 6). All targets fell into one of these two categories of behavior, but one could not determine which until the 6.92 MeV level calibration measurements were made. The uncertainties associated with the use of F_1 were consistent with the quality of the fit and usually were within ± 25% of the actual correction made. For example, if a target thickness factor, $F_1 = 1.08$ was applied to a raw yield of 100 counts and the uncertainty associated with F_1 was ± 25%, then it would be necessary to add 8 ± 2 counts to get the corrected yield.

The tail factor, F_2, was determined by monitoring the ratio, R_t, of the yield of deuterons from the 7.12 MeV level to those from the 6.92 MeV. The expected ratio, $R_0 = 0.235$ was determined from the value achieved with the freshly evaporated targets, extrapolated to the time when no beam had struck the target. There was agreement within 7% for this value for all targets. In addition, the following independent check was performed. The lithium layer was rotated to 180° from the beam direction and the beam energy was raised to compensate for the beam energy loss in the Ni backing. Under these circumstances an independent determination of the value of R_0 is possible. This value fell within 5% of the other determination of R.

The tail factor, F_2, as a function of time was determined by fitting the values $(R_t - R_0)$ measured at various time intervals. The qualitative time-dependent behavior of F_2 was similar to that

for F_1. In general, an uncertainty of about 30% was assigned to the use of this correction factor. The value of F_2 determined in this way agreed with the visible tail located below single deuteron lines, but the generally lower yield of the well separated lines makes it impractical to use them to determine F_2 within 30% accuracy.

When it was determined that the tail of a line A fell within another line B, then the target factor was applied in the following way. A number of counts $N_T = (F_2 \cdot A)$ was subtracted from the number of counts N_B in line B. The uncertainty in this corrected number of counts, $N_B' = N_B - N_T$ was the quadratic sum of the statistical error in N_B plus the uncertainty in the subtracted tail. In addition, this number still had to be corrected by the target thickness factor, F_1. In some cases almost the entire uncertainty in the measured yield was due to tail factor corrections. In the worst cases, where the yield for the 6.92 MeV level deuterons was several times that for the 7.12 MeV level deuterons, the tail corrections amounted to 50% and introduced uncertainties of the order of 20%.

The cross section may be obtained from the yield if the total integrated beam, target thickness, and solid angle are known. The problems of beam current integration are discussed in Appendix I and it is sufficient here to know that 1 microcoulomb of C^{4+} beam equals 1.56×10^{12} particles. The solid angle is determined by the $\Delta\theta$ and $\Delta\phi$ acceptance slit opening of the spectrometer and can be calculated from these settings using data tabulated by Groce (1963). Both of these measurable quantities can be determined to within an

accuracy of a few percent. On the other hand, the target thickness cannot be measured directly and is difficult to determine within a factor of two. This problem has been discussed in Section II. B. If the evaporated layer were pure ^{6}Li a measurement of the energy loss would be sufficient to determine the target thickness. For example, a beam energy loss of 100 keV in traversing this layer would correspond to 2.73×10^{18} atoms per square centimeter.

If we simply set the target thickness equal to $A \times 10^{18}$ atoms/cm^2 we can determine the cross section in terms of A in the following way. Consider a run in which B microcoulombs of beam equal to $B \times 1.56 \times 10^{12}$ particles have passed through the target producing a yield of N counts. The differential cross section in cm^2 in the lab system, if the solid angular aperture is equal to $d\Omega$ steradians, is then given by

$$\left(\frac{d\sigma}{d\Omega}\right)_{LAB} = \frac{N}{(B \times 1.56 \times 10^{12})(A \times 10^{18})(d\Omega)} \qquad \text{(II. C. 3. 1)}$$

Of course, in order to get C. M. cross sections it was necessary to convert all values to unit solid angle in the C. M. system by multiplying by the expression known as the C. M. factor, F_{CM}, equal to

$$\frac{d\Omega_{LAB}}{d\Omega_{CM}} = \left(\frac{\sin\theta_{LAB}}{\sin\theta_{C.M.}}\right)^3 \left(1 + \left[\frac{M_1 M_3}{M_2 M_4}(1 + Q/E_1)(1 + M_1/M_2)\right]^{\frac{1}{2}} \cos\theta_{CM}\right) \qquad \text{(II. C. 3. 2)}$$

and dividing by $d\Omega_{LAB}$ (Evans, 1955).

Even without knowledge of A, if two measurements are taken on the same target, then the ratio of these cross sections can be determined within the accuracy of the other measurable quantities. For example, if two yields, N_1 and N_2 are obtained with the same solid angle opening, $d\Omega$, and the same total integrated beam, B μC, then the ratio of their cross sections is given by

$$\left(\frac{d\Omega}{d\Omega}\right)_1 \Big/ \left(\frac{d\Omega}{d\Omega}\right)_2 = \left(\frac{N_1}{N_2}\right) \times \left(\frac{F_{CM(1)}}{F_{CM(2)}}\right) \qquad \text{(II. C. 3. 3)}$$

In this way all cross sections were measured in a ratio to that of the 6.92 at 30°, whose absolute cross section was determined later as discussed in Section II. C. 4.

There were several special cases in evaluating the cross section. Due to the large natural width for the 9.58 MeV level and the presence of nearby and overlapping levels, the total yield was obtained from only a certain region near the center of this line. (The procedure used in obtaining this total yield for the 9.58 MeV level is discussed in Appendix III).

In the case of the highly excited states above the 7.12 MeV level there was a broad background of deuterons (See Figs. 7 and 8). In this region it is energetically possible for the ^{6}Li to dissociate directly into α + d. Also, at these lower deuteron energies one might expect a greater contribution from target impurities. At any rate it was necessary to subtract a background determined from the region at either side of the line in order to obtain a yield for these

higher levels. This background subtraction averaging about 30% added a considerable contribution to the uncertainties in the cross sections, in the worst cases about 20%.

The 6.06 - 6.14 MeV doublet presented one further difficulty. At forward angles the lines were not totally resolved. We found that it was possible to improve the resolution to the point that with an assumed line shape we could estimate the contribution of each line to the total. The widths of the lines, which were due entirely to the experimental resolution and are expected to be equal, and the positions are known to within a few keV from the kinematics and spectrometer calibration. The line width was due to target thickness, beam spread, and angular acceptance. Under these assumptions, separations were made such as that shown in Figure 9. The uncertainty in separation was estimated from the fit and thus increased the measured uncertainty in the cross sections for these two levels.

As a result of this procedure, the deuteron angular distributions of the ground state, and first eight states of ^{16}O, at E_{CM} = 7 MeV, the deuteron angular distribution of the third, fourth, and fifth excited states at 8 MeV, and the excitation functions at θ_{LAB} = 30° and θ_{LAB} = 50° for these same levels were measured relative to the cross section of the 6.92 MeV level at θ_{LAB} = 30° and E_{CM} = 7 MeV.

C.4 Normalization of the Cross Sections

It remained to measure the cross section for the 6.92

MeV level at $\theta_{LAB} = 30^{o}$ and $E_{CM} = 7$ MeV, in order to achieve an absolute normalization and get the total cross section for all the relative cross sections measured. This was accomplished by re-measuring the elastic scattering of protons, $^{6}Li(p, p)^{6}Li$, under the same circumstances as the calibration point was measured. The scattering of 8 MeV protons was chosen (Harrison and Whitehead, 1962).

The ratios of $d\sigma/d\Omega_p$ to $d\sigma/d\Omega$ (6.92 at $\theta_{LAB} = 30^{o}$) were calculated using Equation (II. C. 3. 1) and the values are listed in Table 3.

Using the values of σ_p measured by Harrison, we obtained three separate values for $d\sigma/d\Omega$ (6.92). These were then averaged with a weight equal to the inverse square of the uncertainty in each ratio, to obtain a single value of this cross section equal to 1.90 ± 0.05 mb/st. The second column in Table 3 shows the values of $d\sigma/d\Omega_p$ measured by Harrison and Whitehead multiplied by the factor 1.19 ± 0.06. This renormalization of their data was due to a later absolute calibration of the total cross section discussed by Harrison (1966). The last column shows the values obtained for $d\sigma/d\Omega$ (6.92) from the measured ratios. The agreement is well within the experimental errors.

Although this procedure did not necessitate the measurement of the actual target thickness, Figure 10 which shows the cross sections calculated from the thickness implied by the energy loss measurements, points out the inaccuracy of the dE/dx method. It

would be safe to say that on the average an overestimate of the lithium content by a factor of two would occur in the dE/dx method.

Due to the uncertainties in the original measurements of Harrison, in the later renormalizations, and in the measurement of the relative cross sections, as well as possible systematic errors introduced by the use of a different beam and possibly different beam spot position, the total uncertainty in the absolute cross section measurement was estimated to be 20%.

The results of the angular distribution at 7 MeV are shown in Figures 11, 12, and 13 and Tables 4, 5, and 6, those at 8 MeV are shown in Figure 14 and Table 7, and the excitation functions are given in Figure 15 and Table 8. The solid lines in the angular distributions are Legendre polynomial fits.

III. INTERPRETATION OF RESULTS

A. Legendre Polynomial Expansions

The Legendre polynomials, $P_L(\cos\theta)$, are a complete orthogonal set of functions covering the polar angles from 0° to 180°. Therefore, it is obvious that one should be able to fit any angular distribution as a sum of these polynomials of the form

$$d\sigma/d\Omega(\theta) = \sum_{L=0}^{L_{max}} A_L P_L(\cos\theta) \qquad \text{(III.A.1)}$$

However, if the fit is to have any meaning the χ^2 distribution should be reasonable.

The total value of the quantity

$$\chi^2 = \sum_{\substack{\text{All data}\\ \text{Points}}} \left(\frac{\text{Experimental Value - Calculated Value}}{\text{Experimental Error}}\right)^2$$

should be approximately equal to one less than the number of degrees of freedom, which is the number of data points minus the number of free parameters used in the polynomial fit. The fitting procedure used was suggested by Harrison (1966), and follows the genera approach of Seeger (1963), Evans (1955), and Mathews and Walker (1964).

The Legendre polynomial fits have been a very powerful analytical tool in many cases with one or at most a few levels in the compound nucleus contributing to the reaction mechanism. This is

discussed by many authors, e.g., see Blatt and Weisskopf (1952).

One especially important result from a Legendre polynomial fitting procedure is the value of the first coefficient, A_0. The total cross section is simply $4\pi A_0$ due to the orthogonality of the Legendre polynomials, and the fact that the expression for the total cross section is given by

$$\sigma_{tot} = \int_0^{\pi} \frac{d\sigma}{d\Omega} \times 2\pi \, d(\cos\theta) = 2\pi \sum_{L=0}^{L_{max}} A_L \int_0^{\pi} P_L(\cos\theta) \, d(\cos\theta) \qquad \text{(III. A. 3)}$$

Since the integral is zero except for the L = 0 term, we have

$$\sigma_{tot} = 4\pi A_0 \qquad \text{(III. A. 4)}$$

After a sufficient number of polynomials have been used to insure a reasonable fit to the data, A_0 should approach a constant value to within its internal uncertainty. This convergence is another test of the goodness of the fit. The total cross sections were calculated from $4\pi A_0$ and these cross sections and the ratios, A_L/A_0, of the higher order coefficients are listed in Table 9. The fits have been plotted with the data points discussed in the previous section, in Figures 11-14.

The uncertainties in the total cross section have been calculated by using the errors of the coefficients, A_0 determined in the fitting procedure, and by estimating the errors due to the incompleteness of the angular distributions. These are also stated in Tables

9 and 13 and are used in the later theoretical analysis of the data.

If a nuclear reaction proceeds through a state of definite parity in the compound nucleus, the angular distribution should be symmetric about $\theta_{CM} = 90^{o}$ (see, for example, Blatt and Weisskopf, 1952). If there are several states of opposite parity in the intermediate state in the compound nucleus, interference effects destroy the symmetry about 90^{o}. However, the net effect of interference decreases as the number of overlapping levels increase and the cross section again approaches symmetry about 90^{o}. This has been extensively discussed in a review by Ericson (1960).

It might therefore be possible to gain insight into the reaction mechanism by examining the coefficients of the odd Legendre polynomials. If the reaction proceeds through the statistical compound nucleus ^{18}F, then the energy average of these coefficients should be zero. In fact, since the target thickness of about 40 - 60 keV in the C. M. system is the main contribution to the beam energy spread in the experiment, the following argument may be made. With such an energy spread we are averaging over many levels, and the odd coefficients themselves should not be significantly different from zero. However, in both this experiment and in that of Heikkinen, many of the odd coefficients were non-zero. This alone is not a compelling argument against statistical compound nuclear contributions to the reaction, but does help confirm other indications discussed later.

The main result of this analysis has been a determination

of the total cross sections. The other coefficients in the expansion may or may not have significance but are presented as an indication of the anisotropy.

B. The Reaction Mechanisms

B.1. General Considerations

A brief inspection of $(d\sigma/d\Omega)_{exp}$ leaves little hope that the reaction takes place through only one reaction mechanism. There is evidence that both direction reaction and compound nucleus formation occurs, and our problem is then to separate these processes.

The formation of the final state in ^{16}O at 8.88 MeV with a spin and parity of 2^- would seem to require a compound nuclear contribution to the reaction mechanism. This level could not be formed from the direct capture of an alpha particle by a ^{12}C nucleus as its unnatural parity $(-)^{\ell+1}$ and the 0^+ spins and parity of both ^{12}C and ^4He are not consistent with the conservation of angular momentum and parity.

On the other hand, the relatively large measured total cross section, σ_{exp}, for the highly excited levels known to have large reduced alpha widths, is a strong indication that there is also a sizeable direct reaction contribution present.

The problem is therefore to separate the two mechanisms and assign the relative strength of each in a quantitative manner. It is important to bear in mind that both descriptions of nuclear processes are models which are most successful when they truly dominate the reaction. Therefore, there is a risk involved when a reaction seems

to be described by a comparable amount of each mechanism that neither model is valid. However, an attempt to divide the total cross section according to the two mechanisms seems the only way to estimate the size of the direct reaction.

A general discussion of the two mechanisms follow, in order that the methods used in the procedure of separation are better understood in a reasonable perspective.

B.2. Compound Nuclear Contribution

The formation of an intermediate compound nucleus which subsequently decays was first suggested by Bohr (1936) as a reaction mechanism and has been a valid model for many reactions. In the case of a single level resonance, spin and parity are well defined quantities and can often be determined for the compound level from considerations such as the resonance shape and angular distributions. If several levels in the compound nucleus contribute, the reaction is more difficult to analyze. However, if a large number of levels overlap, which is the case at higher excitations where the level density and level width, Γ, increase, one can make use of a statistical approach in determining average values for cross sections (Weisskopf 1937). This approach which completely neglects the structure in the cross section due to the existence of compound levels is known as the "Continuum Theory" and has been well described by Blatt and Weisskopf (1952) and further studies based on this model were made by Wolfenstein (1951) and Hauser and Feshbach (1952). The Hauser-Feshbach calculation of statistical compound nuclear cross sections

is widely used today and there exists a Fortran IV computer code ABACUS, written by Auerbach (1964), which is capable of performing Hauser-Feshbach calculations. In the Hauser-Feshbach cross section calculations it is assumed that the density of compound levels is sufficiently great that all incoming waves that penetrate the nuclear surface are absorbed into the compound nucleus. These levels then decay into many outgoing channels, and there are so many levels contributing to each decay channel that the contribution of any one is small compared to the total. Since the phase of each contribution is expected to be random, one may neglect all cross terms and assume each individual process will add incoherently to the others.

It is also assumed that inside the nuclear surface all deuteron decay channels were formed on the average with an equal probability due to the large number of such channels, and that only the transmission coefficients of these outgoing channels determined their relative magnitudes. All other decay channels were ignored. The total cross sections were obtained by a normalization discussed in Section III. C.

These assumptions, which are standard to Hauser-Feshbach calculations and continuum theory, permit us to compute the pure statistical compound nuclear cross sections for each level by the following expression

(III. B. 2. 1)

$$\left(\frac{d\sigma}{d\Omega}\right)_{H.F.} = A(E) \sum_{L=0}^{L_{MAX}} \sum_{M=-L}^{L} C_{LM} \left| Y_L^M(\theta, \phi) \right|^2$$

where A(E) is the normalization factor, and

$$C_{LM} = \sum_{J} \sum_{\ell} \sum_{J_2} \sum_{M_d} \sum_{M_L} |(\ell, 1, 0, M_{Li} | \ell, 1, J, M_{Li})|^2 (2\ell + 1) \times T_{\ell}^{IN}(E)$$

$$\times T_{\ell}^{OUT}(E') \times |(L, j_2, M, M_{Li} - M \,|\, L, j_2, J, M_{Li})|^2$$

$$\times |(S, 1, M_{Li} - M - M_d, M_d \,|\, S, 1, J_2, M_{Li} - M)|^2$$

in which

ℓ = orbital angular momentum of the incoming ^{6}Li and ^{12}C

L = orbital angular momentum of the outgoing d and ^{16}O

M = projection of L along the beam axis

J = angular momentum of the state in the compound nucleus

S = spin of the ^{16}O final state

M_d = spin projection of the spin 1 deuteron along the beam axis

M_{Li} = spin projection of the spin 1 ^{6}Li along the beam axis

J_2 = channel spin of the outgoing channel

$T_{\ell}^{IN}(E)$ = transmission coefficient of the incoming wave at C. M. energy E, calculated by ABACUS. (Table 10)

$T_{\ell}^{OUT}(E')$ = transmission coefficient of the outgoing L wave at C. M. energy corresponding to the proper excitation energy of the ^{16}O level in question, calculated by ABACUS. (Tables 11 and 12.)

These sums are carried out in such a way as to insure conservation of angular momentum and parity. Our use of this

method is discussed in Section III. C.

Another approach to the problem of reactions proceeding through the statistical region of the compound nucleus has been extensively explored and reviewed by Ericson (1960; 1963). Here the emphasis is on the statistical properties of the levels in the compound nucleus, such as their average width and level density in terms of various models. In principle, it might be possible to isolate the contribution of many overlapping compound nuclear levels to the reaction mechanism in a very high resolution ($\Delta E \ll \Gamma$) experiment and determine the direct interaction contribution.

In this experiment the excitation functions (Fig. 15) show no sharp resonance behavior. The excitation energy in the compound nucleus ^{18}F is above 20 MeV where in this odd-odd nucleus there are many overlapping levels. Due largely to the target thickness for ^{12}C ions the incident energy spread was of the order of 60 keV. Since this energy spread is approximately equal to the line widths (also of the order of 50-100 keV which can be estimated (Bohr and Wheeler, 1939), the Ericson fluctuations will be washed out. In turn this implies that the predictions of the average values of cross sections from the over-all statistical theory should be reasonably valid. Although a high resolution experiment which permits fluctuation analysis might be preferable, it would be out of the question with the present beam and target conditions and the rather low cross sections.

B. 3. Direct Reaction Contribution

The major distinction of a direct reaction is the absence

of an intermediate system. The time scale of such a reaction is very short, comparable to the time it would take the projectile to traverse the target nucleus, whereas, the lifetime of a compound nucleus is long compared to this time. A number of reactions fit into this category, such as some inelastic scattering, knock-out, pick-up, and stripping reactions. An extensive discussion of direct reactions may be found in Tobocman (1961). Although in principle all of these direct reactions might be possible in the $^{6}Li + {}^{12}C$ system, we are most interested in the particular "stripping" reaction, the alpha transfer. The heavy particle stripping reaction would require the pick-up of a ^{10}B from the ^{12}C by a ^{6}Li, and it would be expected that this process would be less likely than the alpha transfer, to the same extent that a description of ^{12}C in terms of $^{10}B + d$ is less likely than the description of ^{6}Li as $^{4}He + d$. Therefore, we shall assume that the only direct reaction occurring is the alpha transfer reaction ($^{6}Li, d$), and for simplicity, we shall refer to the ^{6}Li as the projectile in the C.M. system.

A standard method for analyzing such a stripping reaction as this one is to break the system up into 3 indivisible particles, in our case an alpha (α), a deuteron (d) and a ^{12}C nucleus (C). Then the reaction can be written as

$$(d + \alpha) + {}^{12}C \rightarrow d + (\alpha + {}^{12}C) \qquad \text{(III. B. 3. 1)}$$

For this system the Hamiltonian can be written both as

$$H = T_{^6Li\,^{12}C} + T_{(\alpha + d)} + V_{C\alpha} + V_{Cd} + V_{\alpha d}(\text{initial system}) \quad \text{(III. B. 3. 2)}$$

or as,

$$H = T_{d0} + T_{\alpha + C^{12}} + V_{\alpha d} + V_{C\alpha} + V_{Cd}(\text{final system}) \quad \text{(III. B. 3. 3)}$$

At this point in the analysis, however, there are several paths that one may choose to approximate the transition amplitude and the cross section. The basic idea used is the application of a Born approximation through perturbation theory. One chooses an initial state ϕ_i and a final state ϕ_f which are eigenstates of a convenient Hamiltonian, H_o which approximates the real Hamiltonian for the complete system. The remaining part of the Hamiltonian, V, is then the perturbing potential whose matrix element determines the transition probability from the initial to the final state. Therefore, if the initial state is denoted by channel A and the wave number of the incoming waves by K_A and reduced mass by M_A and the final state B has outgoing waves with wave number K_B and reduced mas M_B, then the cross section is

$$\frac{d\sigma}{d\Omega}(A, B) = \frac{M_A M_B}{(2\pi\hbar^2)^2} \left|\frac{K_B}{K_A}\right| \left| \langle \phi_f(K_B) | V | \phi_i(K_A) \rangle \right|^2 \quad \text{(III. B. 3. 4)}$$

An early evaluation of the stripping cross section approximated the initial and final states by plane waves (PWBA). This method was introduced by and then later reviewed by Butler (1957).

In this case, the initial Hamiltonian, H_{oi}, and final Hamiltonian, H_{of}, are taken to be

$$H_{oi} = T_{LiC} + (T_{\alpha d} + V_{\alpha d}) \qquad \text{(III. B. 3. 5)}$$

and

$$H_{of} = T_{0d} + (T_{C\alpha} + V_{C\alpha}) \, . \qquad \text{(III. B. 3. 6)}$$

The initial and final wave functions that are eigenstates of these Hamiltonians are

$$\phi_i = e^{iK_{LiC} \cdot r_{LiC}} \phi_{Li} \qquad \text{(III. B. 3. 7)}$$

$$\phi_f = e^{iK_{0d} \cdot r_{0d}} \phi_0 \qquad \text{(III. B. 3. 8)}$$

where ϕ_{Li} and ϕ_0 are the internal wave functions of the ^{6}Li and ^{16}O respectively, and the plane wave factors are the free particle functions of the incoming and outgoing nuclei. With the use of these approximations, an expression of ϕ_{Li} and ϕ_0 in terms of ϕ_C, ϕ_α, and ϕ_d, and some tedious but straightforward algebra, one can arrive at an expansion for the cross section. Good agreement with experimental angular distributions has been achieved in many cases by using such calculated expressions for (d, p) and (d, n) stripping reactions. The PWBA method has been valuable and easy to use, because the final expressions consist entirely of known tabulated functions, and can be evaluated without the need for high-speed digital computers.

A recent, quite successful approach has been that introduced in a series of papers by Morinigo (1964, 1965). In this method the Hamiltonians in the initial and final states include the Coulomb

potentials and therefore the plane waves in ϕ_i and ϕ_f are replaced by the Coulomb wave functions which are known and can be calculated from hypergeometric functions. This Coulomb wave Born approximation (CWBA) has been successful in fitting angular distributions for stripping reactions below the Coulomb barrier, as it takes into account the Coulomb effects previously ignored.

Another method is the distorted wave Born approximation (DWBA) whose region of validity is not limited to below the Coulomb barrier, and which would be more appropriate to the energy region where this experiment has been carried out. This method includes the optical model potential responsible for elastic scattering within the Hamiltonians H_i and H_f. The optical model parameters are determined from the data of elastic scattering experiments, and from these the distortions in the incoming and outgoing waves are calculated. In this way the calculated ϕ_i and ϕ_f more truly represent the relative motion factors of the initial and final wave functions. However, such a calculation must necessarily be carried out on a high-speed digital computer and there must be additional information concerning the elastic scattering in both the incoming and outgoing channels. Fortunately a program has been written for the IBM-7094 computer which can do such calculations.

This code, TSALLY, is accompanied by a discussion (Bassel, Drisko, and Satchler, 1962) which describes the calculation of DWBA cross sections in great detail. If one has an abundance of data from a predominantly direct reaction, then the DWBA approach

is the most reasonable way to analyze the data. However, in our experiment we know the orbital angular momenta of the states involved and in this case the simplicity of the PWBA method justifies its use over that of the more complicated DWBA.

One of the biggest difficulties in the use of these methods to extract reduced widths has been the over-all normalization of the total calculated cross sections. This arises from a number of causes such as the form taken for bound state wave functions and the penetrability of incoming and outgoing waves. However, if an unbound level is also measured whose reduced width is known from a resonance reaction, then the relative cross sections can give the relative reduced widths and are quite independent of the type of Born approximation used. French (1960) has discussed this problem and the results of his general approach for the extraction of reduced widths using PWBA are followed here.

The final expression relating the cross section for an alpha transfer reaction to the reduced alpha width is a modification of equation (A17) in French for deuteron stripping. When allowance is made for the fact that the incoming particle is a bound state (α + d) rather than a bound state (p + n), and all the numerical expressions are gathered into one constant, U (which must be renormalized at a later step in any case), the PWBA expression relating the cross section and the reduced alpha width θ_α^2 becomes

$$\left(\frac{d\sigma}{d\Omega}\right)_{PWBA} = U\left(\frac{E_A}{E_B}\right)^{\frac{1}{2}} (2S + 1)\theta_\alpha{}^2 \sigma_T{}^\ell(x, y) \qquad \text{(III. B. 3. 9)}$$

and where E_A is the incoming ^{6}Li energy relative to the ^{12}C at rest, E_B is the outgoing deuteron energy relative to the ^{16}0 at rest, and S is the spin of the final state in ^{16}0. The factor $\sigma_T{}^\ell(x, y)$ is a function of the incoming and outgoing energies and outgoing angle, θ, of the deuteron with respect to the beam axis, given by

$$\sigma_T{}^\ell(x, y) = \frac{[W_\ell(x, y)]^2}{(x^2 + |y|^2)[1 + 0.008\,(x^2 + |y|^2)]^2} \qquad \text{(III. B. 3. 10)}$$

where $x = q\, r_0$

q = the momentum transfer, $\left|\vec{K}_A - \frac{M_B}{M_A}\vec{K}_B\right|$

r_0 = is the Butler radius, and

$$y = \left(\frac{2M_A}{M_B}(-E_B)\ \frac{(A.M.U.)}{h^2}\right)^{\frac{1}{2}} r_0$$

where E_B is the energy in MeV by which the alpha particle is bound into the final ^{16}0 state. The parameter, y, is real or imaginary when the final state ^{16}0 state is unbound or bound respectively.

The expression W (x, y) contains the spherical Bessel functions, j_ℓ, and Hankel functions of the first kind $h^{(1)}$ and their derivatives. It is

$$W_\ell(x, y) = x\frac{d}{dx}\, j_\ell(x) - \frac{y j_\ell(x)}{h_\ell{}^{(1)}(y)}\ \frac{d}{dy}\, h_\ell{}^{(1)}(y) \qquad \text{(III. B. 3. 11)}$$

In general, the cross section expression (Eq. III. B. 3.9) is evaluated as a function of the momentum transfer by varying the Butler radius and the angular momentum, ℓ, until the best possible fit to the angular distribution data is achieved. The value of ℓ is important in determining the spin and parity of the final state formed. However, in our experiment the final state spins and parities are known, but not their reduced alpha widths. Because of the suspected presence of a large compound nuclear contribution to the cross section, the standard direct reaction analysis of the data is not appropriate, and further steps are necessary.

C. Isolation of the Two Contributions

Our method for isolating the direct reaction contribution, σ_{DIR}, from the experimentally measured σ_{exp} is based on the following assumptions:

(1) $\sigma_{exp} = \sigma_{DIR} + \sigma_{CN}$. The cross sections add without interference.

(2) $\sigma_{CN} = \sigma_{HF}$ for all the final states in $^{16}0$, and is computed from Equation III. B. 2. 1 except for the factor A(E) which is independent of the $^{16}0$ final state.

(3) The constant A(E) is evaluated by assuming the cross section leading to the 2^- state in $^{16}0$ is due only to the Hauser-Feshbach contribution.

Since the region of excitation in ^{18}F has many overlapping levels and the beam energy spread and the level width is sufficiently large compared to the spacing of these levels, it was assumed that

the effects of fluctuations from the individual levels are negligible. Thus, the Hauser-Feshbach analysis was applied to the problem by calculating the transmission coefficients T_ℓ of the incoming $T_\ell^{IN}(E)$ and outgoing waves $T_\ell^{OUT}(E')$ by using the computer program ABACUS (Auerbach 1964). These transmission coefficients were calculated from elastic scattering cross sections at the appropriate energies for all contributing angular momentum waves using optical potentials. The values of the optical parameters were taken from the scattering experiment of Bennett and Grant (1963) and the tabulation of Hodgson (1963). The values obtained for these coefficients are listed in Tables 10, 11 and 12. These transmission coefficients were then used in Equation (III. B. 2. 1) to calculate the quantities $\sigma_{H.F.}/A(E)$ for each final state in ^{16}O.

Such calculations give the relative cross section for formation of each level. The further assumption discussed earlier that the 8.88 MeV (2^-) level can be formed only by such a compound nuclear process, leads to the following normalization procedure. The factor of normalization, A(E), was chosen so that the calculated total cross section for the 8.88 MeV level agreed with the measured values. A plot of the calculated angular distributions for this level along with the measured values is shown in Figure 16. A weakness is that the angular fit at 7.0 MeV is not very good, but one would expect a better fit to the total cross section than to the differential cross section. A different normalization factor is required for the 7.0 and 8.0 MeV data, as expression (III. C. 2) does not contain the

usual Hauser-Feshbach denominator which takes into account the effect of all the exit channels on the total cross section. As more channels open this factor decreases as would be expected.

The results of these calculations for total cross sections obtained by integrating the differential cross section over all angles are listed under the column labeled '$\sigma_{H.F.}$' in Table 13. When these are compared to the measured cross sections, σ_{exp}, one can see that in all cases the predicted $\sigma_{H.F.}$ is no larger than σ_{exp}, within the experimental errors. This suggests that there may well be a direct reaction mechanism contributing strongly to those levels which display significantly larger cross sections than those predicted by the Hauser-Feshbach calculations.

An examination of the term $\sigma_{exp} - \sigma_{H.F.}$ in Table 13 reveals several significant patterns.

(1) The 9.58 MeV level and the 10.36 MeV level which have the largest reduced alpha widths and would be expected to show the largest σ_{DIR}, have the largest values of $\sigma_{exp} - \sigma_{H.F.}$.

(2) The 9.84 level, with a small reduced alpha width and therefore not expected to have a large direct reaction contribution, has the predicted compound nuclear cross section within the experimental error. Furthermore, of all the other levels measured, none has a smaller cross section than that predicted by the Hauser-Feshbach method.

Since the Hauser-Feshbach calculations are based on the incoherence of many small contributions to a total compound

nuclear cross section, it is not unreasonable to assume that these contributions are also incoherent with the direct reaction taking place simultaneously. In this way an estimate of the total direct reaction cross section 'σ_{DIR}' is obtained by simply subtracting the Hauser-Feshbach contribution from the total. These results are shown in Table 13. This assumption of non-interference was also used by Ericson (1963) in his treatment of separating statistical compound nuclear cross sections from direct reaction by means of fluctuations.

Table 13 also permits a comparison of this direct cross section 'σ_{DIR}' = $\sigma_{exp} - \sigma_{H.F.}$ with the tabulated reduced alpha widths. The extraction of reduced alpha widths from these calculated 'σ_{DIR}' required further assumptions. An alpha transfer reaction would have a cross section proportional to the reduced alpha width for the final state in ^{16}O. In order to complete the analysis, we have assumed only alpha transfer reactions contribute to σ_{DIR}. This is discussed in the next section.

The calculation of 'σ_{DIR}' was carried out for the E_{CM} = 8 MeV data also (Table 13), although since no states with known, non-zero reduced alpha widths were measured, we can compare only the ratios of the 'σ_{DIR}' of the 6.92 to 7.12 MeV levels. These ratios (3.4 ± 0.9 at E_{CM} = 7 MeV and 6.3 ± 4.2 at E_{CM} = 8 MeV) agree within the experimental uncertainty.

As a further check, the same procedure was used to analyze the data of Heikkinen (1966), with a few minor differences.

Since Heikkinen was not able to measure the cross section leading to the 8.88 MeV level nor to resolve the 6.06 and 6.14 MeV levels, it was necessary to use the ground state as the normalization point for the Hauser-Feshbach calculations and to sum the results for the 6.06 - 6.14 MeV doublet. The results of this calculation at E_{CM} = 3.4 MeV are shown in Table 14.

The ratio of the 'σ_{DIR}' of the 6.92 to the 7.12 MeV level is 3.3 ± 0.7 in agreement with the values at 7 and 8 MeV. We are unable to gain any further information about the ground state as its σ_{exp} was used for obtaining the total cross section normalization. In order to study more than just the sum of the 6.06 and 6.14 levels, a rough estimate of the contribution of each to the total was made on the basis of deuteron spectra shown by Heikkinen (1965). The σ_{DIR} extracted from this estimate and shown in parentheses in Table 14 are consistent with the values obtained at 7 MeV, although the uncertainty is very large in each and these uncertainties are correlated and not independent.

These checks on the behavior of 'σ_{DIR}' at 3.4 and 8 MeV add some confidence in the general approach that this subtraction technique takes, and may justify the attempt to extract values of the reduced alpha widths for these levels.

D. Extraction of the Reduced Alpha-Widths

The reduced alpha-widths, θ_α^2, for the levels in ^{16}O investigated in this study were obtained from the values of 'σ_{DIR}'

discussed in the preceding section. The additional necessary assumptions concerning σ_{DIR} discussed above, are that σ_{DIR} represents only an alpha transfer direct reaction and that θ_α^2 is proportional to σ_{DIR}. The determination of the proportionality constant and its spin and energy dependence are described below.

An expression obtained by a PWBA method, given by Equation (III. B. 3. 9) (see page 42) shows that the cross section is proportional to the reduced alpha width, but that its dependence upon the spin, S, and the various energies is rather complicated. There is a general (2S + 1) factor, but the expression $\sigma_T{}^{\ell}(x, y)$ also depends on S since the spinless α and ^{12}C nuclei force ℓ to be equal to S.

Because of the fairly rapid oscillation in stripping cross sections as a function of the momentum transfer, the choice of the Butler radius r_0 can affect the values calculated by Equation (III. B. 3. 9). Therefore, the following procedure was carried out. A complete code was written to evaluate the $(d\sigma/d\Omega)_{PWBA}$ expression of Equation (III. B. 3. 9) as a function of θ and compute the integrated cross section

$$\sigma_{PWBA} = \left(\frac{E_1}{E_0}\right)^{\frac{1}{2}} (2S + 1)\, \theta_\alpha^2 \int_{\theta=0}^{\pi} \sigma_T{}^{\ell}(x(\theta, r_0), y(r_0))\, d\Omega$$

$$= \sigma_{PWBA}(r_0) \qquad \text{(III. D. 1)}$$

We next averaged over a range of volume r_0 = 5 - 10 f to obtain

$$\sigma_{PWBA}(\bar{r}) = U \left(\frac{E_1}{E_0}\right)^{\frac{1}{2}} (2S + 1)\, \theta_\alpha^2 \int_{r_0 = 5f}^{10f} dr_0 \int_0^\pi \sigma_T^{\ell}(\theta, r_0) d\Omega$$

(III. D. 2)

The averaging process over the values of r_0 from 5.0 to 10.0 f can be justified by understanding the need for r_0. Originally it was chosen as the sharp radius of the nuclear surface, so that the integral that had to be evaluated in the external region in a PWBA calculation could be cut-off. Physically, however, a "fuzzy" cut-off would be more realistic and the optical potential in a DWBA calculation does effectively blur the nuclear surface. An averaging over r_0 achieves the same effect, although in a cruder way, perhaps.

The normalization constant U was evaluated by setting $\sigma_{PWBA}(\bar{r}, 9.58 \text{ MeV level}) = \sigma_{DIR}(9.58 \text{ MeV level})$. The 9.58 MeV level was chosen for this normalization because it has the largest $\theta_\alpha^2 = 0.85$ and the largest value of σ_{DIR}. The values of $\sigma_{PWBA}/\theta_\alpha^2$ are shown in Table 15 along with the values of θ_α^2 derived from the ratio of σ_{DIR} to σ_{PWBA}.

The range of values assigned to θ_α^2 is due entirely to the uncertainties in each σ_{exp} and to the uncertainties in the σ_{exp} for the 8.88 and 9.58 MeV levels as they enter into the Hauser-Feshbach and PWBA normalizations. Although the general method used might well introduce even greater uncertainties, there is no good method to estimate these. The θ_α^2 are presented in Table 15 in the form shown,

rather than in the mean value ± standard error form normally used, for the convenience of the reader and as an indication that the uncertainties do not take all possible errors into account.

IV. DISCUSSION OF THE RESULTS

A. The Nucleus ^{16}O

A.1. Comparison with Previous Experiments

We shall now try to compare the results obtained for the reduced widths in the preceding section to those previously measured by other observers. Such a direct comparison is possible in only two cases, since of the nine ^{16}O levels investigated here only four states have open alpha decay channels (see Ajzenberg-Selove and Lauritsen, 1959). Of these, two levels have contributed their θ_α^2 as input data in order to determine the reduced widths for the other seven levels. This leaves only the 9.84 MeV level investigated by Hill (1953) and the 10.36 MeV level investigated by Bittner and Moffat (1954) to check our experimental results. In both of these experiments θ_α^2 was determined from $^{12}C + \alpha$ elastic scattering data. For the 9.84 MeV level we extract a value of $\theta_\alpha^2 \leq 0.06$, whereas Hill measured a value of $\theta_\alpha^2 = 0.0015$. We obtain a range of values for θ_α^2 between 0.23 and 0.53 for the 10.36 MeV level compared to the value 0.26 measured by Bittner and Moffat. In each case we find agreement with the directly measured values of θ_α^2 within the experimental errors.

It is unfortunate that there are no other measurements for θ_α^2 for the levels stable to alpha decay. In order to get any idea of the θ_α^2 for these bound levels, we must rely on independent theoretical predictions discussed in the next section. We should also note that our measured cross sections generally agree in their

relative magnitude in populating the various $^{16}0$ final states with those measured by Heikkinen (1966).

Using the principle of detailed balance and allowing for the momentum and spin factors we find good agreement within the experimental error with the measured magnitude and shape of the cross section for the inverse reaction $^{16}0(d, ^{6}Li)^{12}C$ taken by Daehnick and Denes (1964) at the nearby C.M. energy of 7.3 MeV. This is the only cross section measurement in the same energy range as we have used. Denes et al. (1966) have used a DWBA method applied to this alpha pickup reaction to probe the structure of the $^{16}0$ ground state. This work is discussed in the next section.

A.2. Level Structure Models

The reduced widths extracted here have certain implications for the structure of the corresponding levels in $^{16}0$. The low-lying levels in $^{16}0$ have been treated theoretically in terms of an alpha particle model (Dennison 1940, 1954; Kameny 1956), and alpha particle plus ^{12}C cluster model, (Roth and Wildermuth 1960; Sheline and Wildermuth 1960), a shell model (Gillet and Vinh Mau 1964; Bassichis and Ripka 1965), and a unified shell and collective model (Borysowicz and Sheline 1964; Kelson 1965). Good summaries of these various theoretical treatments are given by Larson (1965) and Heikkinen (1965).

There is much evidence (e.g., Carter et al. 1964, Gorodetsky et al. 1962, Kelson 1965) for the existence of rotational bands in the $^{16}0$ nucleus. This collective behavior can be compatible

with shell model descriptions of nuclei using the concept of intrinsic states as discussed by Kelson. In general, this latter approach seems to be the most satisfactory one. However, the $^{12}C + \alpha$ cluster model does make quite definite predictions for θ_α^2 and it would not be fair to exclude it from this discussion. The discussion will be limited to comparison with the $^{12}C + \alpha$ cluster model and the unified shell-collective model.

The Ground State

The lowest even parity state is, of course, the ground state. The shell model description of this state is that of completely filled $1s^{1/2}$, $2p^{3/2}$ and $2p^{1/2}$ shells. This doubly magic nucleus, however, does have four particles in its least tightly bound shell and might be expected to have a reasonable alpha width for this reason. On the other hand, these four particles are tightly bound and the spherical symmetry might inhibit the breakup of the ^{16}O ground state into such large clusters as an alpha plus ^{12}C. This spherical symmetry also precludes the existence of any rotational bands built on this level which might shed light on the intrinsic structure of the ground state.

The cluster model describes this level as a $^{12}C + \alpha$ in a relative $\ell = 0$ state. The implications of this model would be a large θ_α^2. Our results indicate a value not greater than 0.05. This is not in agreement with the work of Denes et al. (1966) in which a rather large spectroscopic factor, related to θ_α^2, is extracted. However, they did not consider the effects of compound nucleus formation

in their DWBA analysis. Our analysis would indicate that approximately 90% of the total cross section can be attributed to the compound nuclear contribution to the process. If our analysis is correct then their approach could overestimate the reduced width by an order of magnitude. Our value of 0.05 for θ_α^2 would indicate that the ground state of $^{16}0$ is poorly described by a $^{12}C + \alpha$ cluster.

The 6.06, 6.92, and 10.36 MeV Levels

The first excited state of $^{16}0$ at 6.06 MeV has a spin and parity of 0^+. The experiments of Gorodetsky et al. (1962) and Carter et al. (1964) have strongly suggested that this is the 'ground state' of a $K = 0^+$ rotational band. The 2^+ state at 6.92 MeV and the 4^+ state at 10.36 MeV are the other members of this band investigated here. Kelson (1965) describes this band as the angular momentum projections of an intrinsic deformed state ϕ_0 made up of four particles outside the spherical core. This collective state should have a reasonably large θ_α^2 because of the four particles outside the core in this deformation. In addition, the θ_α^2 that one measures should be nearly independent of the angular momentum of the particular state.

The cluster model predicts that these levels are described by $^{12}C + \alpha$ in relative $\ell = 0$, $\ell = 2$, and $\ell = 4$ states and therefore would have large reduced widths. Our results show θ_α^2 for all three levels to be consistent with the value $\theta_\alpha^2 = 0.26$ measured for the unbound 4^+ level by Bittner and Moffat (1954). This band provides the strongest test of our method for extracting θ_α^2

in the case of bound levels and the agreements give somewhat more confidence in the general approach taken here.

9.58 MeV Level

The 9.58 MeV 1^- state has an extremely large $\theta_\alpha^2 = 0.85$ (Hill, 1953) which was used in the extraction procedure for the other levels. The cluster model presents this level as an $\alpha + {}^{12}C$ in a relative $\ell = 1$ state, thus, explaining the large θ_α^2. The similarity of the reduced widths of this level and the 3^- level at 11.63 (not investigated here) and the existence of broad 5^- levels in the region of 16.5 to 18.5 MeV provides evidence for a rotational band of spins and parities 1^-, 3^-, 5^-, etc. Kelson explains this sequence as a $K = 0^-$ band projected from the same deformed state ϕ_0 as the $K = 0^+$ band discussed above. Borysowicz and Sheline explain this deformed set of levels as mainly a 3 particle - 3 hole state. Both approaches would predict a large θ_α^2, but not as large as that measured. Since the known θ_α^2 is used as an input parameter in our analysis, we gain no further information about the level from this experiment.

The 6.14 and 7.12 MeV Levels

The two bound negative parity states of spin 3^- at 6.14 MeV and 1^- at 7.12 MeV are discussed together. The cluster model predicts large θ_α^2 on the basis of single $\ell = 1$ and $\ell = 3$ states of relative orbital momenta. However, since the reduced alpha widths extracted in this experiment are no larger than the order of 0.1, it is likely that another model would be more successful in describing

these levels. Kelson suggests that they are essentially single particle-single hole levels with a 6-7% admixture of the deformed collective states ϕ_0.

A recent treatment has been carried out by Stephenson (1966) based on the earlier work of Brown and Green (1966). In his model there exist intrinsic one particle-one hole and three particle-three hole states identified with representations of the now famous group SU(3). The negative parity states in ^{16}O are then linear combinations of these intrinsic states and one can derive certain properties of these levels. The reduced width predicted in Stephenson's model (0.06 - 0.14) is in good agreement with our value for the 7.12 MeV level, but his prediction (0.1 - 0.2) is larger than our value of < 0.02 for the 6.14 MeV level.

8.88 MeV Level

The only other unbound negative parity state studied here is unique in that it is the only level in which decay to an $\alpha + {}^{12}C$ is strongly forbidden by the necessity to conserve parity and angular momentum. In the analysis of the data this 'zero' reduced alpha width was used as an input parameter. The cluster model describes this level as an alpha coupled to an excited $^{12}C^*$ in a relative $\ell = 1$ state. Kelson calls the state 100% "spherical" with a one-particle-one hole configuration. The possible relationships of this level to other negative parity states is not clear due to the general lack of precise understanding of the negative parity levels.

9.84 MeV Level

The remaining positive parity state studied here is the unbound 2^+ state at 9.84 MeV. The value of θ_α^2 that we extract is in agreement with the measured value of 0.0015. The cluster model describes this level as an $\ell = 0$ state of an alpha plus a $^{12}C^*$ excited core, and thus a small θ_α^2 is predicted. Borysowicz and Sheline (1964) suggest that this level is the base state of a band of levels with positive parity and spins 2^+, 3^+, 4^+, etc. This experiment sheds no further light on the nature of this state but the agreement with the previously measured θ_α^2 does instill more confidence in the general method used.

The extraction of the bound level reduced widths in this experiment may help to understand the level structure in $^{16}0$. There seem to be no great surprises from the data and the collective plus shell model theoretical approach to the general $^{16}0$ problem appears to give the most satisfactory conclusions concerning the level structure.

B. Astrophysical Implications

The major uncertainty in tracing the evolution of ^4He burning stars has been the lack of knowledge of the cross section for the $^{12}C(\alpha,\gamma)^{16}0$ reaction. Since the temperature at which the $3\alpha \rightarrow {}^{12}C$ reaction ignites in most stellar models is at about 10^8 degrees ($T_8 = 1$) this is the temperature at which the $^{12}C(\alpha,\gamma)^{16}0$ reaction rate is of most importance as the main mechanism for forming $^{16}0$ and thereby depleting the carbon built up by the 3α

reaction. The reaction mechanism is non-resonant at this energy just above the $^{12}C + \alpha$ threshold, but due to the nearness of the bound level at 7.12 MeV (see Fig. 1) this level is presumed to provide the major contribution to the alpha capture cross section. In order to calculate this cross section it is necessary to know the reduced alpha width, θ_α^2, for the 7.12 MeV level.

Tombrello (private communication, 1964) has pointed out that since the 9.58 and 7.12 MeV levels both have spin and parity of 1^-, the (α,γ) cross section may be modified by either constructive or destructive interference in the region between the resonances. Using a two-level formula, he has estimated that at an energy corresponding to $T_8 = 1$, the effect of interference should not change the estimated cross section by more than ± 20% for a value of $\theta_\alpha^2 (7.12) = 0.1$.

Using the reaction rates derived by Reeves (1964), Deinzer and Salpeter (1964) have calculated final (defined to be total core helium depletion) carbon abundances as a function of stellar mass between 0.3 and 10^2 solar masses. Their model assumed equilibrium conditions, pure helium burning, important radiation pressure, and $\theta_\alpha^2 = 0.1$ in agreement with our value. The results show a carbon abundance of 40% at 0.3 solar masses rising to a maximum of 60% at one solar mass, and then falling off to about 10% above 10^2 solar masses. The conclusion drawn from this is that, except for extremely massive stars, the carbon abundance is sufficiently large that the next probable stage in the evolution of

such stars must be the ignition of $^{12}C + {}^{12}C$ reactions at about $T_8 = 6$. Other models (e.g., Iben, 1966) reach the same general conclusions.

The further development of the star is critically dependent upon the rate of the $^{12}C + {}^{12}C$ reaction, which may be in competition with neutrino processes at the temperatures involved in this stage of stellar evolution (Fowler and Hoyle, 1964). It is now important to reduce the present uncertainty in the $^{12}C + {}^{12}C$ cross sections in order to calculate the conditions of the next stage in stellar evolution more accurately.

C. Summary and Conclusions

The reaction cross section for the formation of the ground state and first eight excited states of ^{16}O in the heavy ion reaction $^{6}Li(^{12}C, d)^{16}O^*$ have been measured and used to extract the reduced alpha widths for the bound states. This analysis depends upon the assumption that the compound nuclear contribution to the total cross section can be calculated and then subtracted with no interference to leave a direct alpha transfer cross section proportional to the reduced widths, θ_α^2. Tests of the analysis method in the prediction of previously known reduced widths and theoretical predictions of the bound state reduced widths have not pointed out any striking shortcomings in the results and the general approach rests on fairly reasonable assumptions.

This method of analysis might be a powerful tool for measuring reduced widths of bound levels in the presence of

considerable compound nuclear formation. In particular, the use of ^{6}Li as a beam or target at energies above the Coulomb barrier might measure the reduced alpha widths of various alpha bound levels such as in the reaction $^{6}Li(^{16}O, d)^{20}Ne^{*}$. The measurements of such reduced widths would be a considerable prize to the theorists attempting to understand the nature of the low-lying excited states of light weight nuclei.

Due to deterioration of the ^{6}Li target and because of unfavorable kinematics, a ^{6}Li beam would have been preferable. Further efforts to inject a sizable negative or neutral Li beam into the Tandem accelerator might be rewarded by the ability to perform such experiments as these mentioned above and to extend the work done at lower energies with Li beams into the tandem energy region.

The reduced alpha width determined for the 7.12 MeV level in ^{16}O, which is necessary in order to predict the $^{12}C(\alpha,\gamma)^{16}O^{*}$ cross section in the region above threshold important in astrophysical calculations, has been determined to be of the order of 0.1. This value had been used in previous astrophysical models dealing with the evolution of helium burning stars, and confirms that in most cases a considerable fraction of the residual core after the exhaustion of helium is ^{12}C. This then implies that the next stage of stellar evolution involves the reaction $^{12}C + {}^{12}C$.

It is desirable to extend the $^{12}C(\alpha,\gamma)$ measurements to as low an alpha energy as possible as the reaction rate in the energy region corresponding to temperatures below $T_8 = 20$ are still quite

uncertain. However, if we are satisfied that we now know the stellar reaction rate of $^{12}C(\alpha, \gamma)$ at the appropriate energy near $T_8 = 1$, the most useful nuclear experiment that could shed more light on the evolution of helium burning stars would be the study of the $^{12}C + {}^{12}C$ reaction. This reaction rate helps determine the future development of such stars and the experiment could take advantage of much of the technology utilized in the $^{6}Li(^{12}C, d)^{16}O^{*}$ experiment.

APPENDIX I. CHARGE STATES OF HEAVY IONS IN MATTER

The equilibrium charge states of heavy ions are often of essential interest in the design and analysis of experiments which involve the acceleration or detection of charged particles heavier than helium. The calculation of such charge fractions is sufficiently complicated that it is necessary to rely on experimental data for the purpose of estimating the various fractions of a beam to be found in a given charge state at any energy.

For a given ion beam, these equilibrium fractions, ϕ_i, depend upon the nature of the material in which equilibrium has been achieved and upon the velocity of the ions upon leaving this material. A previous review of the experimental information concerning the ions Li, Be, B, C, N, O, F, and Ne, discussed the general problem in some detail (Zaidins, 1962). Other general discussions have been given by Northcliffe (1963) and Allison (1958).

This treatment is intended to present a more recent calculation of curves for ϕ_1 with which one can make a <u>good guess</u> as to the charge states fractions for solid target materials. The reason for this restriction is that the values of ϕ_i are insensitive to the nature of the solid material in which equilibrium is established, but are more dependent upon the nature of a target gas. This may be due to the fact that only a very thin target [< 0.5 μg at 0.5 MeV/A (Hubbard and Lauer, 1955) and < 50 μgrams/cm^2 for 10 MeV/A (Heckman et al. 1963)] is necessary to establish equilibrium, and

many solids have that much surface "dirt" unless special precautions are taken. The discussion is also restricted to positive ions.

The charge state curves for Lithium (Fig. 17), Beryllium (Fig. 18), Boron (Fig. 19), Carbon (Fig. 20), Nitrogen (Fig. 21), Oxygen (Fig. 22), Fluorine (Fig. 23), and Neon (Fig. 24) have been calculated using an extension of the ideas introduced by Dimitriev (1957).

The basic assumption of the Dimitriev approach is that the Z electrons in a given atom may be treated independently and ordered with respect to the successive ionization potentials of the atom, U_j. The importance of these ionization potentials was explored in an early series of papers by Bohr (1940, 1941) and Brunings, Knipp, and Teller (1941). Next, the probability of the loss of a given electron is described by a function of velocity, (e.g., $P_j(v)$ for the jth electron). Thus, we can also define another function $M_j(v) = 1 - P_j(v)$ which is the probability that the jth electron is not lost. Using the laws of probability, an atom with atomic charge Z will have 2^Z possible states, α, each of whose probability is described by

$$\psi_\alpha(v) = \prod_{j=1}^{Z} \begin{pmatrix} M_j(v) \\ \text{or} \\ P_j(v) \end{pmatrix} \qquad \text{(AI. 1)}$$

A convenient symbol for α is a Z-digit binary representation where the value of the jth digit signifies whether the jth

electron is present (0) or has been lost (1). For example, 0000 would stand for a neutral Boron atom and 1111 a totally ionized Be^{++++} ion. In this way, the value of the jth digit would determine the choice of $M_j(v)$ or $P_j(v)$ in the product of equation (AI. 1).

In this model an ion with a total positive charge i could be made up of any of the $Z!/i!(Z - i)!$ states which have lost i electrons. Therefore, the probability, ϕ_i, of the ion having a total positive charge i is the sum over all ψ_α in which α has i non-zero digits. For example, the probability of a Lithium ion having charge +1 is given by

$$\phi_1 = \psi_{001} + \psi_{010} + \psi_{100} \qquad \text{(AI. 2)}$$

where

$$\begin{cases} \psi_{001} = M_3 M_2 P_1 \\ \psi_{010} = M_3 P_2 M_1 \\ \psi_{100} = P_3 M_2 M_1 \end{cases} \qquad \text{(AI. 3)}$$

At this stage it would be wise to say a word about the model. The assumption of the independence of the electrons is not physically justified in view of our knowledge of the behavior of identical fermions. It is true that the measured values of ϕ_i could be used to determine a set of M_j, but these functions would not be expected to have any physical meaning. The importance of the M_j functions lies instead in their use in calculating good approximations to the experimental values of ϕ_i with reasonable extrapolations to regions with no experimental data. This method also insures the

normalization condition that

$$\sum_{i=0}^{Z_1} \phi_i = 1.$$

The fitting procedure made use of two free parameters per electron. The probability functions were chosen for convenience to be of the form

$$M_j(v) = e^{-A_j \left(\frac{v}{v_j}\right)^{B_j}}$$

where A_j is a completely free, real parameter; B_j, the exponent parameter of the dimensionless velocity ratio, is constrained to integer or half integer values in order to facilitate the calculations; and V_j is the velocity corresponding to the kinetic energy necessary for the jth electron to overcome its ionization potential U_j. The values of U_j are taken from tables in Landolt-Bornstein (1962) and then the V_j are calculated from the non-relativistic expression

$$V_j = \sqrt{\frac{U_j}{2m_0}} \qquad \text{(AI. 5)}$$

The non-linear, least-squares fitting method made use of a computer code written for the CIT-IBM 7090-7094 system. The sum of the squares of the deviations between the calculated and experimental values of ϕ_i was minimized with respect to the parameters A_j by a steepest descent (gradient) method. Then the values of B_j

were changed manually and the sum of the squares of the deviations was again minimized with respect to A_j. The parameters of the smallest values of these minima were chosen to generate the curves for ϕ_i (Fig. 17 through Fig. 24). All the parameters for the final curves are listed in order of increasing atomic number in Table 16. The experimental data points used in the fitting procedure and plotted in Figure 17 through Figure 24 were taken from equilibrium fractions established in various materials listed below.

Beam	Target Material	Reference
Lithium	Celluloid	Teplova et al. (1957)
	Boron	Young et al. (1965, private communication)
Beryllium	Beryllium	Tombrello, Parker and Bacher (1962, private communication)
	Boron	Purdom (1965, private communication)
Boron	Celluloid	Nikolaev et al. (1958, 1961)
Carbon	Vanadium Nitride	Seegar and Kavanagh (1963)
	Zapon	Heckman et al. (1963)
	Nickel	Loebenstein, Mingay, and Zaidins (1964, private communication)
Nitrogen	Celluloid	Nikolaev et al. (1957, 1961)
	Formvar	Reynolds et al. (1955)
	Zapon	Heckman et al. (1963)
		Stephens and Walker (1966)
Oxygen	Celluloid	Nikolaev et al. (1958)
	Zapon	Heckman et al. (1963)
	Zapon	Stephens and Walker (1955)
	Aluminum	Northcliffe (1960)
	Iron	Simpson et al. (1965)
	Nickel	Loebenstein, Mingay, and Zaidins (1964, private communication)

Fluorine	Carbon	Almquist et al. (1962)
	Zapon	Stephens and Walker (1955)
Neon	Celluloid	Nikolaev et al. (1958, 1961)
	Zapon	Heckman et al. (1963)

In those cases (C, F, and Ne) where insufficient data were present to determine all the free parameters, the parameters that were set arbirarily to values consistent with those for nearby atoms are given in parentheses and all others were varied in the standard way to achieve a least squares fit.

APPENDIX II. CARBON BEAMS

A. Beam Production

The purpose of this section is to describe the procedures used in the production of a carbon beam in the CIT-ONR Tandem Van de Graaff accelerator. The initial step of injecting a negative carbon beam is still not a routine matter nor is the exact nature of what occurs in the negative ion source totally understood.

Various source gases were tried in order to obtain a negative carbon beam. Carbon dioxide (CO_2), ethanol (C_2H_5OH), and methanol (CH_3OH) were discarded because of the strong oxygen beams that they produced. Some mixtures of methane (CH_4) and hydrogen (H_2) were used and the pure methane proved to give the most intense beam. Acetylene (C_2H_2) might given an even stronger beam, and is being tried presently, but there may be danger in using acetylene with copper. The presence of copper fixtures in the gas handling system might allow the formation of explosive copper acetylide (Cu_2C_2).

Methane gas is admitted to the duoplasmatron source at pressures in the region between 50μ and 200μ under the plasma conditions. Hydrogen gas is used in the exchange canal at pressures in the region of 3×10^{-4} mm(Hg) after passing through a liquid N_2 trap which dries it. This is to supress further the oxygen beams which originate in the exchange canal. Of course, these pressure readings are only an indication of the right region as under each individual set of beam conditions, they are adjusted so as to maximize

the beam. If it is possible to operate under conditions of low source pressure (50μ), the filament life may easily exceed 90 hours and carbon build up in the source chamber is minimized. This build up of solid carbon is a serious beam inhibitor and an oversized (0.6 mm diameter) hole through which the positive beam is extracted from the plasma supresses this deposit considerably.

Other average settings for a reasonable beam are:

Filament current	40 Amps
Source magnetic current	1 Amp
Filament bias	120-130 volts
Probe bias	60-70 volts
Arc current	300 milliamps
Exchange voltage	42.5 kilovolts
Focus voltage	4-5 kilovolts
Lens I	15 kilovolts
Lens II	17 kilovolts

Again, these settings should be taken to be only approximate.

Special precautions are necessary because of the nature of negative heavy ion beams. The large cross sections for electron loss require an especially good vacuum at the low energy side of the tandem. Pressures that would only slightly attenuate H^- beams will reduce C^- beams significantly. Pressures of less than 10^{-5} mm Hg at this point are advisable.

Heavy ion beams of energy less than 100 keV require

quite precise steering. This often necessitates physically positioning the entire duoplasmatron probe head by means of the movable set screws provided on the back of the ion source box.

A most important setting is the magnetic field in the 20° analyzing magnet. This is measured to sufficient accuracy by the current output of the magnet power supply in units of D. C. milliamperes. We find that for an exchange voltage of 42.5 K. V., this current setting should be 285 mA. This does not seem to correspond to the process of acceleration denoted by (C^+, C^-), where a positive carbon ion is extracted from the plasma and is charge exchanged at the exchange canal to a singly charged negative carbon ion which is then accelerated to ground potential and then injected into the tandem at an energy which is twice the exchange potential energy in keV. The equation governing the relation between the analyzing magnet current and the beam mass and energy is

$$I(mA) = \frac{K\sqrt{A \times E(keV)}}{Q} \qquad \text{(AII. 1)}$$

where $K = 10.25$ as determined from the best fit to the (He^+, He^-) (d_2^+, d^-) and (H_3^+, H^-) accelerating processes. Table 17, compiled with the aid of R. G. Miller (1966), lists several C^- and various other accelerating processes which may take place and the recorded current settings for these processes. On the assumption that it is actually C^- ions that are injected into the tandem, the processes such as (C_2^+, C^-) or (CH_5^+, C^-) are the best candidates for what actually takes place. However, it would be extremely difficult to

analyze exactly what the acceleration procedure is prior to injection.

After injection the negative beam (of about 0.1 μA) is accelerated to the terminal where it encounters the increased gas pressure in the stripper canal. It then establishes a new charge state equilibrium in the canal which is operated at pressures approximately 20% higher than that of normal for a proton beam. These positive beams are then accelerated to the high energy end of the tandem and each beam, corresponding to different ionic charge, has a different energy as determined by Equation II.A.1. The NMR frequency setting of the 90^0 magnet will pass a beam of $^{16}0$ with charge Q' having an energy equal to $3/4 \left(\frac{Q'}{Q}\right)^2 E_c$, the factor 3/4 being due to the ratio of the masses. By coincidence it turns out that for Q' = Q + 1 such a $^{16}0$ beam requires a terminal voltage sufficiently close to that for the desired ^{12}C beam that the methods described in the next section are necessary to be sure that it is the proper beam that has been analyzed.

For a $^{12}C^{4+}$ beam of 21 MeV with 4.2 million volts on the terminal one may expect 50-60 nanoamps on the image after the 90^o magnet if the object current reading before the analyzing magnetic is about 300 nA.

B. Beam Identification

Beam identification must be performed after the acceleration and analysis of the positive carbon beam, due to the similarity of the carbon beams and the many oxygen beams which are also injected. Bromley et al. (1961) at Chalk River have used

a deuterium target and detected the characteristic gamma rays from the reactions $d(C^{12}, p\gamma)C^{13}$ and $d(O^{16}, p\gamma)O^{17}$ as a method of beam identification. We have used the elastically scattered beams for the 1000 Å nickel target foils analyzed in the 61 cm magnet spectrometer to identify the mass of ions whose energy is known.

The problems of beam current integration in a small target chamber such as that in the 61 cm magnetic spectrometer has been discussed by Loebenstein et al. (1965). The heavy ions passing through the target produce high energy δ-rays (electrons) in various ways (Zupancic and Huus, 1954). Due to these electrons and the secondary electron emission from the walls resulting from the impact of the δ-rays, a positive bias on the target of the order of 3 kilovolts is necessary in order to achieve current readings accurate to 5%.

For this experiment with carbon beams of the order of 20 MeV, the arrangement described in Loebenstein et al. (1965) was used. The Faraday cup was placed close to the target and both were biased to + 1800 volts and connected to a current integrator a common electrical connection. The six 300 volt dry cell batteries connected in series had to be insulated from ground by a sheet of lucite approximately 15 cm in thickness. In addition, a screen cage made of 16 gauge bronze mesh was placed inside the chamber about 5 mm from the chamber walls by means of insulating nylon screws. This cage was then biased to - 1200 volts. In this way there was a strong suppression of the emission of electrons induced by any

source from the target chamber walls and the total effective bias on the target Faraday cup assembly with respect to the cage was 3000 volts. These precautions along with the constant check from the monitor counter mentioned in Section II. A brought about an estimated reduction in the uncertainty of current integrations to less than 5% for the average currents of less than 15nA on target.

APPENDIX III. THE 9.58 MeV LEVEL CROSS SECTION

The cross sections deduced from the 9.58 MeV data were computed in a somewhat different manner from those for the other levels. The great width of this level (650 keV) and the existence of nearby and overlapping levels made it inconvenient to measure and extract the cross section from the entire line shape in most cases. The following method, using only part of the area under the line shape, was employed.

The large width of the deuteron line corresponding to the 9.58 level in ^{16}O is due to the natural width of the level. The shape of the deuteron line depends on the phase shift extracted from $^{12}C(\alpha,\alpha)^{12}C$ experiments (Jones et al., 1962) in the region of this level. It also depends upon penetration factors between the deuterons and $^{16}O^{*}$ due to Coulomb effects and relative orbital angular momentum of the deuteron, ℓ'. Theoretical deuteron line shapes were calculated using the spectral shape computer program of Bacher (1965).

Using the measured $^{12}C + \alpha$ phase shifts and values of $\ell' = 0$ and $\ell' = 4$ at angles from $\theta_{lab} = 0^{\circ}$ to $\theta_{lab} = 70^{\circ}$, this program calculated the theoretical line shapes as a function of spectrometer frequency for the deuteron. The total areas under the curves were normalized to unity and then the percentage of the total area under the curve between the frequencies corresponding to excitation energies of 9.184 and 9.749 MeV in ^{16}O was measured. These

excitation values were chosen for experimental convenience, being just far enough from the levels at 8.88 and 9.84 to avoid background problems. These values ranged between 74% and 82% and averaged 77%. Figure 25 shows the theoretical line shape normalized to unit area for the case of $\ell' = 0$ and $\ell' = 4$ at $\theta_{lab} = 5^{o}$. The statistical error in the measured data is too large to permit the clear determination of the value of ℓ'. Due to the uncertainty in the actual value or range of values for ℓ' and other uncertainties in the procedure, it was decided that measurements between excitation energies of 9.184 and 9.749 MeV contained 77 ± 8% of the total counts that could be attributed to the broad level at 9.58 MeV in ^{16}O.

At 30^{o}, special efforts were made to obtain a complete spectrum and background was subtracted to yield an independent cross section measurement for the 9.58 level. This measurement agreed to within 5% with the one taken by the method used above while the combined experimental error was 14%. It seems reasonable that this method of measuring a significant part of the spectrum and allowing for the part not measured introduces no major error and facilitates the measurement considerably.

References

Ajzenberg-Selove, F., and Lauritsen, T., 1959, Nucl. Phys. 11, 1.

Allison, S. K., 1958, Rev. Mod. Phys. 30, 1137.

Almqvist, E., Broude, C., Clark, M.A., Kuehner, J.A., and Litherland, A.E., 1962, Can. J. Phys. 40, 954.

Auerbach, E. H., 1964, Brookhaven National Laboratory Report 6562 (unpublished).

Bacher, A. D., 1965, private communication.

Bashkin, S., Hurt, V. P., and Seale, W. A., 1963, Phys. Rev. 129, 1750.

Bassel, R. H., Drisco, R. M., and Satchler, G. R., 1962, ORNL-3240 (unpublished).

Bassichis, W., and Ripka, G., 1965, Physics Letters 15, 320.

Bennett, J. R. J., and Grant, I. S., 1963, Proceedings of the Third Conference on Reactions between Complex Nuclei, University of California Press, 50.

Bittner, J. W., and Moffatt, R. D., 1965, Phys. Rev. 96, 374.

Blair, J. M., and Hobbie, R. K., 1962, Phys. Rev. 128, 2282.

Blatt, J. M., and Weisskopf, V. F., 1952, Theoretical Nuclear Physics, John Wiley and Sons, New York.

Bohr, N., 1936, Nature, 137, 344.

Bohr, N., 1940, Phys. Rev. 58, 654.

Bohr, N., 1941, Phys. Rev. 59, 270.

Bohr, N., and Wheeler, J. A., 1939, Phys. Rev. 56, 426.

Borysowicz, J., and Sheline, R. K., 1964, Physics Letters 12, 219.

Breit, G., and Wigner, E. P., 1936, Phys. Rev. 49, 519.

Bromley, D. A., Kuehner, J. A., and Almqvist, E., 1961, Phys. Rev. 123, 878.

Brown, G. E., and Green, A. M., 1966, Nucl. Phys. 75, 410.

Brunings, J., Knipp, J., and Teller, E., 1941, Phys. Rev. 50, 657.

Burbidge, E. M., Burbidge, G. R., Fowler, W. A., and Hoyle, F., 1957, Revs. Mod. Phys. 29, 547.

Butler, S. T., 1957, Nuclear Stripping Reactions, John Wiley and Sons, New York.

Carter, E., Mitchell, G., and Davis, R., 1964, Phys. Rev. 133, B1421.

Dachnick, W. W., and Denes, L. J., 1964, Phys. Rev. 134, B74.

Demirlioglo, D., and Whaling, W., 1962, California Institute of Technology Report (unpublished).

Denes, L. J., Daehnick, W. W., and Drisko, R. M., 1966, Phys. Rev. 148, 1097.

Dennison, D. M., 1940, Phys. Rev. 57, 454; 1954, Phys. Rev. 96, 378.

Dienzer, W., and Salpeter, E. E., 1964, Ap. J., 140, 499.

Dmitriev, I. S., 1957, Soviet Phys. JETP, 5, 473.

Erickson, T., 1960, Adv. Phys. 9, 425.

Ericson, T., 1963, Ann. Phys. 23, 390.

Evans, R. D., 1955, The Atomic Nucleus, McGraw-Hill Book Company.

Fowler, W. A., and Hoyle, F., 1964, Ap. J. Suppl. No. 91, IX, 201.

French, J. B., 1960, Nuclear Spectroscopy, Part B, (Academic Press, New York), 890.

Gillet, V., and Vinh Mau, N., 1964, Nucl. Phys. 54, 321.

Gorodetsky, S., Mennrath, P., Chevallier, P., Scheibling, F., and Sutter, G., 1962, Physics Letters, 1, 14.

Groce, D. E., 1963, Ph.D. Thesis, California Institute of Technology.

Harrison, W. D., 1966, Ph.D. Thesis, California Institute of Technology.

Harrison, W. D., and Whitehead, A. B., 1962, Phys. Rev., 132, 2607.

Hauser, W., and Feshbach, H., 1952, Phys. Rev. 87, 366.

Heckman, H. H., Hubbard, E. L., and Simon, W. G., 1963, Phys. Rev. 129, 1240.

Heikkinen, D. W., 1965, Ph.D. Thesis, The University of Iowa.

Heikkinen, D. W., 1966, Phys. Rev. 141, 1007.

Hill, R. W., 1953, Phys. Rev. 90, 845.

Hodgson, P. E., 1963, The Optical Model of Elastic Scattering, Oxford University Press, London.

Hubbard, E. L., and Lauer, E. J., 1955, Phys. Rev. 98, 1814.

Iben, I., Jr., 1966, Ap. J. 143, 483; Ap. J. 143, 516.

Jones, C. M., Phillips, G. C., Harris, R. W., and Beckner, E. H., 1962, Nuclear Phys. 37, 1.

Kameny, S. L., 1956, Phys. Rev. 103, 358.

Kelson, I., 1965, Physics Letters 16, 143.

Knipp, J., and Teller, E., 1941, Phys. Rev. 59, 659.

Landolt-Bornstein, 1962, G. Auflage, I Band, 1. Teil, 211.

Lang, D., 1961, Nuclear Phys. 26, 434.

Larson, J. D., 1965, Ph.D. Thesis, California Institute of Technology.

Loebenstein, H. M., Mingay, D. W., and Zaidins, C. S., 1965, Nucl. Instr. and Meth. 33, 175.

Loebenstein, H. M., Mingay, D. W., and Zaidins, C. S., 1964, private communication.

MacDonald, N., 1962, Nuclear Phys. 33, 110.

Macfarlane, M. H., and French, J. B., 1960, Revs. Mod. Phys. 32, 567.

Mathews, J., and Walker, R. L., 1964, Mathematical Methods of Physics (W. A. Benjamin, Inc.).

McNally, J. H., 1966, Ph. D. Thesis, California Institute of Technology.

Miller, R. G., 1966, private communication.

Morinigo, F. B., 1964, Phys. Rev. 134, B1243; Phys. Rev. 133, B65, Nuclear Phys. 50, 136.

Morinigo, F. B., 1965, Nuclear Phys. 62, 373.

Nikolaev, Dmitriev, Fateeva, and Teplova, 1957, Soviet Physics JETP, 5, 789; 1958, Soviet Physics JETP 6, 1019; 1961 Soviet Physics JETP 12, 627.

Norbeck, E., Coon, S. A., Carlson, R. R., and Berkowitz, F., 1963, Phys. Rev. 130, 1971.

Northcliffe, L. C., 1960, Phys. Rev. 120, 1744.

Northcliffe, L. C., 1963, Ann. Rev. of Nuclear Science 13, 67.

Ollerhead, R. W., Chasman, C., and Bromley, D. A., 1964, Phys. Rev. 134, B74.

Purdom, P. W., 1965, private communication.

Reeves, H., and Salpeter, E. E., 1959, Phys. Rev. 116, 1505.

Reeves, H., 1964, "Stellar Energy Sources," in Stellar Structure, Vol. VIII of Stars and Stellar Systems (University of Chicago Press).

Reynolds, H. L., Wyly, L. D., and Zucker, A., 1955, Phys. Rev. 98, 474.

Roth, B., and Wildermuth, K., 1960, Nuclear Physics 20, 10.

Salpeter, E. E., 1957, Phys. Rev., 107, 516.

Seeger, P. A., 1963, California Institute of Technology Report, (unpublished).

Seeger, P. A., and Kavanagh, R. W., 1963, Nuclear Phys. 40, 577.

Sheline, R. K., and Wildermuth, K., 1960, Nuclear Phys. 21, 10.

Simpson, J. J., Cookson, J. A., Eccleshall, D., and Yates, M. J. L., 1965, Nuclear Phys. 62, 385.

Snyder, C. W., Rubin, S., Fowler, W. A., and Lauritsen, C. C., 1950, Rev. Sci. Instr. 21, 852.

Stephens, K. G., and Walker, D., 1955, Proc. Roy. Soc. (London) A229, 376.

Stephenson, G. J., Jr., 1966, Ap. J. 146, 950.

Tang, Y. C., Wildermuth, K., and Pearlstein, L., 1961, Phys. Rev. 123, 548.

Teichmann, T., and Wigner, E. P., 1952, Phys. Rev. 87, 123.

Teplova, Dmitriev, Nikolaev, and Fateeva, 1957, Soviet Physics JETP 5, 797.

Tobocman, W., 1961, Theory of Direct Nuclear Reactions, Oxford University Press, London.

Tombrello, T. A., 1964, private communication.

Tombrello, T. A., Parker, P. D. M., and Bacher, A. D., 1962, private communication.

Weisskopf, V. F., 1937, Phys. Rev. 52, 295.

Wolfenstein, L., 1951, Phys. Rev. 82, 690.

Young, F. C., Forsyth, P. D., Roush, M. L., Hornyak, W. F., and Marion, J. B., 1965, private communication.

Zaidins, C. S., 1962, California Institute of Technology Report (unpublished).

Zucker, A., 1960, Ann. Rev. of Nuclear Science 10, 27.

Zupancic, C., and Huus, T., 1954, Phys. Rev. 94, 205.

Table 1

Comparative Kinematics of ^{6}Li and ^{12}C Beams at E_{CM} = 7.0 MeV

		Deuteron Energies in MeV			
		^{6}Li on $^{12}C \rightarrow d + ^{16}O$		^{12}C on $^{6}Li \rightarrow d + ^{16}O$	
^{16}O Level	θ_{LAB}	0^{o}	180^{o}	0^{o}	180^{o}
g.s.		15.86	7.46	21.25	4.44
6.06		9.32	3.24	13.48	1.37
7.12		8.12	2.55	12.23	0.99
8.88		6.08	1.47	9.57	0.35
10.36		4.26	0.66	7.25	0.04

Comparison of the maximum and minimum deuteron energies occuring at $\theta_{LAB} = 0^{o}$ and 180^{o} for E_{CM} = 7.0 MeV for various levels. This requires a beam energy of 10.5 MeV ^{6}Li or 21 MeV ^{12}C.

Table 2

Frequency and yield factors for the 16-counter array (Pages 19,20)

Counter	Frequency Factor	Yield Factor
1	.98149	.903
2	.98416	1.086
3	.98689	.943
4	.98961	.957
5	.99230	.958
6	.99494	.986
7	.99749	.998
8	1.0	1.0
9	1.00257	1.026
10	1.00502	1.053
11	1.00749	1.093
12	1.00984	1.056
13	1.01222	1.108
14	1.01453	1.131
15	1.01692	1.131
16	1.01912	1.127

Table 3

Normalization Data for $^{6}Li(^{12}C,d_3)^{16}O$ at $\theta_{LAB} = 30^{o}$ Related to $^{6}Li(p,p)^{6}Li$ at $E_p = 8.0$ MeV

Reaction	θ_{LAB}	$d\sigma/d\Omega$ [a] mb/ster	Particle Yield	μC [c]	$d\Omega$ in 10^{-3} ster	C.M. Factor F_{CM}	$d\sigma/d\Omega_p$ Ratio to $d\sigma/d\Omega$ (6.92)	$d\sigma/d\Omega$ [b] (6.92) mb/ster
$^{6}Li(p,p)$	47.6^{o}	126 ± 4	26143	18	3.025	0.8119	65.9 ± 5.0	1.92 ± 0.15
$^{6}Li(p,p)$	65.0^{o}	40.9 ± 1.2	24230	54	3.025	0.8810	22.0 ± 1.1	1.85 ± 0.08
$^{6}Li(p,p)$	80.5^{o}	23.9 ± 0.8	12613	54	3.025	0.9593	12.5 ± 0.5	1.92 ± 0.07
$^{6}Li(^{12}C,d_3)$	30^{o}	-	1560	162 [c]	1.982	0.4640	1	1.90 ± 0.05

a) 1.19 times the values measured by Harrison and Whitehead (1962).

b) Determined as a best fit to preceding column and the resulting ratio yields the normalized value of the $^{6}Li(^{12}C,d_3)$ cross section listed above.

c) There are only 1/4 as many incident particles/μc for a $^{12}C^{4+}$ beam.

Table 4

Differential Cross Sections (mb/ster) of the Ground, First and Second Excited States of ^{16}O at E_{CM} = 7.0 MeV

$^{6}Li(^{12}C,d)^{16}O^{*}$

Ground State		6.06 MeV Level		8.14 MeV Level	
θ_{CM}	$d\sigma/d\Omega$	θ_{CM}	$d\sigma/d\Omega$	θ_{CM}	$d\sigma/d\Omega$
90.5	0.30 ± 0.03	22.7	1.18 ± 0.17	22.7	1.66 ± 0.18
101.5	0.30 ± 0.05	30.1	0.64 ± 0.09	30.2	1.81 ± 0.12
111.9	0.31 ± 0.04	44.9	0.27 ± 0.07	45.0	1.51 ± 0.10
121.5	0.17 ± 0.03	59.3	0.21 ± 0.07	59.4	1.36 ± 0.10
130.5	0.14 ± 0.03	73.2	0.29 ± 0.08	73.4	1.19 ± 0.11
138.8	0.40 ± 0.05	86.5	0.48 ± 0.18	86.6	0.89 ± 0.18
146.6	0.83 ± 0.11	98.9	0.32 ± 0.12	99.1	1.20 ± 0.14
153.9	1.08 ± 0.09	110.5	0.41 ± 0.10	110.7	0.91 ± 0.14
160.7	1.33 ± 0.13	121.0	0.28 ± 0.11	121.2	0.51 ± 0.13
		130.5	0.26 ± 0.05	130.7	0.78 ± 0.09
		138.9	0.43 ± 0.08	139.1	0.89 ± 0.11
		146.5	0.56 ± 0.10	146.6	1.35 ± 0.15
		153.2	1.30 ± 0.17	153.4	1.39 ± 0.17
		159.3	0.96 ± 0.15	159.4	1.31 ± 0.18
		164.9	1.07 ± 0.17	165.0	1.39 ± 0.22

Table 5

Differential Cross Sections (mb/ster) of the Third, Fourth, and Fifth Excited States of ^{16}O at E_{CM} = 7.0 MeV .
$^{6}Li\ (^{12}C,d)^{16}O^{*}$

6.92 MeV Level		7.12 MeV Level		8.88 MeV Level	
θ_{CM}	$d\sigma/d\Omega$	θ_{CM}	$d\sigma/d\Omega$	θ_{CM}	$d\sigma/d\Omega$
1.6	3.05 ± 0.14	1.6	1.73 ± 0.13	1.7	1.00 ± 0.10
7.8	2.91 ± 0.10	7.8	1.61 ± 0.10	8.4	0.94 ± 0.05
15.5	2.40 ± 0.10	15.6	1.56 ± 0.11	16.8	0.90 ± 0.06
23.2	1.90 ± 0.08	23.4	1.45 ± 0.08	25.1	0.87 ± 0.05
30.9	1.78 ± 0.07	31.1	1.19 ± 0.07	33.4	0.79 ± 0.06
38.5	1.85 ± 0.08	38.7	0.74 ± 0.06	49.8	0.53 ± 0.04
44.5	1.83 ± 0.06	44.8	0.39 ± 0.04	65.9	0.33 ± 0.04
46.0	1.90 ± 0.05	46.3	0.44 ± 0.03	81.3	0.22 ± 0.03
60.8	1.58 ± 0.08	61.2	0.38 ± 0.03	96.0	0.24 ± 0.04
75.0	0.80 ± 0.06	75.5	0.67 ± 0.04	109.6	0.40 ± 0.06
88.6	0.93 ± 0.08	89.1	0.82 ± 0.07	121.9	0.42 ± 0.21
101.3	1.48 ± 0.10	101.8	0.62 ± 0.09	132.7	0.53 ± 0.17
112.9	1.28 ± 0.12	113.6	0.59 ± 0.06	141.9	0.48 ± 0.27
123.5	1.74 ± 0.13	124.2	0.79 ± 0.10		
132.9	2.10 ± 0.15	133.6	0.80 ± 0.14		
141.3	3.04 ± 0.15	141.9	1.13 ± 0.12		
148.6	3.82 ± 0.31	149.1	1.34 ± 0.24		
155.0	4.23 ± 0.38	155.5	1.13 ± 0.25		
160.8	3.73 ± 0.39	161.2	1.37 ± 0.29		
166.0	3.97 ± 0.44	166.3	1.72 ± 0.36		

Table 6

Differential Cross Sections (mb/ster) of the Sixth, Seventh, and Eighth Excited States of ^{16}O at E_{CM} = 7.0 MeV

$^{6}Li(^{12}C,d)^{16}O^{*}$

9.58 MeV Level		9.84 MeV Level		10.26 MeV Level	
θ_{CM}	$d\sigma/d\Omega$	θ_{CM}	$d\sigma/d\Omega$	θ_{CM}	$d\sigma/d\Omega$
8.8	3.26 ± 0.36	8.9	0.63 ± 0.15	9.3	1.59 ± 0.24
26.2	1.78 ± 0.23	26.7	0.32 ± 0.19	28.0	0.99 ± 0.26
52.1	2.05 ± 0.10	53.1	0.18 ± 0.09	55.7	0.79 ± 0.12
68.9	1.70 ± 0.20	70.3	0.39 ± 0.10	73.9	0.95 ± 0.15
85.1	1.83 ± 0.28	87.0	0.16 ± 0.16	91.7	1.22 ± 0.21
100.6	1.51 ± 0.26	102.8	0.26 ± 0.20	108.7	1.77 ± 0.29
114.9	2.24 ± 0.36				

Table 7

Differential Cross Sections (mb/ster) of the Third, Fourth, and Fifth Excited States of ^{16}O at E_{CM} = 8.0 MeV

$^{6}Li(^{12}C,d)^{16}O^{*}$

6.92 MeV Level		7.12 MeV Level		8.88 MeV Level	
θ_{CM}	$d\sigma/d\Omega$	θ_{CM}	$d\sigma/d\Omega$	θ_{CM}	$d\sigma/d\Omega$
15.5	1.47 ± 0.10	15.5	0.89 ± 0.09	16.5	0.34 ± 0.03
45.8	0.88 ± 0.08	46.1	0.59 ± 0.12	48.8	0.43 ± 0.05
74.7	1.15 ± 0.09	75.3	0.45 ± 0.14	79.6	0.34 ± 0.04
100.8	1.23 ± 0.12	101.3	0.39 ± 0.07	94.0	0.30 ± 0.05
123.0	1.44 ± 0.16	123.6	0.39 ± 0.08	107.4	0.40 ± 0.05
144.6	2.41 ± 0.28	145.1	0.66 ± 0.14	130.2	0.59 ± 0.08
165.8	3.18 ± 0.43	166.1	0.89 ± 0.22	147.4	0.65 ± 0.11
				150.8	0.52 ± 0.12

Table 8

Excitation Functions (mb/ster) at $\theta_{LAB} = 30^{o}$ and 50^{o} for the Third, Fourth, and Fifth Excited States of ^{16}O

$^{6}Li(^{12}C,d)^{16}O^{*}$

E_{CM}	$\frac{d\sigma}{d\Omega}$ (6.92)	$\frac{d\sigma}{d\Omega}$ (7.12)	$\frac{d\sigma}{d\Omega}$ (8.88)
	$\theta_{LAB} = 30^{o}$ in mb/ster)		
6.00	1.78 ± 0.08	0.66 ± 0.06	0.53 ± 0.06
6.33	1.83 ± 0.08	0.52 ± 0.06	0.64 ± 0.06
6.67	1.77 ± 0.07	0.42 ± 0.06	0.58 ± 0.04
7.00	1.90 ± 0.05	0.44 ± 0.07	0.53 ± 0.04
7.33	1.54 ± 0.09	0.55 ± 0.09	0.47 ± 0.06
7.67	1.15 ± 0.10	0.57 ± 0.13	0.32 ± 0.05
8.00	0.88 ± 0.08	0.59 ± 0.12	0.43 ± 0.05
8.15	1.00 ± 0.14	0.32 ± 0.13	0.36 ± 0.06
	$\theta_{LAB} = 50^{o}$		
6.00	1.33 ± 0.12	0.96 ± 0.18	0.40 ± 0.07
6.33	1.13 ± 0.11	0.98 ± 0.16	0.43 ± 0.07
6.67	1.09 ± 0.09	1.00 ± 0.15	0.34 ± 0.06
7.00	0.80 ± 0.06	0.67 ± 0.04	0.22 ± 0.03
7.33	0.99 ± 0.08	0.45 ± 0.12	0.26 ± 0.04
7.67	0.96 ± 0.08	0.57 ± 0.14	0.39 ± 0.07
8.00	1.15 ± 0.09	0.45 ± 0.14	0.34 ± 0.04

Table 9

Coefficients and total cross sections determined in Legendre polynomial fits to the measured angular distribution

Level	$\sigma_{TOT}=4\pi A_0$ [a] in millibarns	A_1/A_0	A_2/A_0	A_3/A_0	A_4/A_0	A_5/A_0	A_6/A_0	A_7/A_0
$E_{CM}=7.0$								
g.s.	5.3±0.5	(0) [b]	1.5±0.1	(0) [b]	1.7±0.1			
6.06	5.5±0.5	-0.1 ±0.1	1.0±0.1	0.1±0.2	1.3 ±0.2			
6.14	14.9±0.6	0.3 ±0.1	0.3±0.1	-0.2±0.1	0.2±0.1	-0.04±0.12	-0.2 ±0.1	0.2±0.1
6.92	22.0±0.7	-0.37±0.03	0.9±0.1	-0.2±0.1	0.2±0.06	-0.04±0.06	-0.04±0.07	0.5±0.1
7.12	10.0±0.4	-0.20±0.05	0.6±0.1	0.2±0.1	0.8±0.1	0.8 ±0.1	0.2 ±0.1	-0.2±0.1
8.88	6.1±0.6	-0.09±0.13	1.1±0.1					
9.58	26.3± 7	-0.1 ±0.1	0.3±0.1					
9.84	4.1 ±1.5	-0.4 ±0.9	0.7±0.6					
10.36	18.2±4	-0.6 ±0.2	0.3±0.2	0.3±0.2				
$E_{CM}=8.0$								
6.92	17.6±1	-0.5 ±0.1	0.5±0.1	-0.2±0.1	0.4±0.1			
7.12	6.5±1	-0.1 ±0.1	0.7±0.2					
8.88	5.4±1	-0.2 ±0.1	0.3±0.1	0.0±0.2	-0.3±0.2			

a) Errors in σ_{TOT} include the effect of incomplete angular distributions as well as uncertainties in A_0.
b) Ground state was fit with even polynomials only.

Table 10

Incoming Transmission Coefficients for $^{6}Li + ^{12}C$ System Calculated from Computer Code ABACUS

$T_L^{IN}(E)$ $^{6}Li + ^{12}C$

L \ E_{CM}	3.4	7.0	8.0
0	0.55847	0.98826	0.99418
1	0.46737	0.98522	0.99280
2	0.29669	0.97683	0.98908
3	0.12362	0.95408	0.97923
4	0.03251	0.88904	0.95106
5	0.00594	0.70788	0.86371
6	0.00085	0.37260	0.62514
7		0.11092	0.27264
8		0.02345	0.07174
9		0.00437	0.01523'
10		0.00075	0.00298

Table 11

Outgoing Transmission Coefficients for d + ^{16}O System Calculated from Computer Code ABACUS at E_{CM} = 7.0 MeV

$T_L^{OUT}(E')$	^{16}O + d					E_{CM} = 7.0 MeV			
L Level	g.s.	6.06	6.14	6.92	7.12	8.88	9.58	9.84	10.36
0	0.99106	0.96976	0.96900	0.95966	0.95655	0.90221	0.84847	0.81804	0.72838
1	0.99677	0.98990	0.98927	0.98044	0.97712	0.90285	0.81622	0.76563	0.61960
2	0.98818	0.92042	0.91762	0.88237	0.87036	0.66136	0.48831	0.40975	0.24575
3	0.98316	0.85148	0.84415	0.74955	0.71739	0.30187	0.13931	0.09542	0.03742
4	0.95431	0.37599	0.36201	0.23246	0.20262	0.03490	0.01160	0.00710	0.00223
5	0.72448	0.07126	0.06668	0.03255	0.02650	0.00257	0.00067	0.00037	
6	0.26314	0.00547	0.00506	0.00222	0.00176				
7	0.033817	0.00048	0.00044						
8	0.00527								
9	0.00082								

Table 12

Outgoing Transmission Coefficients for d + ^{16}O System Calculated from Computer Code ABACUS at E_{CM} = 3.4 and 8 MeV

$T_L^{OUT}(E')$	^{16}O + d				
	E_{CM} = 3.4 MeV				
L Level	g.s.	6.06	6.14	6.92	7.12
0	0.98375	0.84102	0.83305	0.68819	0.62654
1	0.99771	0.80388	0.79062	0.55804	0.47005
2	0.96819	0.46782	0.44681	0.19658	0.14054
3	0.95929	0.12654	0.11446	0.02612	0.01576
4	0.74737	0.01022	0.00897	0.00145	0.00090
5	0.31830	0.00058	0.00049		
6	0.03912				
7	0.00419				
8	0.00051				

E_{CM} = 8.0 MeV

	6.92	7.17	8.88
0	0.97103	0.96019	0.94065
1	0.99091	0.98943	0.95802
2	0.92503	0.91833	0.80798
3	0.86341	0.84601	0.56186
4	0.40052	0.36548	0.10832
5	0.07980	0.06780	0.01102
6	0.00626	0.00516	0.00066
7	0.00056	0.00045	

Table 13

Comparison of Measured Total Cross Sections With Those Calculated by the Hauser-Feshbach Method ($\sigma_{H.F.}$)

E_{CM}	Level	σ_{exp} (mb)	$\sigma_{H.F.}$ (mb) [a]	σ_{DIR} [b] $\sigma_{exp}-\sigma_{H.F.}$	Tabulated [c] θ^2_α
7.0	g.s.	5.3 ± 0.5	4.8	0.5 ± 0.7	--
7.0	6.06	5.5 ± 0.5	2.8	2.7 ± 0.6	--
7.0	6.14	14.9 ± 0.6	14.7	0.2 ± 1.6	
7.0	6.92	22.0 ± 0.7	10.6	11.4 ± 1.3	--
7.0	7.12	10.0 ± 0.4	6.6	3.4 ± 0.8	--
7.0	8.88	6.1 ± 0.6	(6.1)	(0)	0
7.0	9.58	26.3 ± 7	3.1	23.2 ± 7	0.85
7.0	9.84	4.1 ± 1.5	4.3	-0.2 ± 1.5	0.0015
7.0	10.36	18.2 ± 4	4.3	13.9 ± 4	0.26
8.0	6.92	17.6 ± 1	8.2	9.4 ± 1	
8.0	7.12	6.5 ± 1	5.0	1.5 ± 1	
8.0	8.88	5.4 ± 1	(5.4)	(0)	

a) The error in this column is ± 10% for the 7 MeV and ± 19% for the 8 MeV data, arising from the use of σ_{TOT} of the 8.88 state for normalization.

b) $\sigma_{DIR} = \sigma_{TOT} - \sigma_{H.F.}$ The errors of σ_{TOT} and $\sigma_{H.F.}$ were combined quadratically.

c) Ajzenberg-Selove and Lauritsen (1959).

Table 14

Comparison of Measured Total Cross Section (σ_{exp}) at E_{CM} = 3.4 MeV (Heikkinen, 1966) with those Calculated by the Hauser-Feshbach Method ($\sigma_{H.F.}$)

Level	σ_{exp}	$\sigma_{H.F.}$	$\sigma_{DIR} = \sigma_{exp} - \sigma_{H.F.}$	σ_{DIR} [b] at E_{CM} = 7.0 MeV
g.s.	2.3 ± 0.2	(2.9)	(0)	0.5 ± 0.7
6.06	(7 ± 3) [a]	1.1	(6 ± 3)	2.7 ± 0.6
6.14	(4 ± 3) [a]	2.8	(1 ± 3)	0.2 ± 1.6
sum 6.06 + 6.14	11.3 ± 1.1	3.9	7.4 ± 1.1	2.9 ± 1.8
6.92	16.5 ± 1.6	1.9	14.6 ± 1.6	11.4 ± 1.3
7.12	5.7 ± 0.5	1.3	4.4 ± 0.6	3.4 ± 0.8

a) Estimated from deuteron spectra line shape for unresolved doublet

b) From Table 13.

Table 15

Reduced Alpha Widths of ^{16}O Levels

Level	σ_{DIR} (mb)	$\sigma_{PWBA}/\theta_\alpha^2$ a) (mb)	Extracted θ_α^2 d)	Previously Tabulated θ_α^2 b)
g.s.	0.5 ± 0.7	22.2	$\leq$ 0.05	--
6.06	2.7 ± 0.6	13.7	0.14-0.30	--
6.14	0.2 ± 1.6	99.8	$\leq$ 0.02	--
6.92	11.4 ± 1.3	54.2	0.15-0.27	--
7.12	3.4 ± 0.8	33.6	0.06-0.14	--
8.88	--	--	(0) c)	0
9.58	23.2 ± 7	27.4	(0.85) c)	0.85
9.84	-0.2 ± 1.5	19.1	$\leq$ 0.06	0.0015
10.36	13.9 ± 4	36.2	0.23-0.53	0.26

a) For calculation of σ_{PWBA} see Page 42.

b) Ajzenberg-Selove and Lauritsen (1959).

c) These values were not extracted, but serve as input data for normalization.

d) Range of values stated due to uncertainty in error estimation and for convenience of reader.

Table 16

The Parameters A_J, and B_J Determined in the Least Squares Fitting of the Heavy Ion Charge State Curves, listed along with the Ionization Velocities V_J. (Page 65)

	J =	1	2	3	4	5	6	7	8	9	10
	A_J	0.209	0.723	0.587							
Li	B_J	2.5	3.5	2							
	V_J	1.41	5.18	6.61							
	A_J	0.257	0.694	0.901	0.460						
Be	B_J	2	2	2	2.5						
	V_J	1.82	3.04	7.39	8.81						
	A_J	0.674	0.107	0.348	0.750	0.464					
B	B_J	2	2	3	3	3					
	V_J	1.72	1.99	2.69	9.58	10.98					
	A_J	(1.0)	0.753	0.428	0.212	0.218	0.519				
C	B_J	(2)	2	3	3	5	2				
	V_J	2.00	2.95	4.13	4.75	11.92	13.70				
	A_J	1.223	1.011	0.870	0.293	0.437	0.314	0.780			
N	B_J	2	2	2	3.5	2	2.5	3.5			
	V_J	2.27	3.26	4.13	5.26	5.89	13.99	15.32			
	A_J	0.685	1.640	1.255	0.456	0.632	0.113	0.460	0.681		
O	B_J	2	3	3	2.5	3.5	3.5	2	3		
	V_J	2.21	3.55	4.41	5.28	6.32	7.00	16.18	17.15		
	A_J	(2.5)	(2.5)	(1.2)	(1.2)	0.410	0.400	0.959	0.276	1.025	
F	B_J	(3)	(2)	(2)	(3)	2	2	2.5	2.5	3.5	
	V_J	2.48	3.58	4.71	5.59	6.33	7.42	8.11	18.20	19.67	
	A_J	(2.5)	2.661	2.358	1.333	1.310	1.167	0.405	0.140	0.647	0.427
Ne	B_J	(2)	3	2	2	3	4	2.5	3.5	2.5	3.5
	V_J	2.75	3.78	4.72	5.81	6.67	7.42	8.53	9.19	20.23	21.88

Values in parentheses have been set arbitrarily without minimization procedure due to scarcity of data.

Table 17

Source Magnet Current Settings for Injection of Various Negative Beams into the Tandem Accelerator. Calculated Current Settings are from

$$I_{CALC} = 10.25\sqrt{E.A}$$ (see page

Process Exchange in Exchange out	Beam	A Mass	E in keV	I_{CALC} (m.A)	I_{EXP} (m.A)
(α^0, α^-)	$^4He^-$	4	40	130	134
(α^+, α^-)	$^4He^-$	4	80	183	195
(α^+, α^-)	$^4He^-$	4	90	195	210
$(^3He^+, ^3He^-)$	$^3He^-$	3	90	169	170
(H_3^+, H^-)	H^-	1	53.3	75	72
(H^0, H^-)	H^-	1	40	65	63
(H_2^+, H^-)	H^-	1	60	79	77
(D_2^+, D^-)	D^-	2	60	112	112
(O_3^+, O^-)	$^{16}O^-$	16	66.7	336	360
(O^+, O^-)	$^{16}O^-$	16	80	316	410
(O^0, O^-)	$^{16}O^-$	16	40	259	?
(S^0, S^-)	$^{32}S^-$	32	40	366	415
(C_2^+, C^-)	$^{12}C^-$	12	63.8	287	290
(CH_4^+, C^-)	$^{12}C^-$	12	74.5	299	290
(C^+, C^-)	$^{12}C^-$	12	85	320	290
(C^0, C^-)	$^{12}C^-$	12	42.5	232	290
(CH_5^+, C^-)	$^{12}C^-$	12	72.6	295	290

Figure 1

Energy level diagram showing the excited states of the nucleus ^{16}O and the systems $^{12}C + \alpha$, ^{18}F - d, and $^{6}Li + ^{12}C$ - d relative to the ground state energy of ^{16}O. (Pages 1, 9, and 58.)

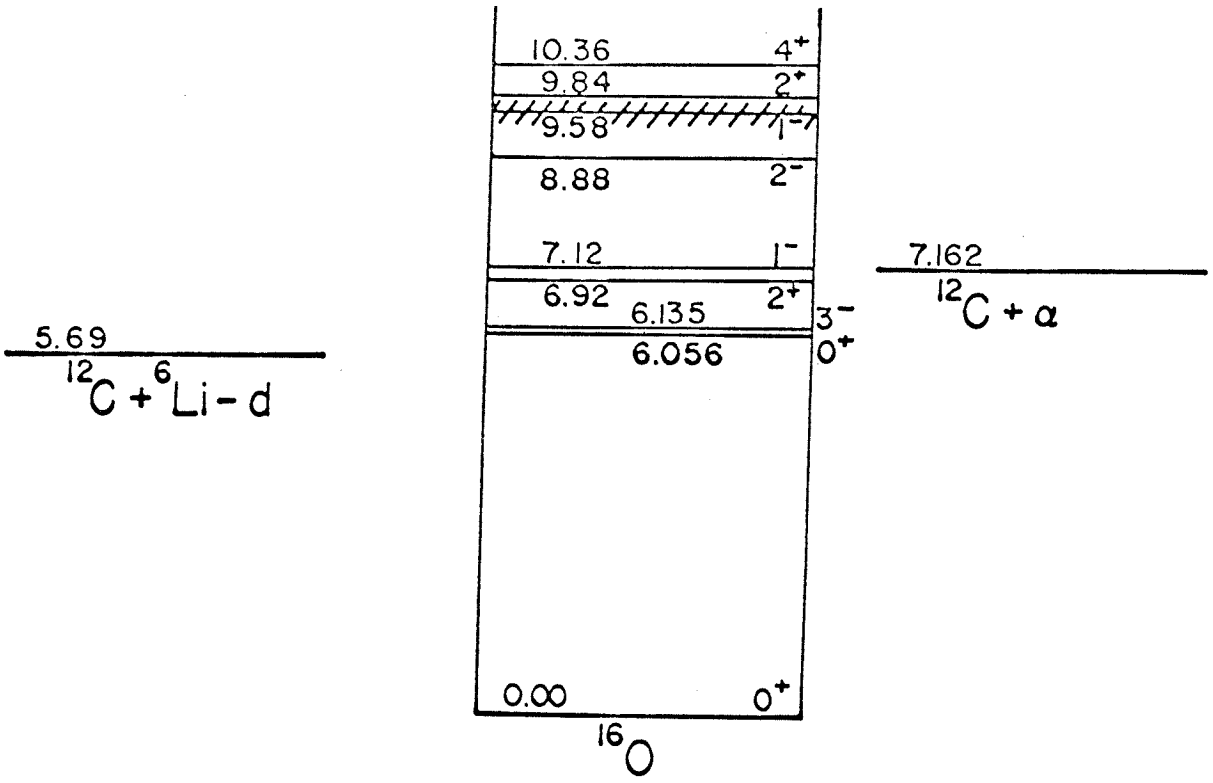
10.36
4+
9.84
2+
9.58
1-
8.88
2-
7.12
1-
6.92
2+
6.135
3-
6.056
0+
0.00
0+
16O
5.69
12C + 6Li - d
7.162
12C + α
-7.154
18F - d

FIGURE 1

Figure 2

Schematic diagram of target chamber viewed from the top. The target is turned to 45° with respect to the beam direction. The beam catcher and target are electrically connected and biased to + 1800 volts. The cage has openings for the beam entrance and spectrometer entrance aperture, and is biased to -1500 volts. The monitor counter is at $\theta_{LAB} = 135^{o}$. (Page 13.)

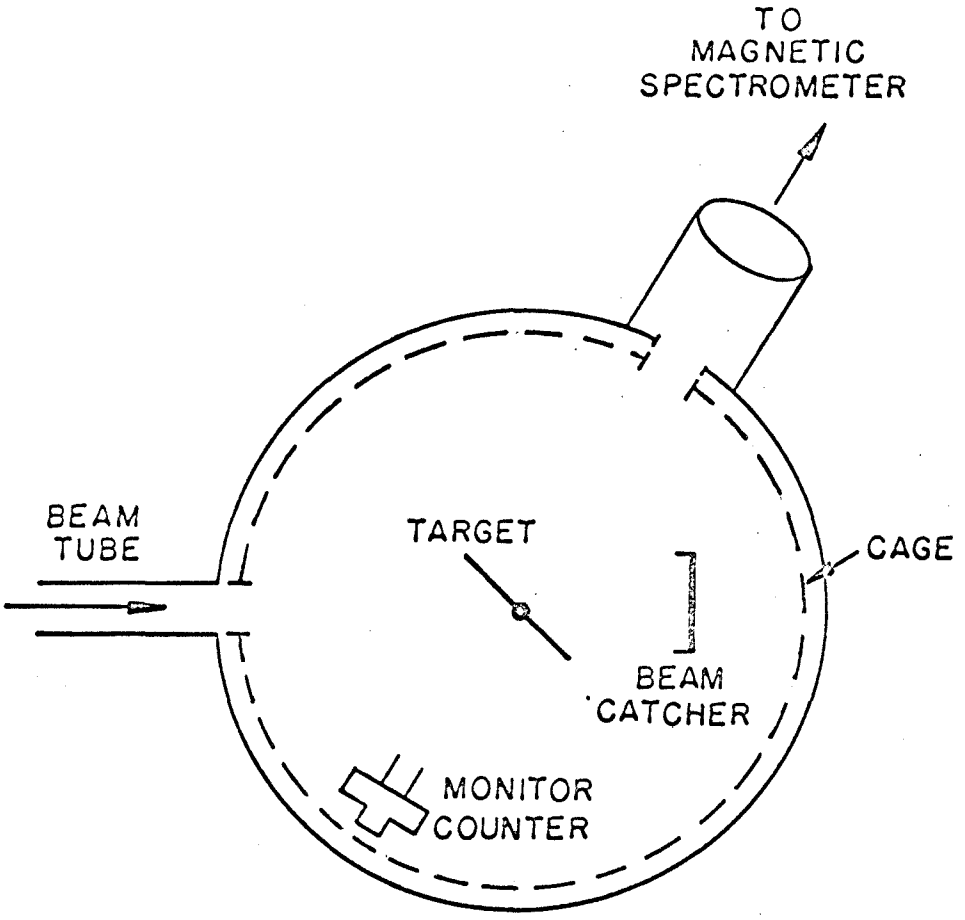
TO
MAGNETIC
SPECTROMETER
BEAM
TUBE
TARGET
CAGE
BEAM
CATCHER
MONITOR
COUNTER

FIGURE 2

Figure 3

Schematic diagram of the target chamber and furnace system with the target in position for lithium evaporation. The furnaces and target chamber are drawn as if they were made of transparent material. (Page 14.)

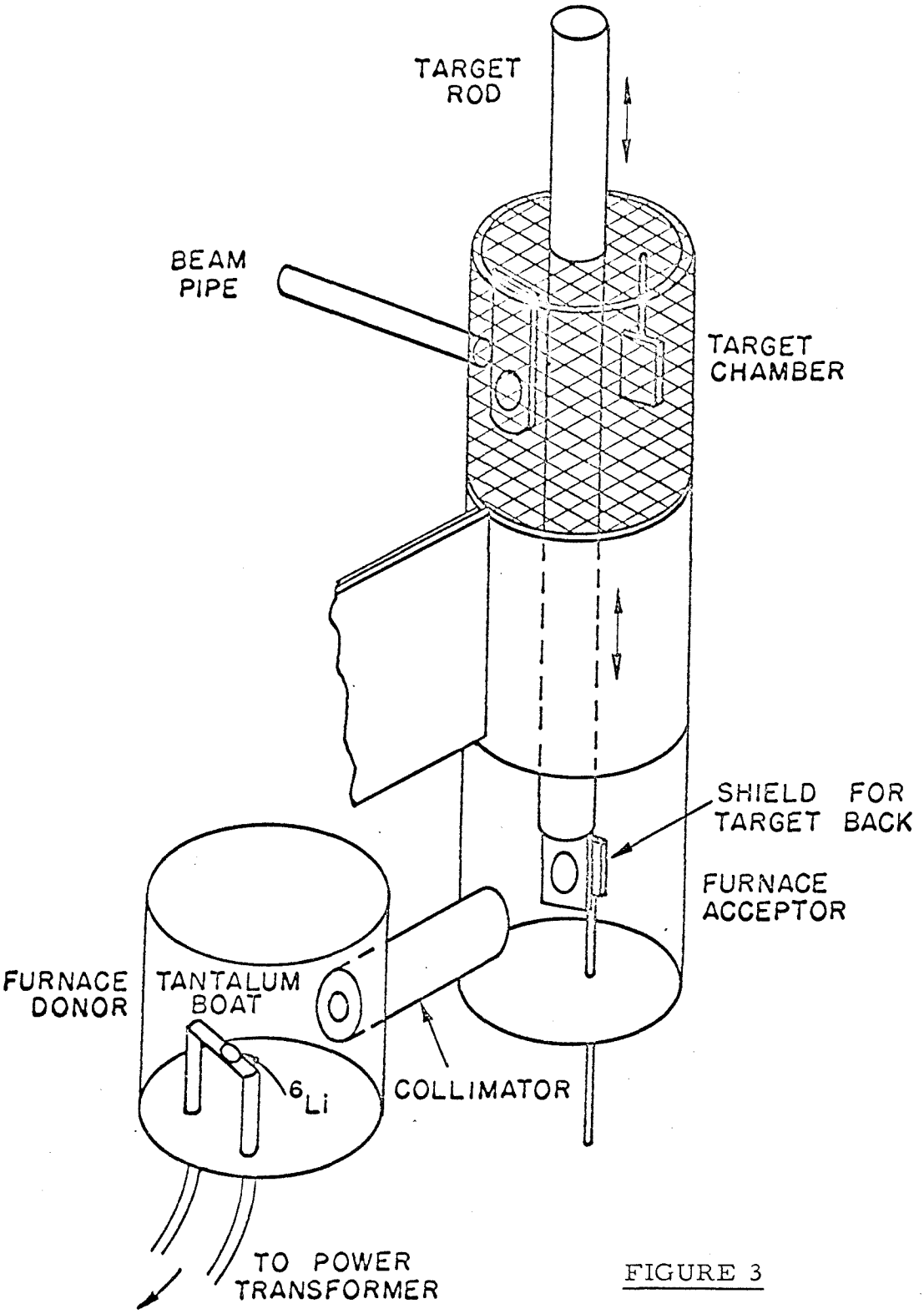
TARGET ROD
BEAM PIPE
TARGET CHAMBER
SHIELD FOR TARGET BACK
FURNACE ACCEPTOR
FURNACE DONOR
TANTALUM BOAT
^6Li
COLLIMATOR
TO POWER TRANSFORMER

FIGURE 3

Figure 4

A typical spectrum of ^{12}C peaks taken before and after evaporation of ^{6}Li on the Ni foil backing. These spectra show the elastically scattered ^{12}C particles in 5+ charge state as detected in the magnetic spectrometer. The scattered particles are detected at $\theta_{LAB} = 30^{o}$ and have been scattered from the 1000 Å Ni foil. This data was obtained in the preparation of the target on October 24, 1965 and the change in the center of the peak position of 77 kHz corresponds to a thickness in energy loss of 113 keV. (Page 15.)

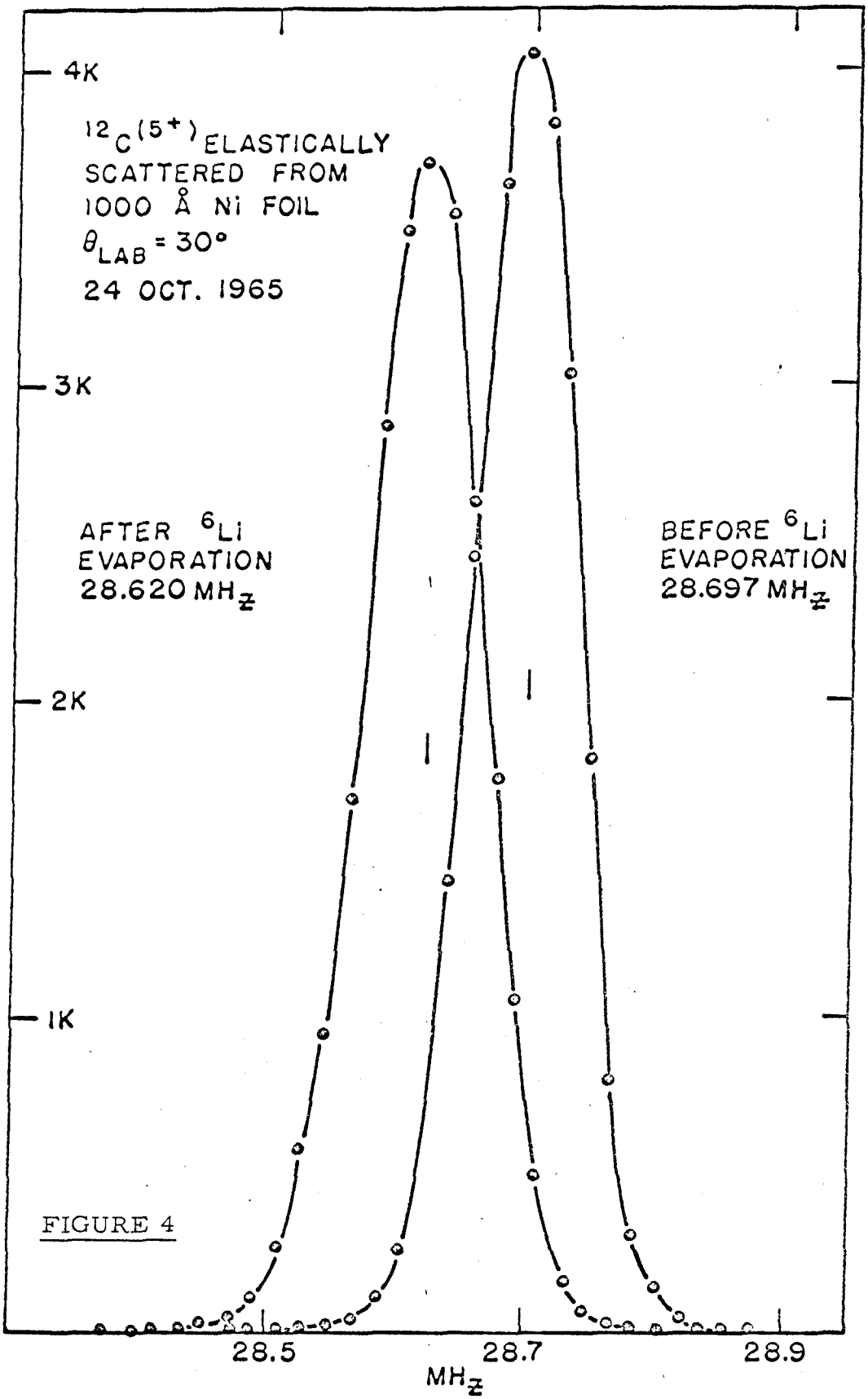
4K
3K
2K
1K
$^{12}C(5^+)$ ELASTICALLY SCATTERED FROM 1000 Å Ni FOIL
$\theta_{LAB} = 30°$
24 OCT. 1965
AFTER ^6Li EVAPORATION
28.620 MH_Z
BEFORE ^6Li EVAPORATION
28.697 MH_Z
28.5
28.7
28.9
MH_Z

FIGURE 4

Figure 5

Plot of target and tail factors F_1 and F_2 as a function of time for a case in which the behavior becomes independent of time, July 12, 1965. (Page 21.)

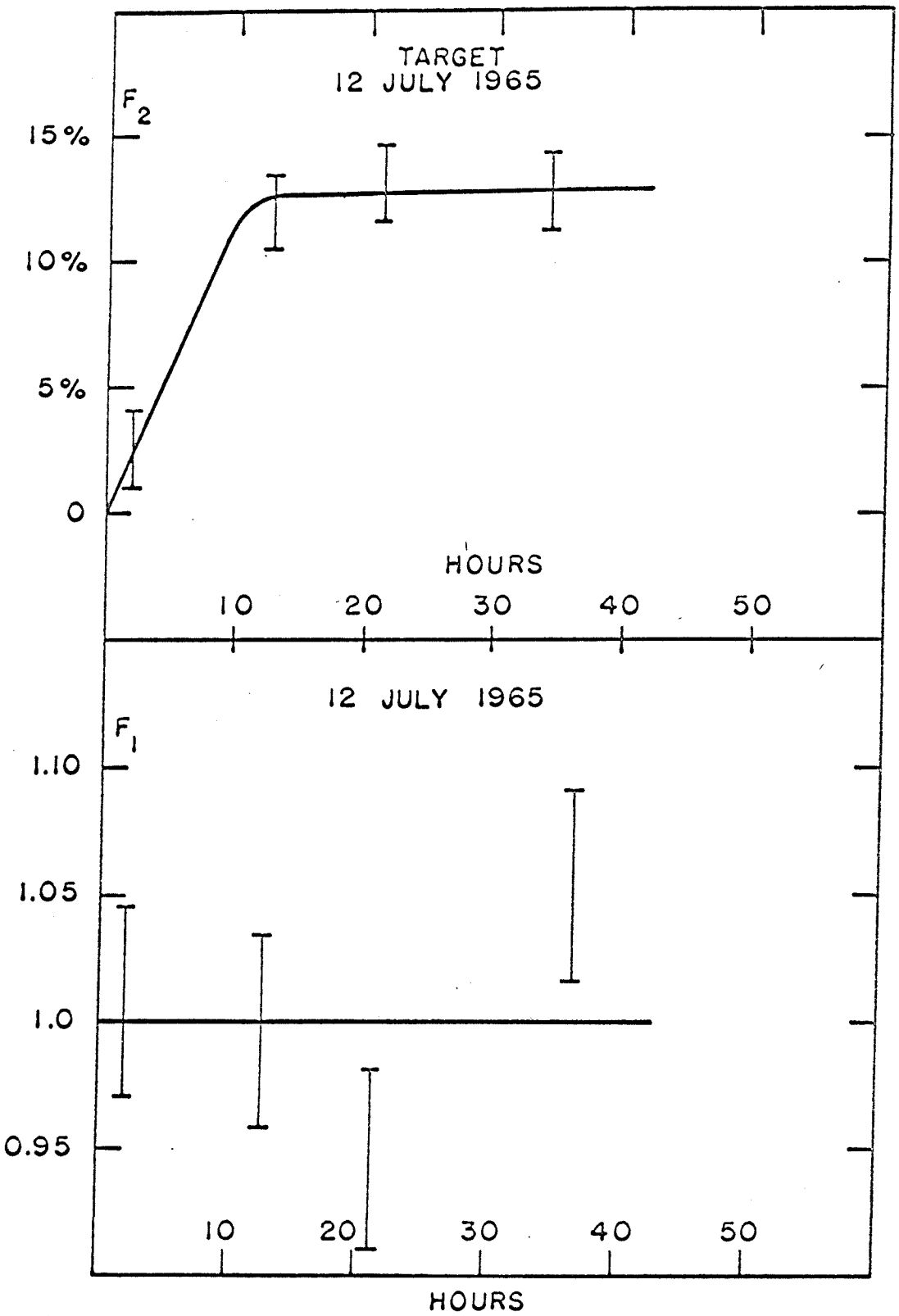
TARGET
12 JULY 1965
F2
15%
10%
5%
0
HOURS
10
20
30
40
50
12 JULY 1965
F1
1.10
1.05
1.0
0.95
10
20
30
40
50
HOURS

FIGURE 5

Figure 6

Plot of target and tail factors F_1 and F_2 as a function of time for a case in which the behavior in which the behavior is linear with time, October 24, 1965. (Page 21.)

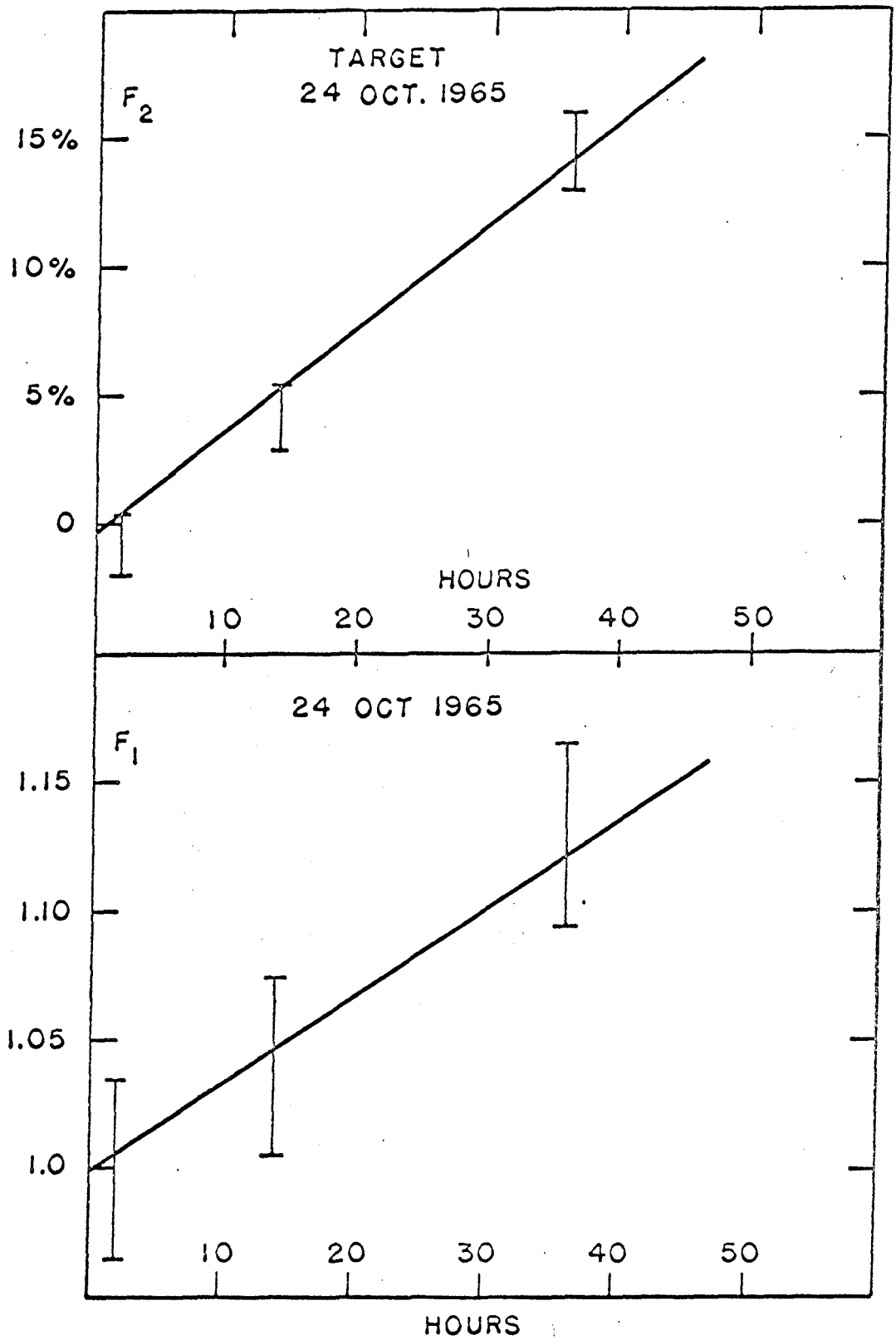
TARGET
24 OCT. 1965
F_2
15%
10%
5%
0
HOURS
10
20
30
40
50
24 OCT 1965
F_1
1.15
1.10
1.05
1.0
10
20
30
40
50
HOURS

FIGURE 6

Figure 7

Deuteron spectrum taken in the magnetic spectrometer at $\theta_{LAB} = 15^{o}$ and $E_{CM} = 7.0$ MeV. The arrows indicate the calculated positions of deuteron peaks corresponding to various excited states in ^{16}O. (Page 18, 21, and 25.)

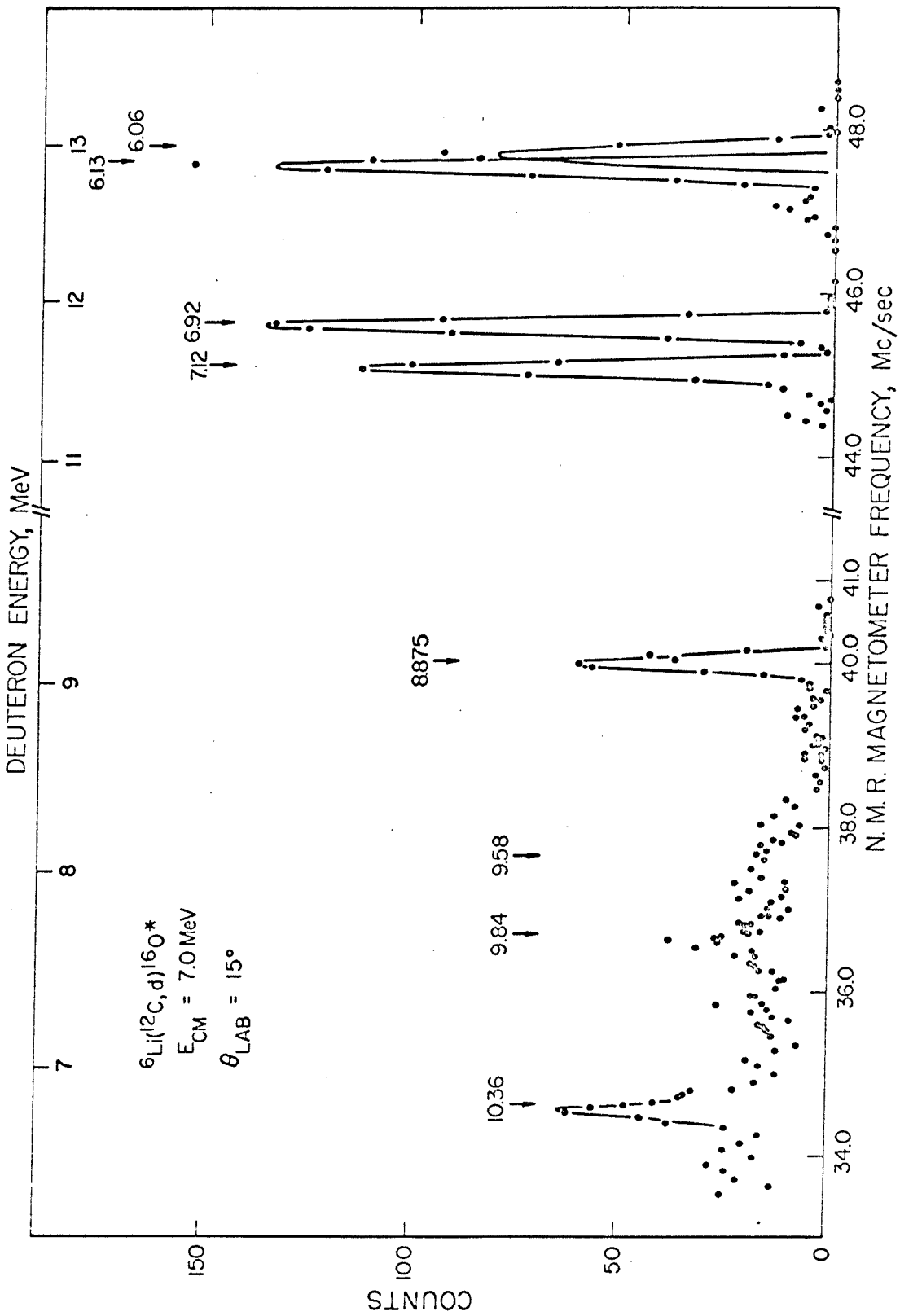
DEUTERON ENERGY, MeV
7
8
9
11
12
13
N. M. R. MAGNETOMETER FREQUENCY, Mc/sec
34.0
36.0
38.0
40.0
41.0
44.0
46.0
48.0
COUNTS
0
50
100
150
$^6Li(^{12}C, d)^{16}O^*$
E_{CM} = 7.0 MeV
θ_{LAB} = 15°
10.36
9.84
9.58
8875
7.12
6.92
6.13
6.06

Figure 7

Figure 8

Deuteron spectrum taken in the magnetic spectrometer at $\theta_{LAB} = 30^{o}$ and $E_{CM} = 7.0$ MeV. The arrows indicate the calculated positions of deuteron peaks corresponding to various excited states in $^{16}0$. (Pages 18 and 25)

FIGURE 8

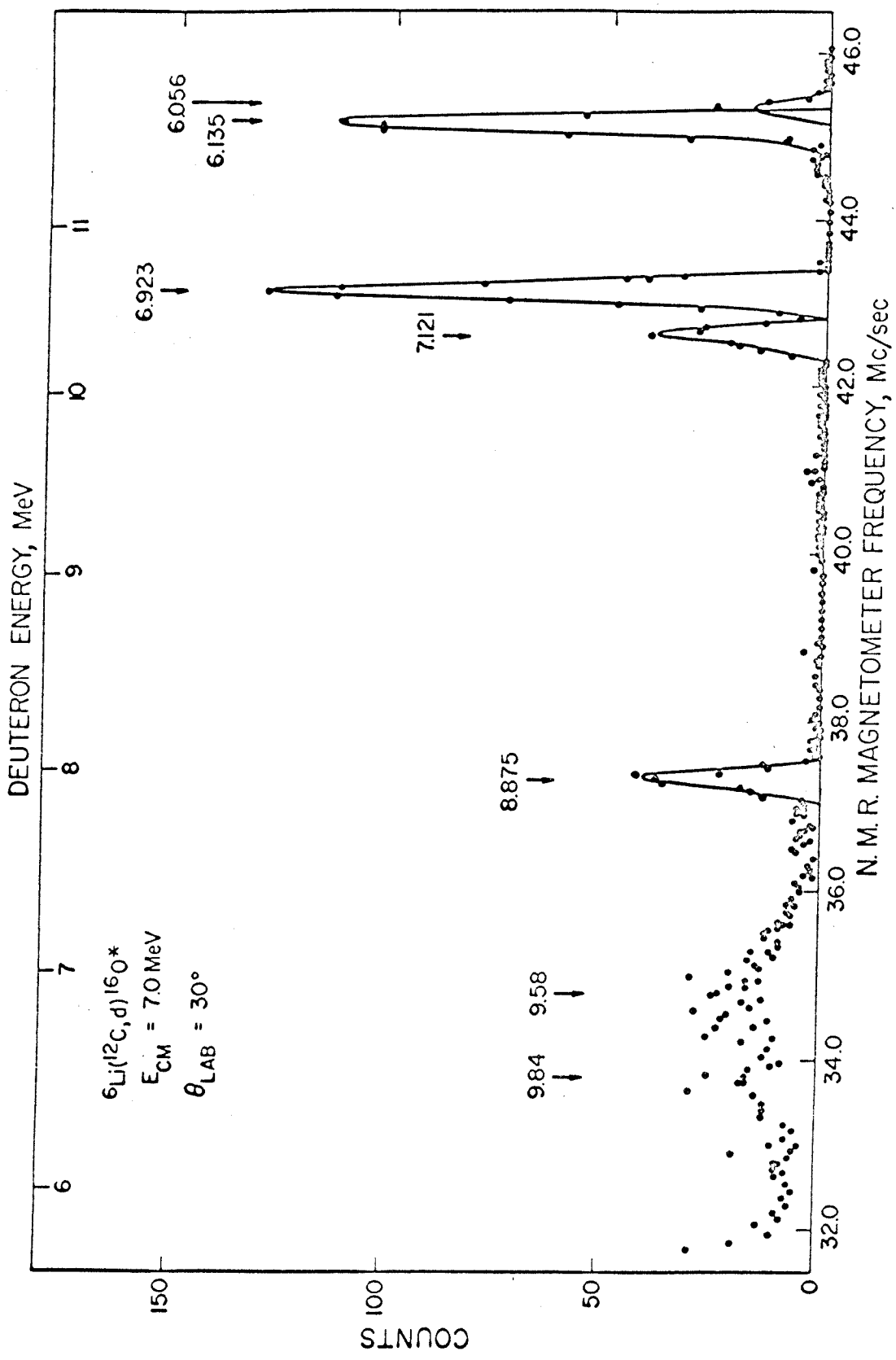
DEUTERON ENERGY, MeV
6
7
8
9
10
11
N. M. R. MAGNETOMETER FREQUENCY, Mc/sec
32.0
34.0
36.0
38.0
40.0
42.0
44.0
46.0
COUNTS
0
50
100
150
$^{6}Li(^{12}C,d)^{16}O^{*}$
E_{CM} = 7.0 MeV
θ_{LAB} = 30°
9.84
9.58
8.875
7.121
6.923
6.135
6.056

Figure 9

Spectrum of deuterons in the region of excitation of the 6.1 MeV doublet at $\theta_{LAB} = 15^{o}$ and $E_{CM} = 7.0$ MeV. The solid curves show the line shapes used in separating the yields from the two levels. (Page 26.)

FIGURE 9

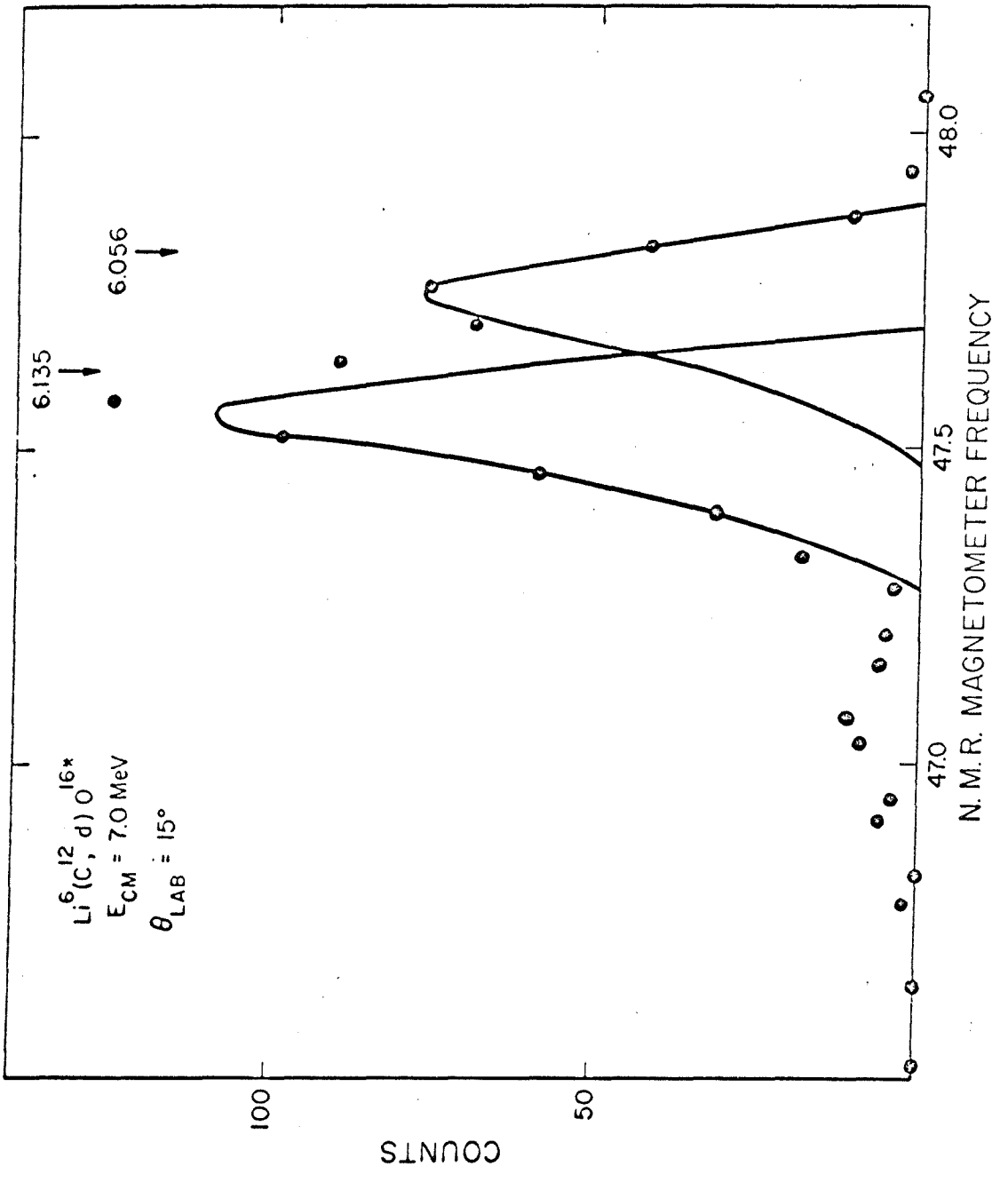
6.056
6.135
$Li^6(C^{12}, d)O^{16*}$
E_{CM} = 7.0 MeV
θ_{LAB} = 15°
100
50
COUNTS
47.0
47.5
48.0
N.M.R. MAGNETOMETER FREQUENCY

Figure 10

Histogram of the values of $d\sigma/dr$ for the formation of the third excited state of $^{16}0$ at $\theta_{LAB} = 30^{o}$ and $E_{CM} = 7.0$ MeV obtained from using the energy loss determination of the target thickness. The arrow indicates the value obtained by the normalization procedure applied to the measurements. (Page 27)

FIGURE 10

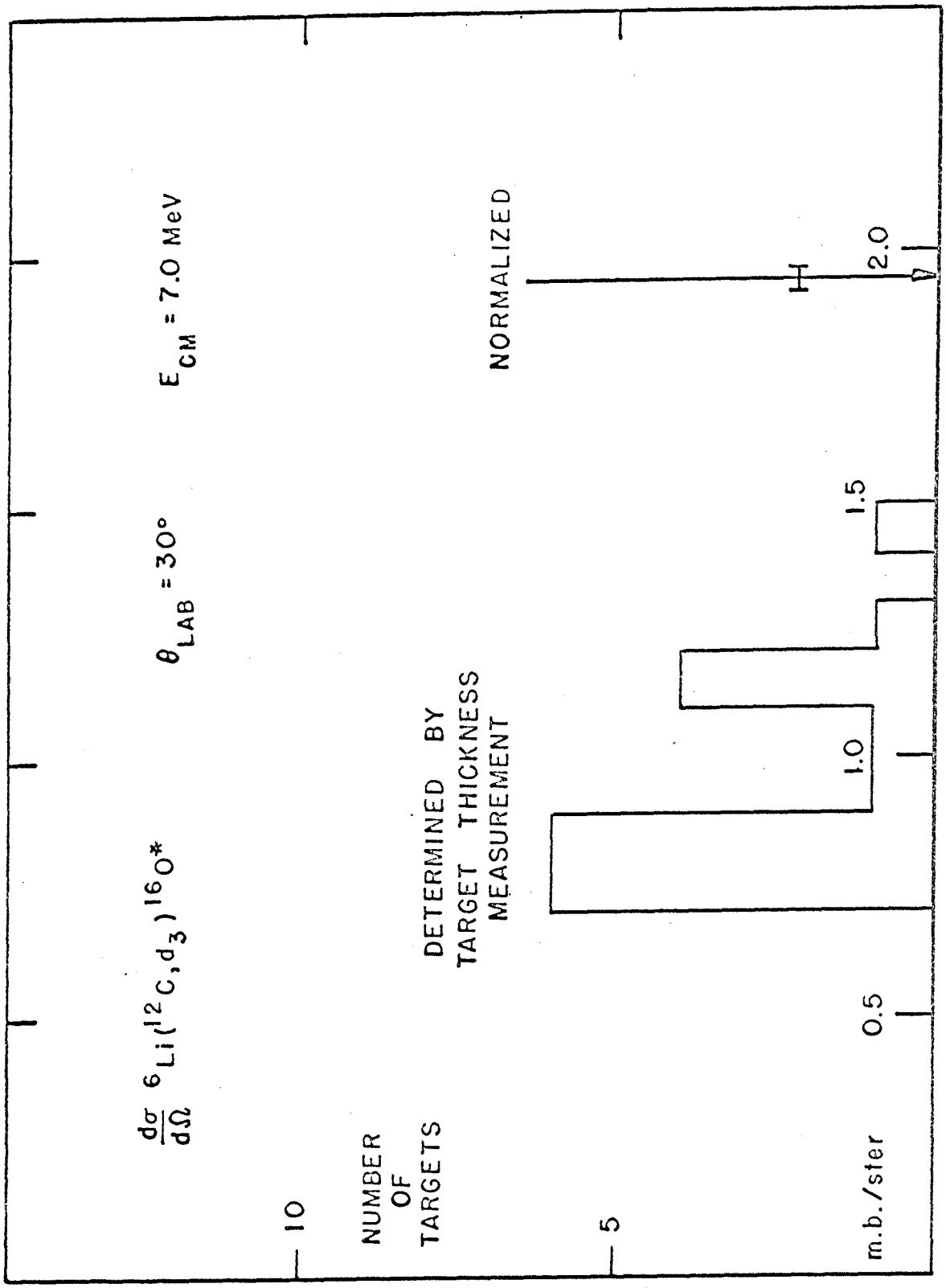
$\frac{d\sigma}{d\Omega}$ $^{6}Li(^{12}C,d_3)^{16}O^*$
$\theta_{LAB} = 30°$
$E_{CM} = 7.0$ MeV
NORMALIZED
DETERMINED BY TARGET THICKNESS MEASUREMENT
NUMBER OF TARGETS
10
5
m.b./ster
0.5
1.0
1.5
2.0

Figure 11

Angular distribution of deuterons leading to the ground, first, and second excited states of ^{16}O at E_{CM} = 7.0 MeV. The solid curves are calculated from the Legendre polynomial fits. (Page 28.)

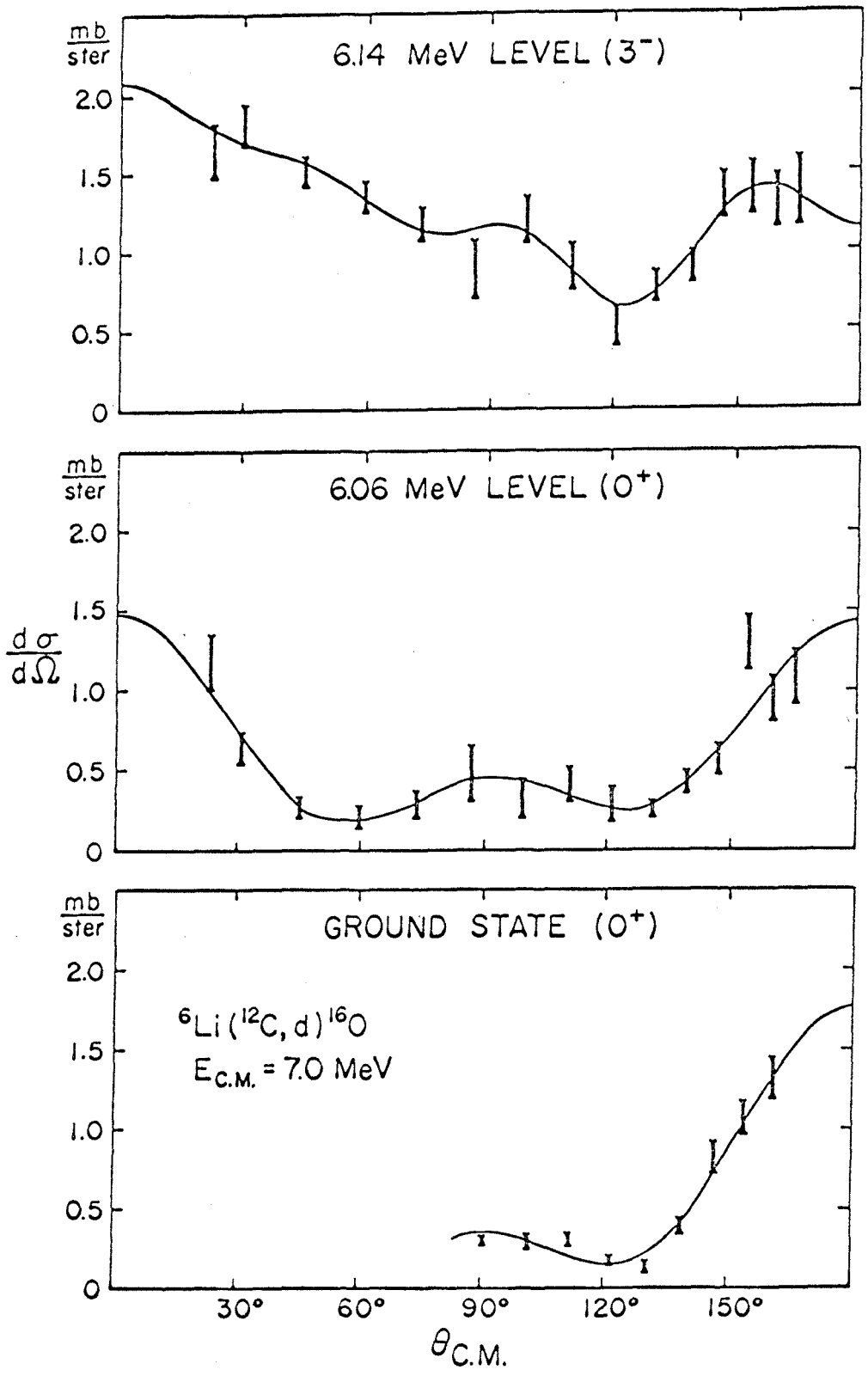
6.14 MeV LEVEL (3⁻)
6.06 MeV LEVEL (0⁺)
GROUND STATE (0⁺)
mb/ster
dσ/dΩ
2.0
1.5
1.0
0.5
0
$^{6}Li(^{12}C, d)^{16}O$
$E_{C.M.}$ = 7.0 MeV
30°
60°
90°
120°
150°
$\theta_{C.M.}$

FIGURE 11

Figure 12

Angular distribution of deuterons leading to the third, fourth, and fifth excited states of ^{16}O at E_{CM} = 7.0 MeV. The solid curves are calculated from the Legendre polynomial fits. (Page 28.)

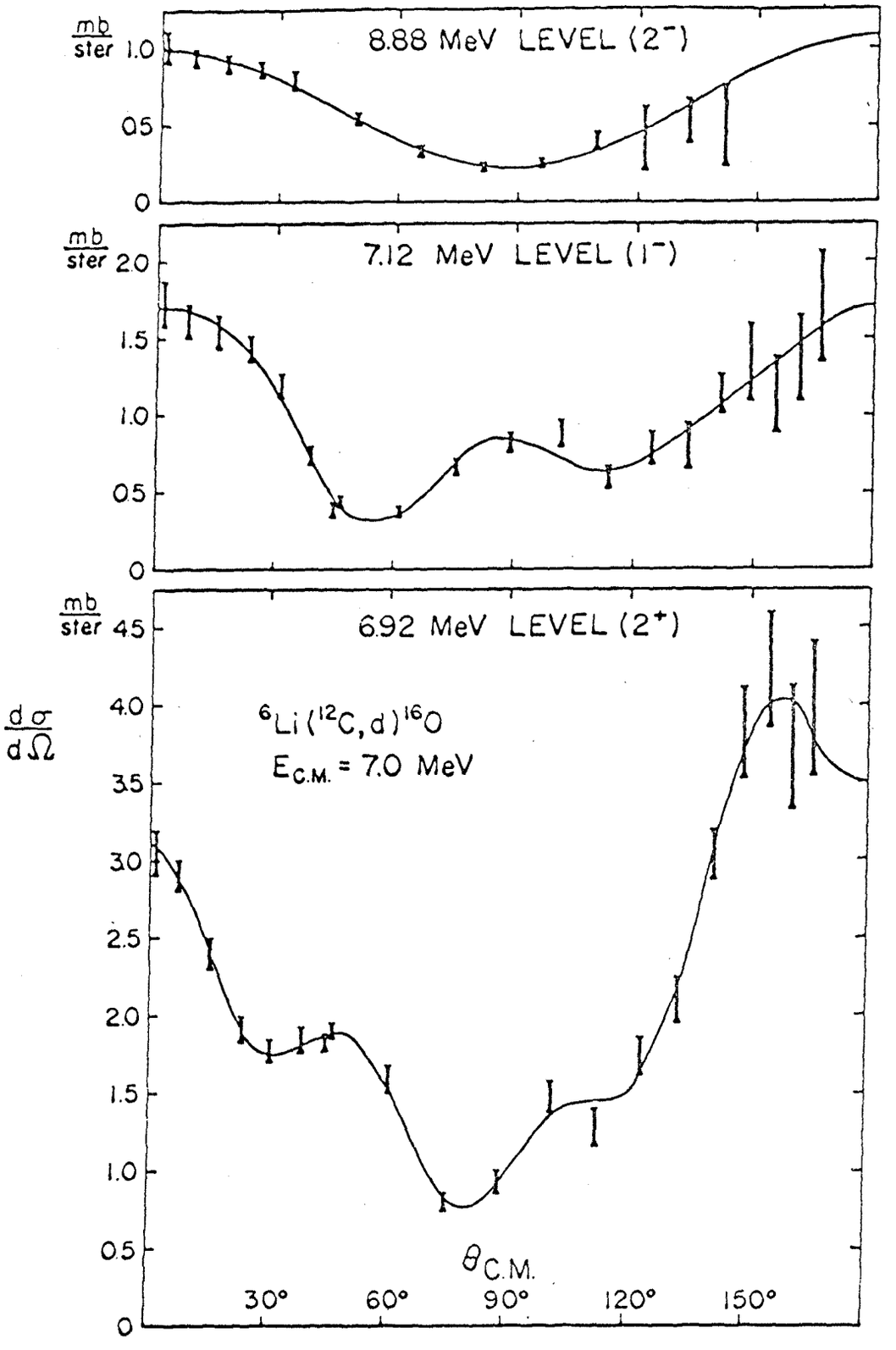
8.88 MeV LEVEL (2⁻)
7.12 MeV LEVEL (1⁻)
6.92 MeV LEVEL (2⁺)
mb/ster
dσ/dΩ
⁶Li(¹²C,d)¹⁶O
E c.m. = 7.0 MeV
θ C.M.
1.0
0.5
0
2.0
1.5
4.5
4.0
3.5
3.0
2.5
30°
60°
90°
120°
150°

FIGURE 12

Figure 13

Angular distribution of deuterons leading to the sixth, seventh, and eighth excited states of ^{16}O at E_{CM} = 7.0 MeV. The solid curves are calculated from the Legendre polynomial fits. (Page 28.)

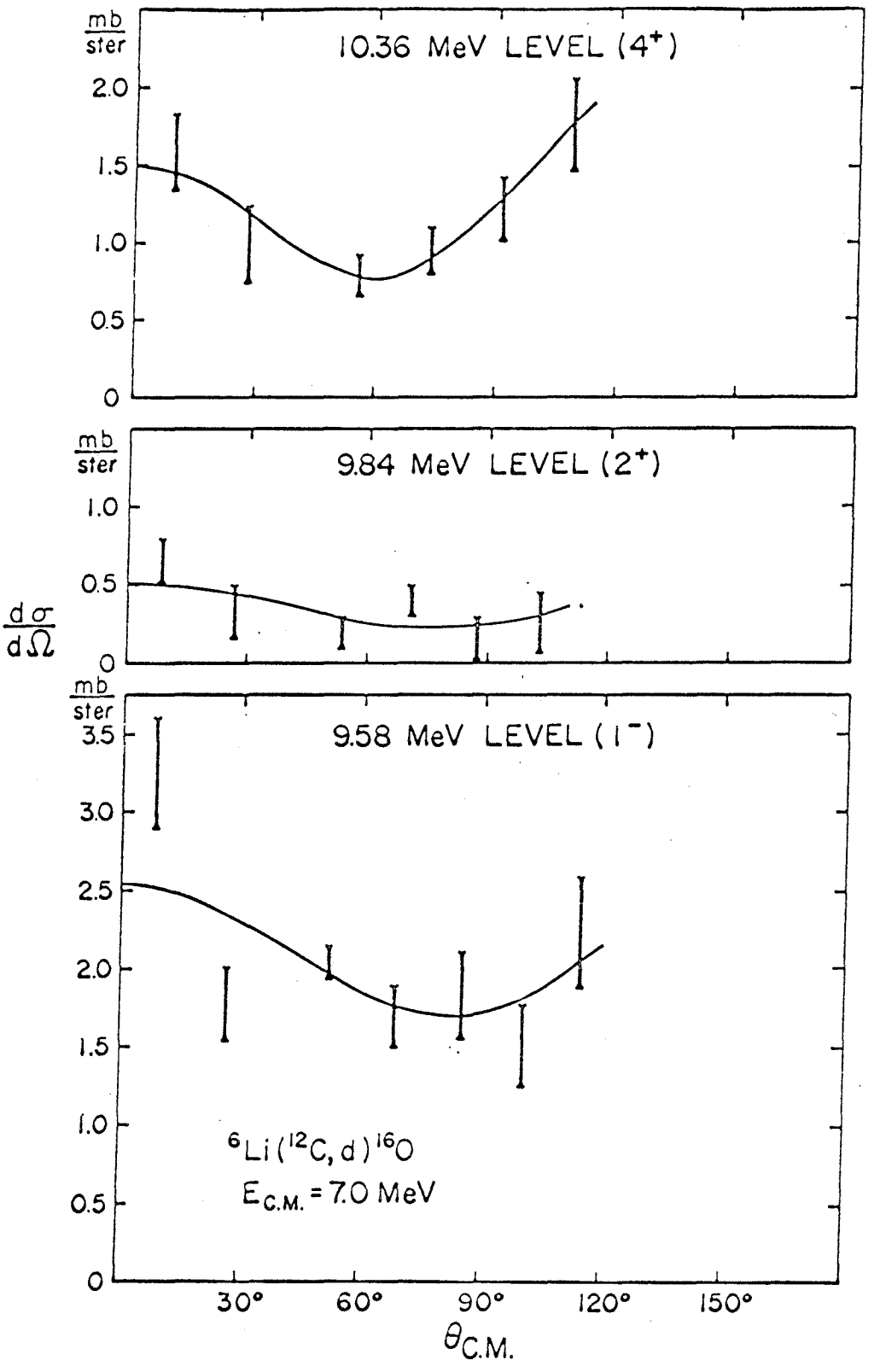
10.36 MeV LEVEL (4+)
9.84 MeV LEVEL (2+)
9.58 MeV LEVEL (1−)
mb/ster
dσ/dΩ
2.0
1.5
1.0
0.5
0
3.5
3.0
2.5
30°
60°
90°
120°
150°
θC.M.
6Li(12C, d)16O
EC.M. = 7.0 MeV

FIGURE 13

Figure 14

Angular distributions of deuterons leading to the third, fourth, and fifth excited states of $^{16}0$ at E_{CM} = 8.0 MeV. The solid curves are calculated from the Legendre polynomial fits. (Page 28.)

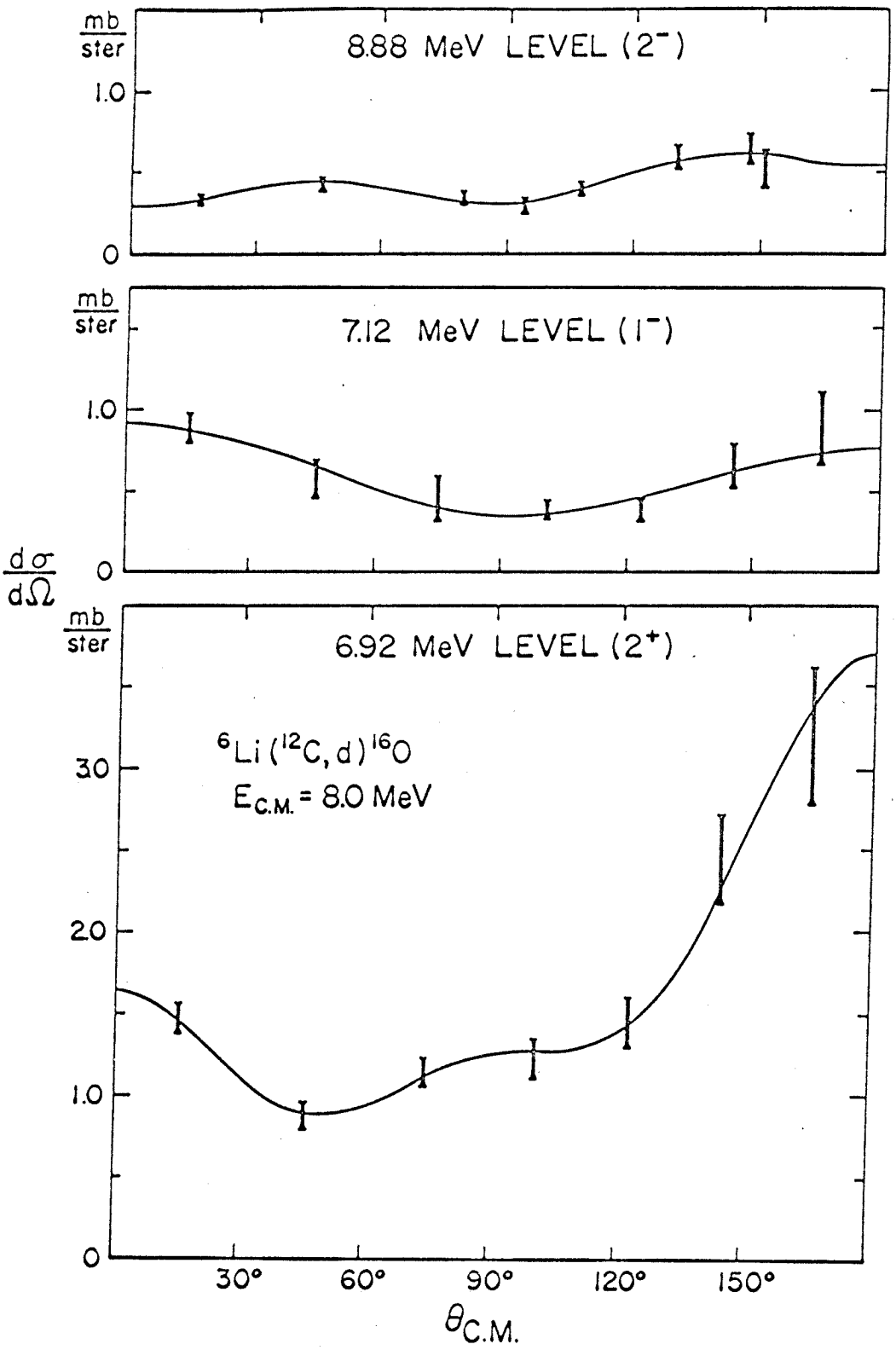
mb/ster
8.88 MeV LEVEL (2⁻)
1.0
0
mb/ster
7.12 MeV LEVEL (1⁻)
1.0
0
dσ/dΩ
mb/ster
6.92 MeV LEVEL (2⁺)
$^{6}Li(^{12}C,d)^{16}O$
$E_{C.M.}$ = 8.0 MeV
30
20
1.0
0
30°
60°
90°
120°
150°
$\theta_{C.M.}$

FIGURE 14

Figure 15

Excitation functions for the third, fourth, and fifth excited states of ^{16}O formation at $\theta_{LAB} = 30^{o}$ and $\theta_{LAB} = 50^{o}$. (Page 28.)

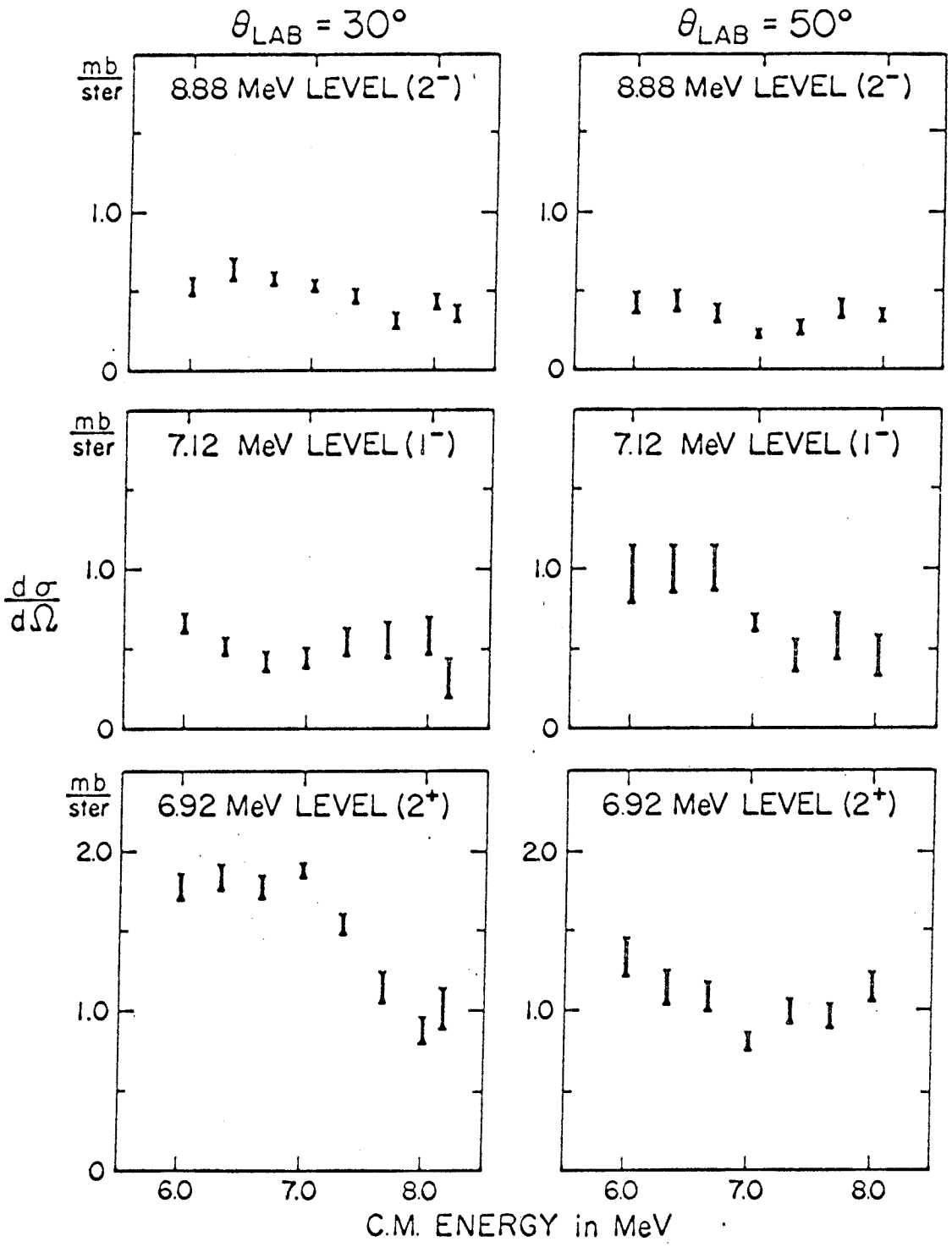
θLAB = 30°
θLAB = 50°
mb/ster
8.88 MeV LEVEL (2⁻)
7.12 MeV LEVEL (1⁻)
6.92 MeV LEVEL (2⁺)
dσ/dΩ
1.0
0
2.0
6.0
7.0
8.0
C.M. ENERGY in MeV

FIGURE 15

Figure 16

Deuteron angular distributions to the fifth excited state of ^{16}O at E_{CM} = 7.0 and 8.0 MeV compared with the calculated Hauser-Feshbach angular distributions normalized to the total cross section for these levels. (Page 44.)

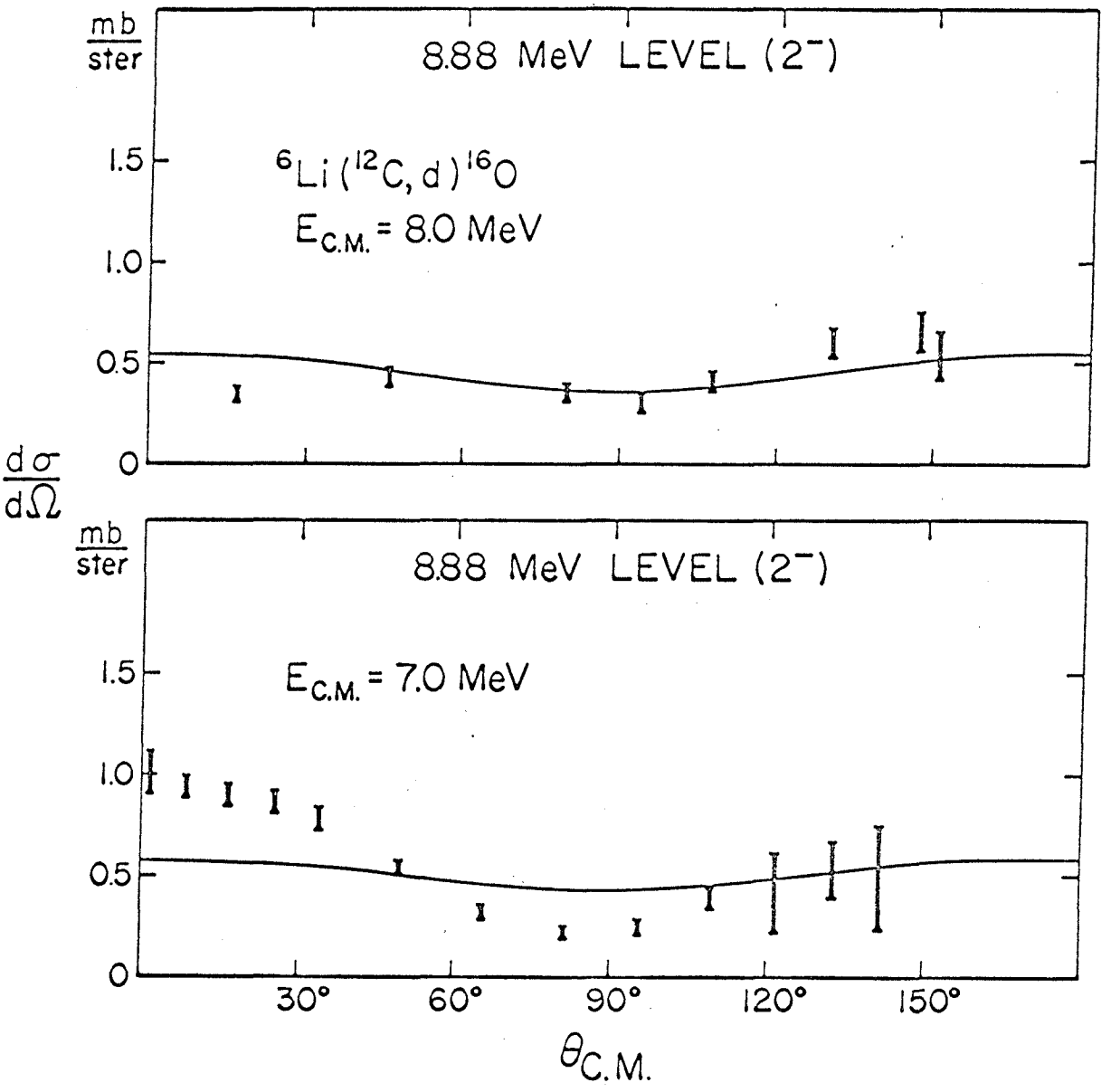
mb
ster
8.88 MeV LEVEL (2⁻)
$^{6}Li(^{12}C, d)^{16}O$
$E_{C.M.}$ = 8.0 MeV
1.5
1.0
0.5
0
$\frac{d\sigma}{d\Omega}$
mb
ster
8.88 MeV LEVEL (2⁻)
$E_{C.M.}$ = 7.0 MeV
1.5
1.0
0.5
0
30°
60°
90°
120°
150°
$\theta_{C.M.}$

FIGURE 16

Figure 17

Lithium charge state curves. Solid curves have been calculated using the parameters, A_J, B_J, and V_J listed below and discussed in Appendix I. The data points have been plotted with the symbols: $\phi_0 = 0$, $\phi_1 = \bullet$, $\phi_2 = x$, $\phi_3 = \Delta$. The parameters used were: (Pgs. 63 and 66.)

J	A_J	B_J	V_J (in 10^8 cm/sec)
1	0.209	2.5	1.41
2	0.723	3.5	5.18
3	0.587	2	6.61

The average deviation per point is 0.03.

FIGURE 17

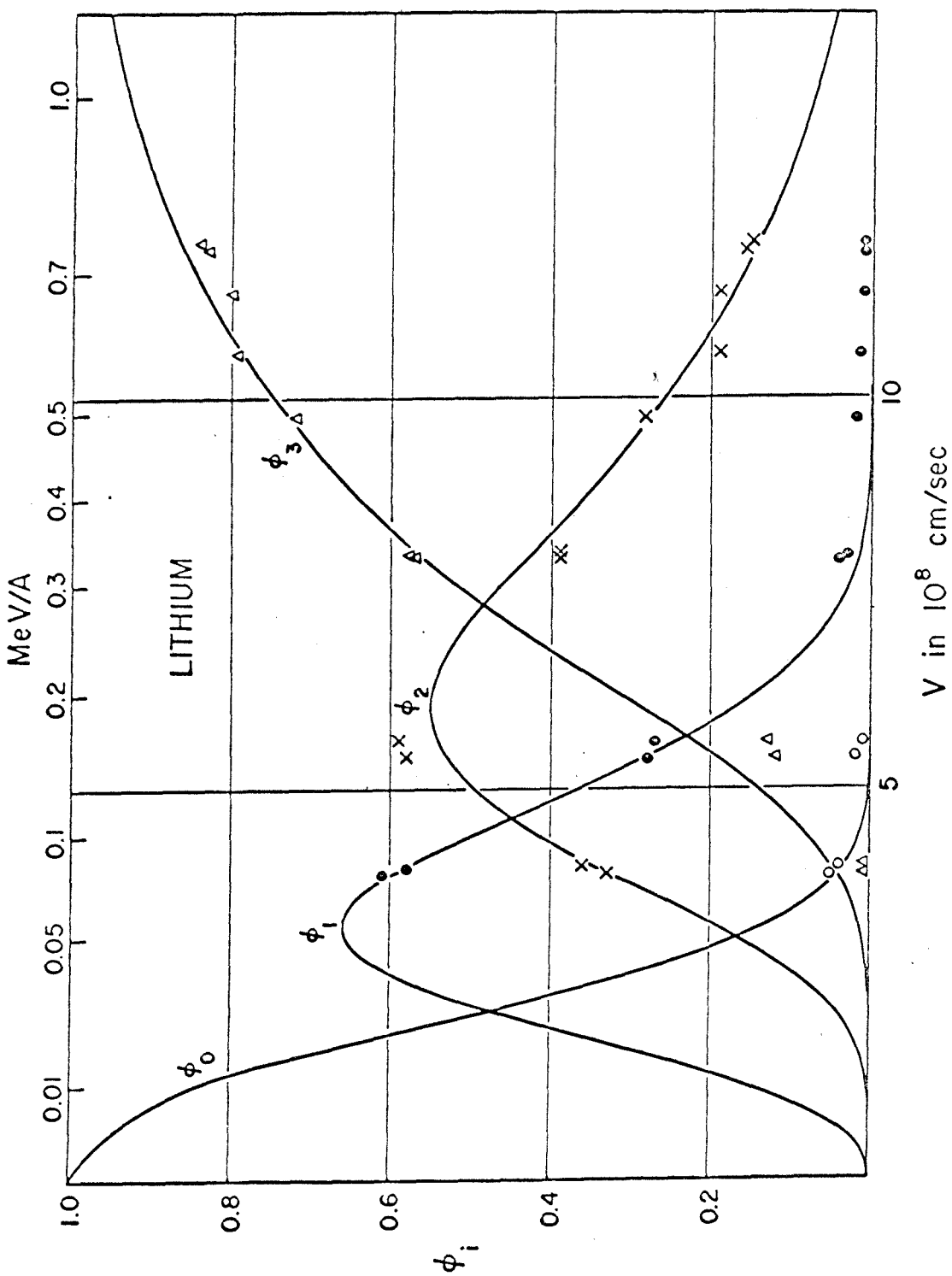
LITHIUM
MeV/A
1.0
0.7
0.5
0.4
0.3
0.2
0.1
0.05
0.01
ϕ_0
ϕ_1
ϕ_2
ϕ_3
ϕ_i
1.0
0.8
0.6
0.4
0.2
V in 10^8 cm/sec
10
5

Figure 18

Beryllium charge state curves. Solid curves have been calculated using the parameters, A_J, B_J, and V_J listed below and discussed in Appendix I. The data points have been plotted with the symbols: $\phi_0 = 0$, $\phi_1 = \bullet$, $\phi_2 = x$, $\phi_3 = \Delta$, and $\phi_4 = \square$. The parameters used were: (Pages 63 and 66.)

J	A_J	B_J	V_J (in 10^8 cm/sec)
1	0.257	2	1.82
2	0.694	2	3.04
3	0.901	2	7.39
4	0.460	2.5	8.81

The average deviation per point is 0.015.

FIGURE 18

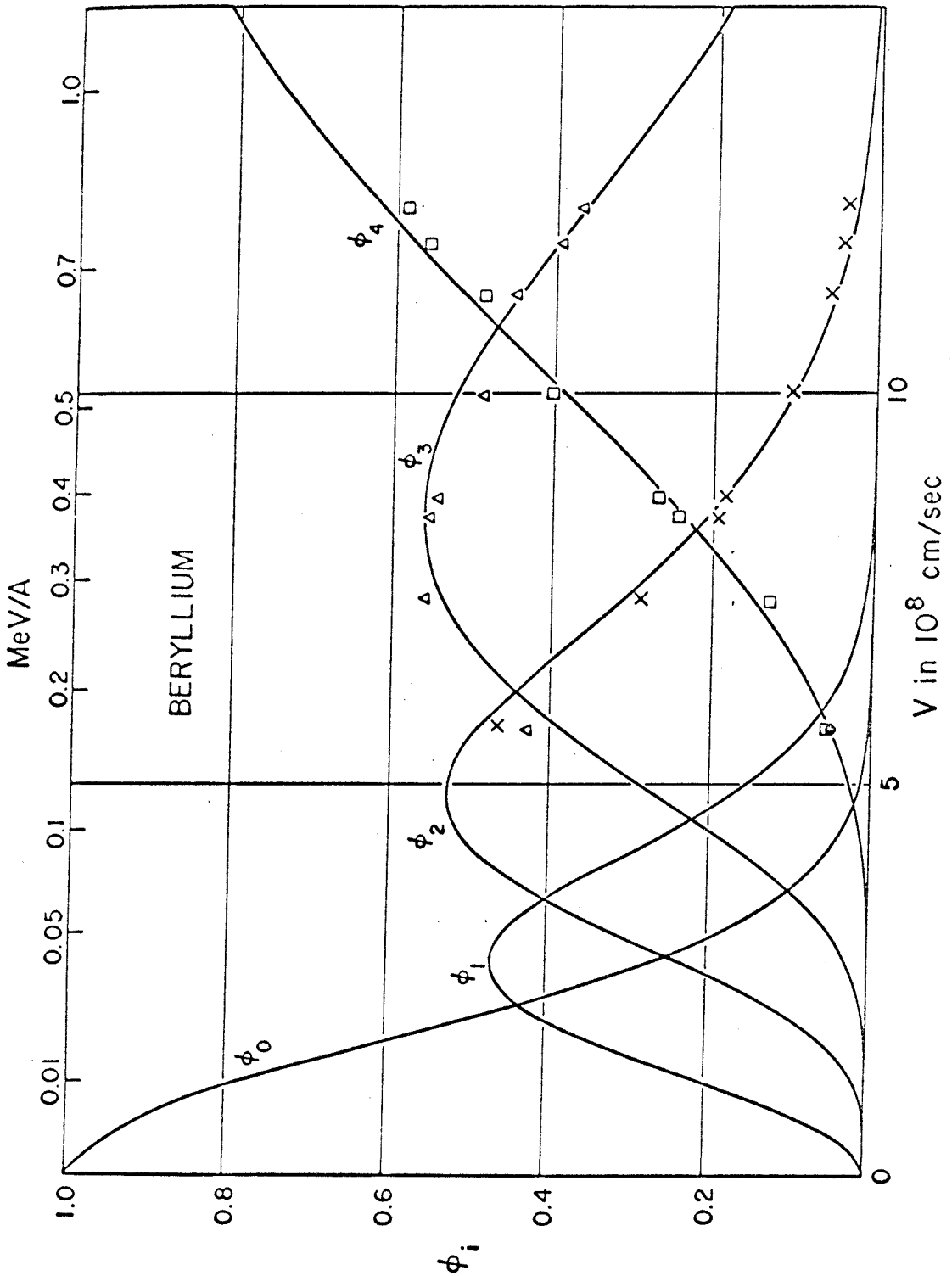

Figure 19

Boron charge state curves. Solid curves have been calculated using the parameters, A_J, B_J, and V_J listed below and discussed in Appendix I. The data points have been plotted with the symbols: $\emptyset_0 = 0$, $\emptyset_1 = \bullet$, $\emptyset_2 = x$, $\emptyset_3 = \Delta$, $\emptyset_4 = \square$, and $\emptyset_5 = +$.
The parameters used were: (Pages 63 and 66.)

J	A_J	B_J	V_J (in 10^8 cm/sec)
1	0.674	2	1.72
2	0.107	2	1.99
3	0.348	3	2.69
4	0.750	3	9.58
5	0.464	3	10.98

The average deviation per point is 0.015.

Figure 19

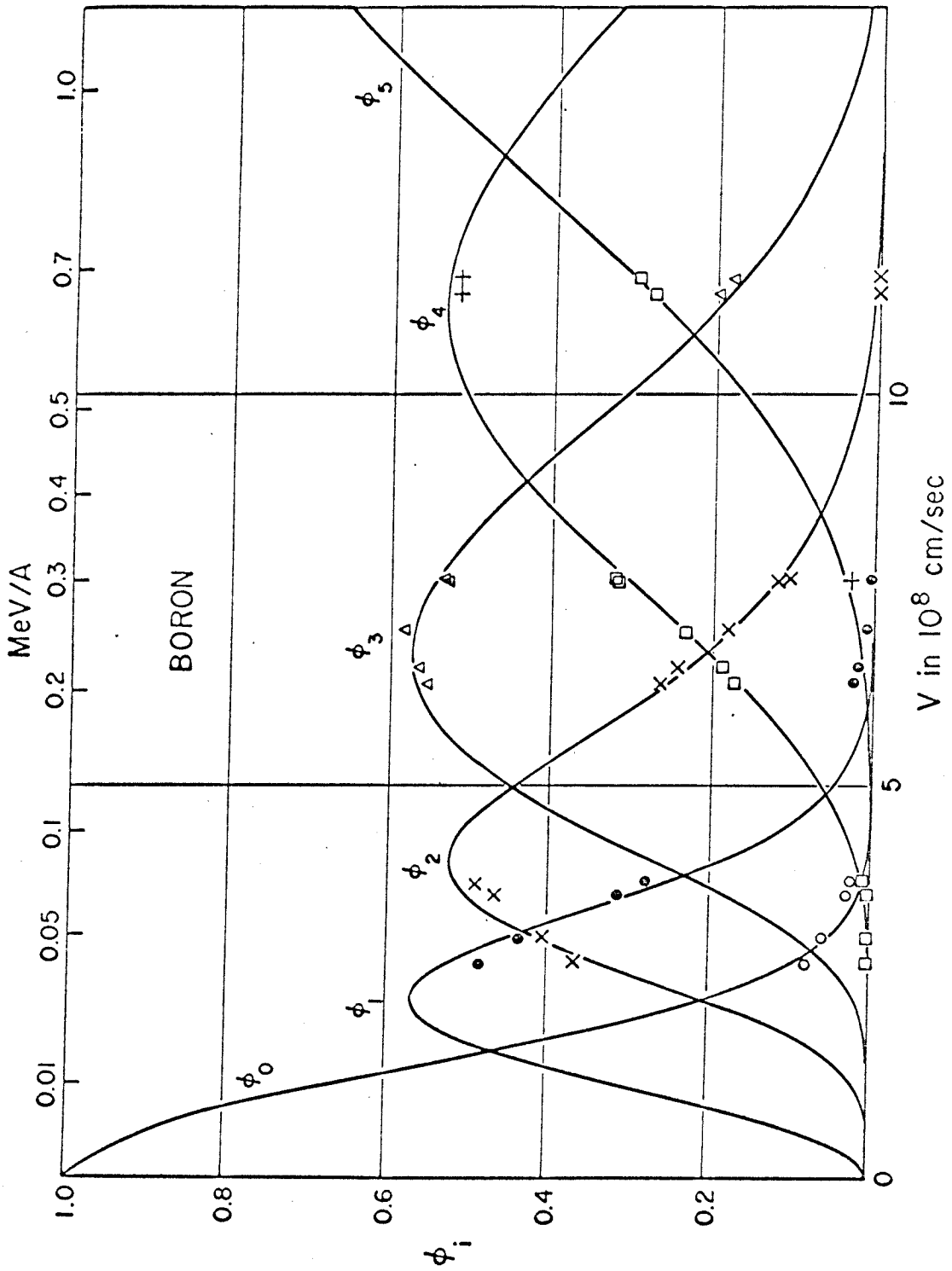
BORON
MeV/A
1.0
0.7
0.5
0.4
0.3
0.2
0.1
0.05
0.01
ϕ_5
ϕ_4
ϕ_3
ϕ_2
ϕ_1
ϕ_0
1.0
0.8
0.6
0.4
0.2
ϕ_i
0
5
10
V in 10^8 cm/sec

Figure 20

Carbon charge state curves. Solid curves have been calculated using the parameters, A_J, B_J, and V_J listed below and discussed in Appendix I. The data points have been plotted with the symbols: ϕ_0 = 0, ϕ_1 = •, ϕ_2 = x, ϕ_3 = Δ, ϕ_4 = □, ϕ_5 = +, ϕ_6 = ⬡.

The parameters used were: (Pages 63 and 66.)

J	A_J	B_J	V_J (in 10^8 cm/sec)
1	1.0	2	2.0
2	0.753	2	2.95
3	0.428	3	4.13
4	0.212	3	4.75
5	0.218	5	11.92
6	0.519	2	13.20

The average deviation per point is 0.01.

Figure 20

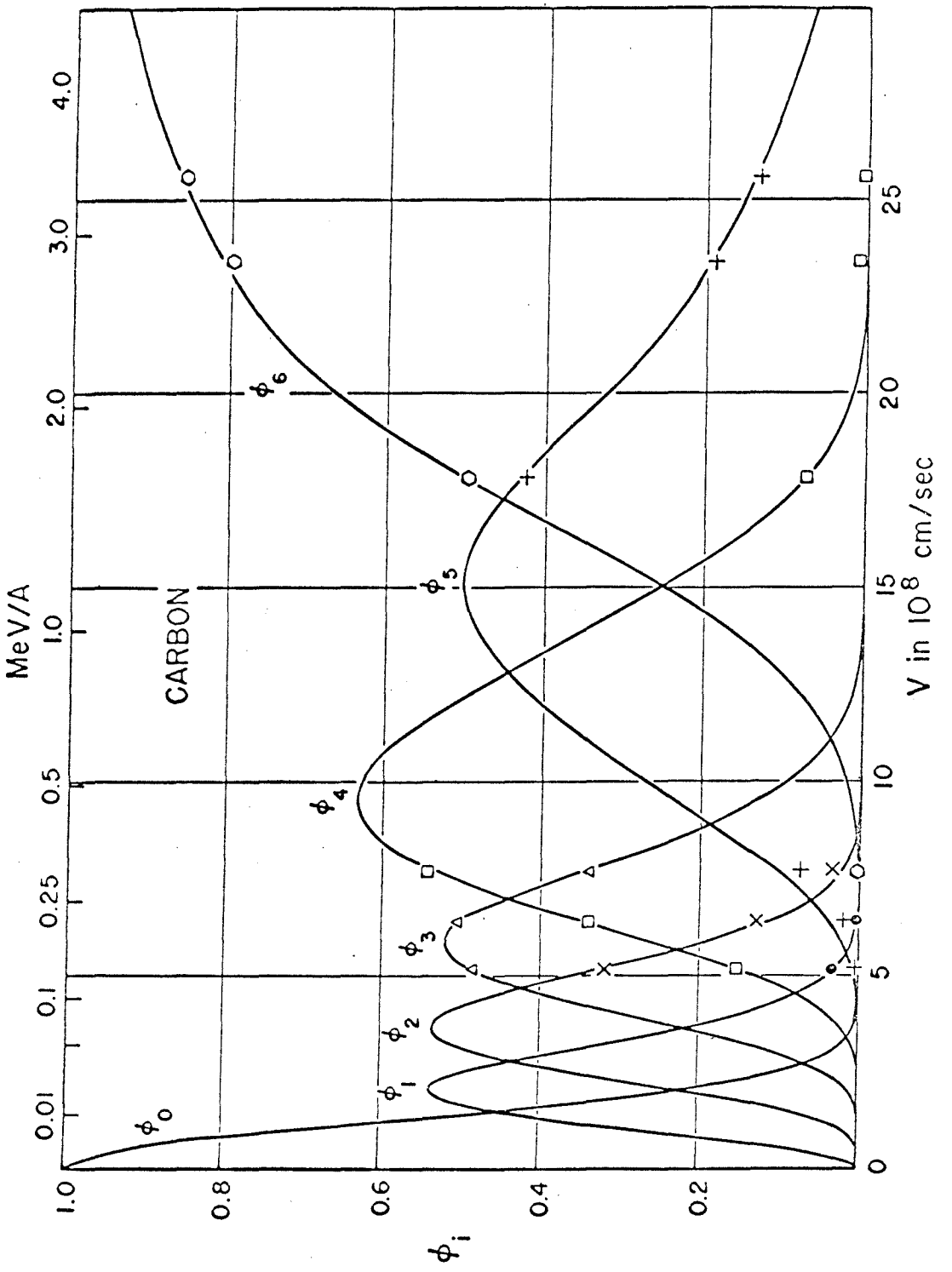
MeV/A
CARBON
V in 10^8 cm/sec
ϕ_i
ϕ_0
ϕ_1
ϕ_2
ϕ_3
ϕ_4
ϕ_5
ϕ_6
4.0
3.0
2.0
1.0
0.5
0.25
0.1
0.01
25
20
15
10
5
0
1.0
0.8
0.6
0.4
0.2

Figure 21

Nitrogen charge state curves. Solid curves have been calculated using the parameters, A_J, B_J, and V_J listed below and discussed in Appendix I. The data points have been plotted with the symbols: $\phi_0 = 0$, $\phi_1 = \bullet$, $\phi_2 = x$, $\phi_3 = \Delta$, $\phi_4 = \square$, $\phi_5 = +$, $\phi_6 = \bigcirc$, $\phi = \diamond$.

The parameters used were: (Pages 63 and 66.)

J	A_J	B_J	V_J (in 10^8 cm/sec)
1	1.223	2	2.27
2	1.011	2	3.26
3	0.870	2	4.13
4	0.293	3.5	5.26
5	0.437	2	5.89
6	0.314	2.5	13.99
7	0.780	3.5	15.32

The average deviation per point is 0.03.

FIGURE 21

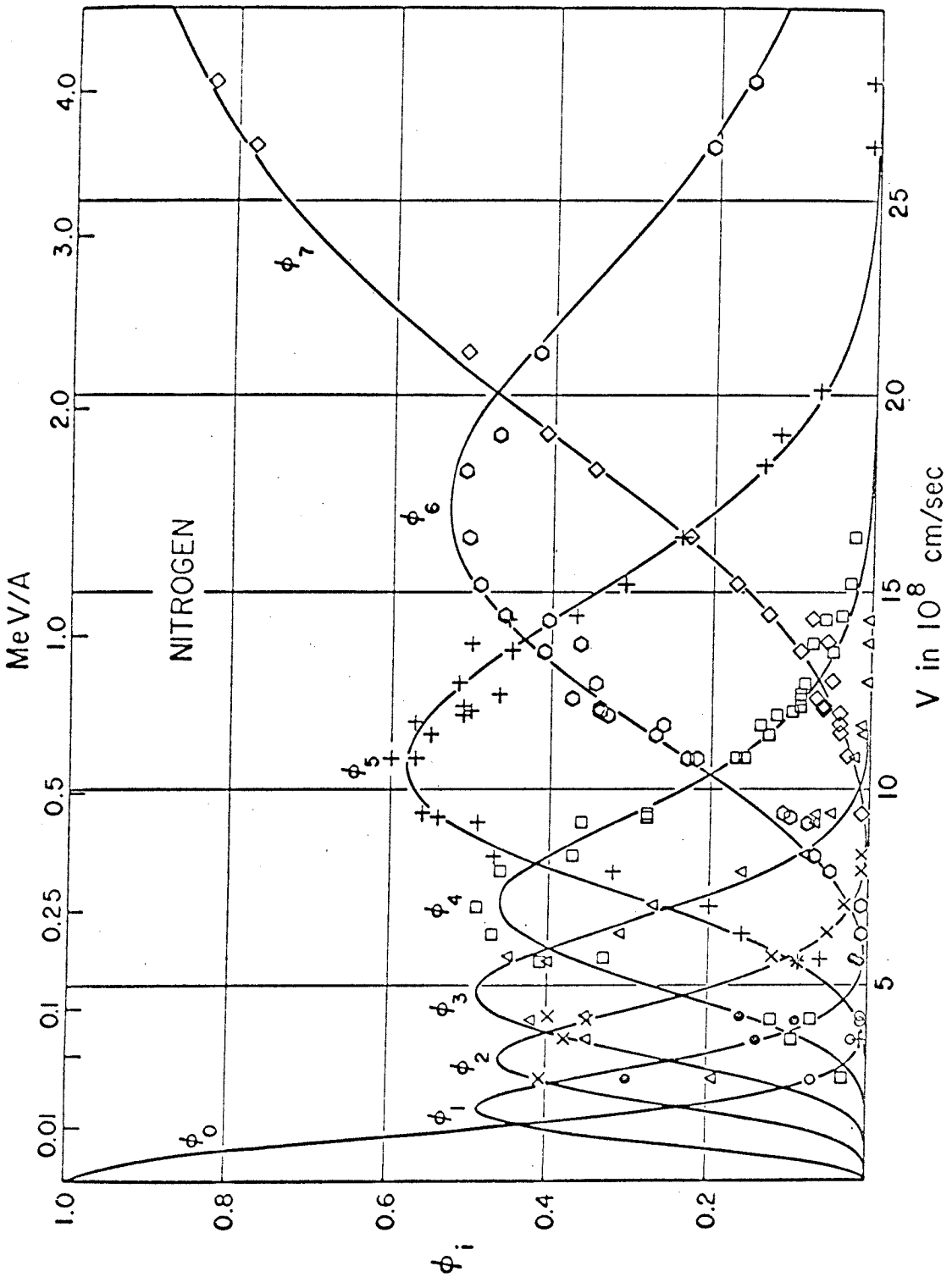
MeV/A
NITROGEN
V in 10^8 cm/sec
ϕ_i
ϕ_0
ϕ_1
ϕ_2
ϕ_3
ϕ_4
ϕ_5
ϕ_6
ϕ_7
4.0
3.0
2.0
1.0
0.5
0.25
0.1
0.01
1.0
0.8
0.6
0.4
0.2
25
20
15
10
5

Figure 22

Oxygen charge state curves. Solid curves have been calculated using the parameters, A_J, B_J, and V_J listed below and discussed in Appendix I. The data points have been plotted with the symbols: $\emptyset_0 = 0$, $\emptyset_1 = \bullet$, $\emptyset_2 = x$, $\emptyset_3 = \Delta$, $\emptyset_4 = \square$, $\emptyset_5 = +$, $\emptyset_6 = \diamond$, $\emptyset_7 = \diamond$, and $\emptyset_8 =$ ▪. The parameters used were: (Pgs. 63 and 66.)

J	A_J	B_J	V_J (in 10^8 cm/sec)
1	0.685	2	2.21
2	1.640	3	3.55
3	1.255	3	4.41
4	0.456	2.5	5.28
5	0.632	3.5	6.32
6	0.113	3.5	7.00
7	0.460	2	16.18
8	0.681	3	17.15

The average deviation per pont is 0.035 .

FIGURE 22

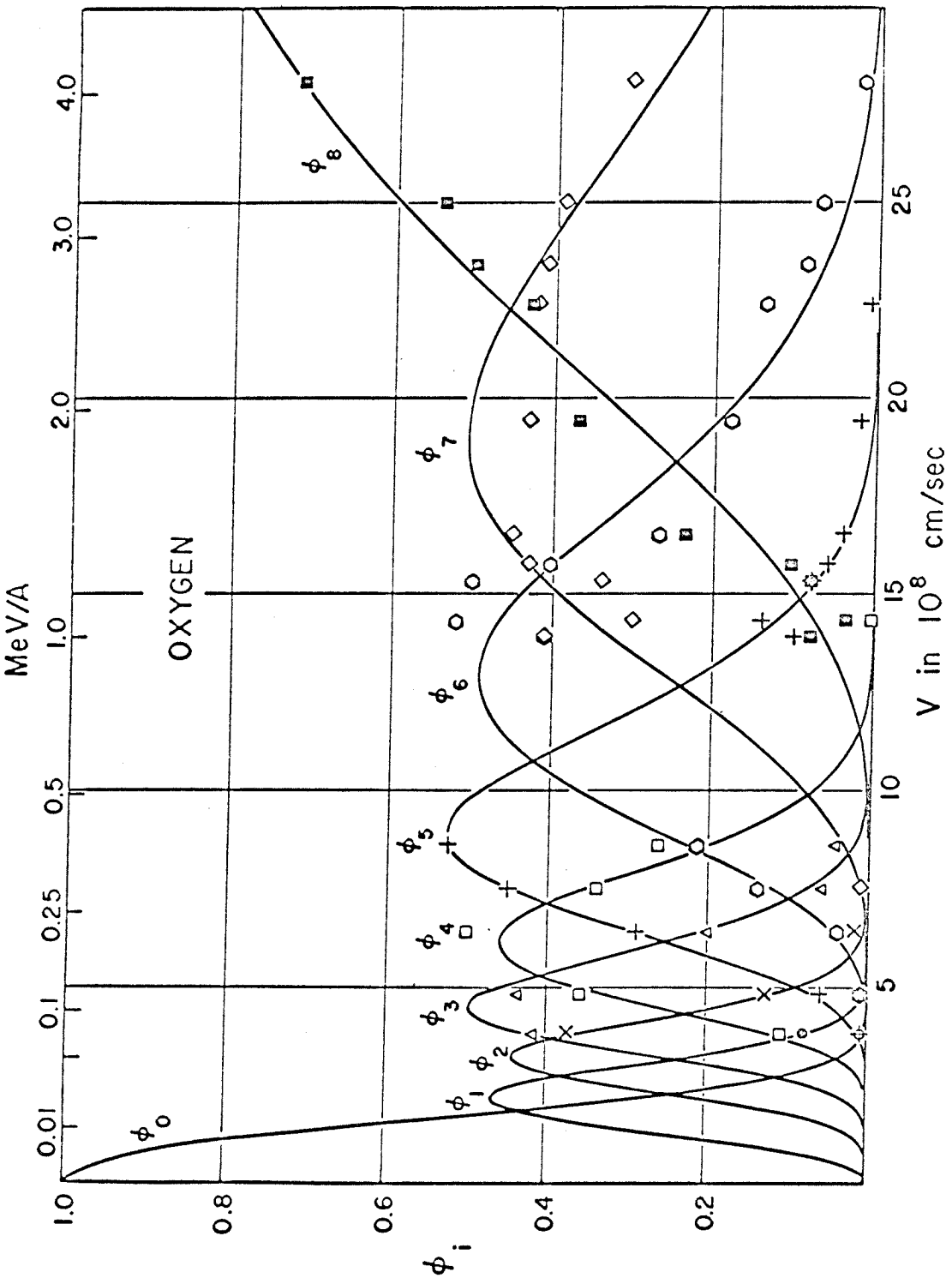
OXYGEN
MeV/A
4.0
3.0
2.0
1.0
0.5
0.25
0.1
0.01
ϕ_8
ϕ_7
ϕ_6
ϕ_5
ϕ_4
ϕ_3
ϕ_2
ϕ_1
ϕ_0
1.0
0.8
0.6
0.4
0.2
ϕ_i
25
20
15
10
5
V in 10^8 cm/sec

Figure 23

Fluorine charge state curves. Solid curves have been calculated using the parameters, A_J, B_J, and V_J listed below and discussed in Appendix I. The data points have been plotted with the symbols: $\emptyset_0 = 0$, $\emptyset_1 = \bullet$, $\emptyset_2 = x$, $\emptyset_3 = \Delta$, $\emptyset_4 = \square$, $\emptyset_5 = +$, $\emptyset_6 = \hexagon$, $\emptyset_7 = \diamond$, $0_8 =$ ▩, $\emptyset_9 = \blacktriangle$. The parameters used were: (Pgs. 63, 66)

J	A_J	B_J	V_J (in 10^8 cm/sec)
1	2.5	3	2.48
2	2.5	2	3.58
3	1.2	2	4.71
4	1.2	3	5.59
5	0.410	2	6.33
6	0.400	2	7.42
7	0.959	2.5	8.11
8	0.276	2.5	18.20
9	1.025	3.5	19.67

The average deviation per point is 0.04 .

Figure 23

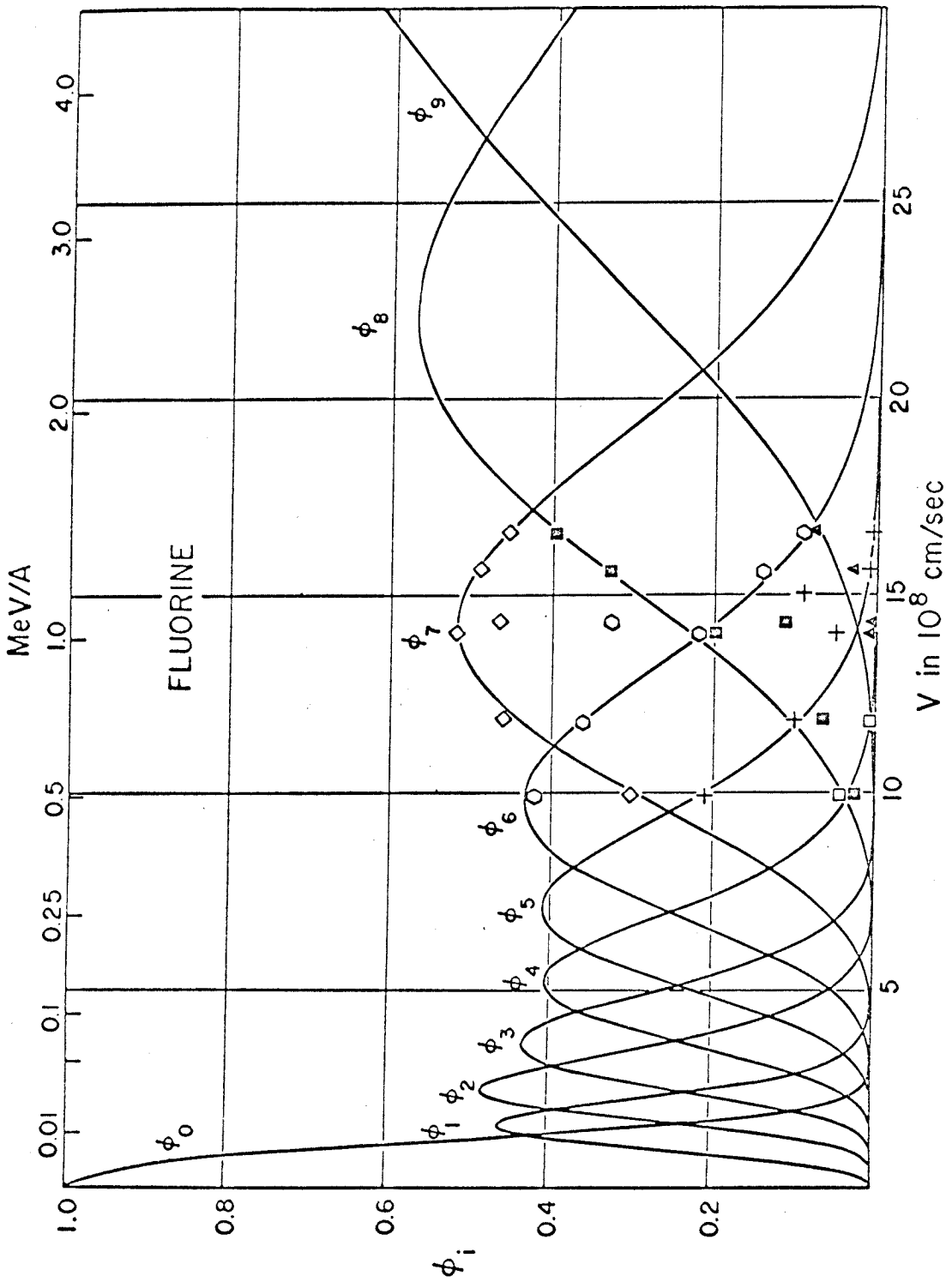
MeV/A
FLUORINE
V in 10^8 cm/sec
ϕ_i
ϕ_0
ϕ_1
ϕ_2
ϕ_3
ϕ_4
ϕ_5
ϕ_6
ϕ_7
ϕ_8
ϕ_9
0.01
0.1
0.25
0.5
1.0
2.0
3.0
4.0
5
10
15
20
25
1.0
0.8
0.6
0.4
0.2

Figure 24

Neon charge state curves. Solid curves have been calculated using the parameters, A_J, B_J, and V_J listed below and discussed in Appendix I. The data points have been plotted with the symbols:

$\phi_0 = 0$, $\phi_1 =$ ●, $\phi_2 =$ x, $\phi_3 = \Delta$, $\phi_4 = \square$, $\phi_5 = +$, $\phi_6 =$ ⬡, $\phi_7 =$ ◇, $\phi_8 =$ ▣, $\phi_9 =$ ▲, $\phi_{10} =$ ◆. (Pages 63 and 67.)

The parameters used were:

J	A_J	B_J	V_J (in 10^8 cm/sec)
1	2.5	2	2.75
2	2.661	3	3.78
3	2.358	2	4.72
4	1.333	2	5.81
5	1.310	3	6.67
6	1.167	4	7.42
7	0.405	2.5	8.53
8	0.140	3.5	9.19
9	0.647	2.5	20.23
10	0.427	3.5	21.88

The average deviation per point is 0.015.

Figure 24

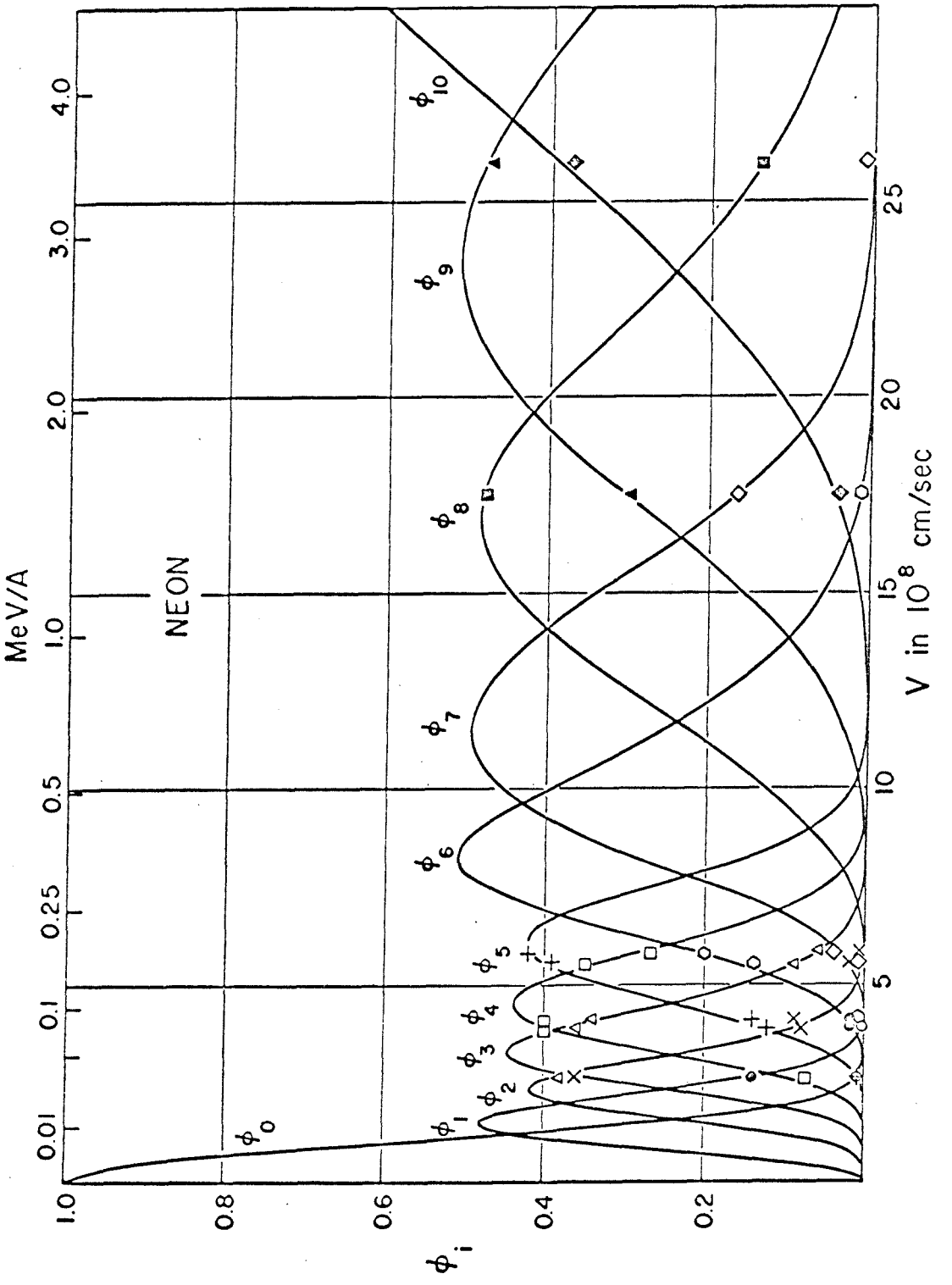
NEON
MeV/A
V in 10^8 cm/sec
ϕ_i
ϕ_0
ϕ_1
ϕ_2
ϕ_3
ϕ_4
ϕ_5
ϕ_6
ϕ_7
ϕ_8
ϕ_9
ϕ_{10}
0.01
0.1
0.25
0.5
1.0
2.0
3.0
4.0
1.0
0.8
0.6
0.4
0.2
5
10
15
20
25

Figure 25

Calculated line shape of the broad deuteron spectrum associated with the 9.58 MeV level in ^{16}O, for relative orbital angular momenta 0 and 4. The region included between the outer arrows is that used in determining the total yield of deuterons from the states.

(Page 75.)

Figure 25

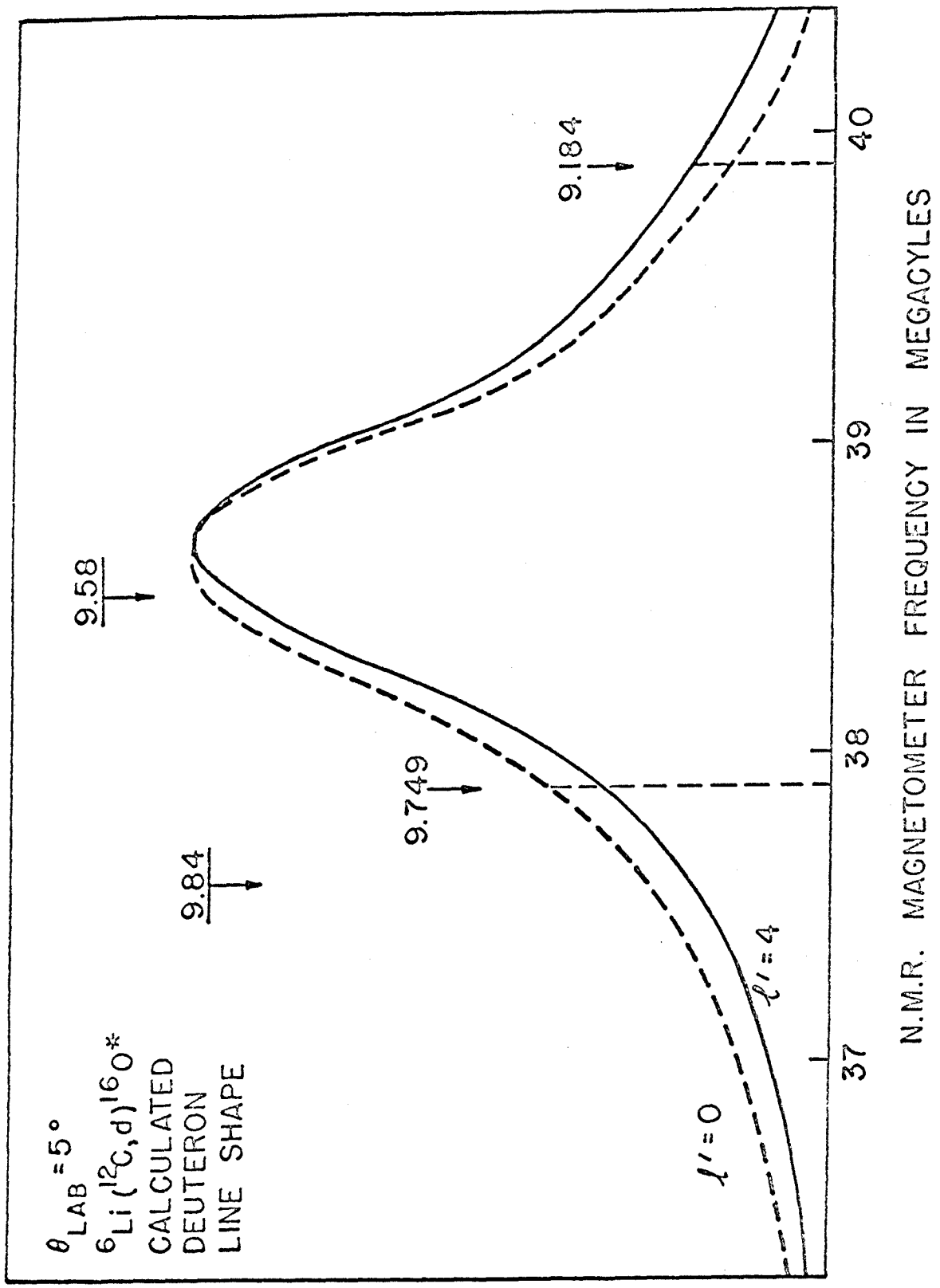
θ LAB =5°
6Li (12C,d) 16O*
CALCULATED
DEUTERON
LINE SHAPE
9.58
9.84
9.749
9.184
l'=0
l'=4
37
38
39
40
N.M.R. MAGNETOMETER FREQUENCY IN MEGACYLES